50X1-HUM

Declassified in Part - Sanitized Copy Approved for Release @ 50-Yr 2014/02/05 : CIA-RDP81-01043R002800240003-8

[redacted]

[redacted]

STAT

NONMETALLIC FERROMAGNETIC MATERIALS AND DEVICES

JOHN M. BLANK
ROBERT W. JOHNSTON
HAROLD W. KATZ
GERALD G. PALMER
NATHAN SCHWARTZ

GENERAL ELECTRIC COMPANY

OCTOBER 1957

WRIGHT AIR DEVELOPMENT CENTER

STAT

ABSTRACT

This report covers research and development performed on the study of nonmetallic ferromagnetic materials and devices by the Electronics Laboratory of the General Electric Company during the contract period.

The work presented in this report describes the effort expended in the various areas of ferrite development covered by the subject contract. These areas include the development of ferrite materials for high power applications, low signal applications, and dynamic magnetostrictive applications for operation in the temperature range -65°C to +250°C; and a high frequency, narrow band (30 mc) modulated delay line.

PUBLICATION REVIEW

The publication of this report does not constitute approval by the Air Force of the findings or conclusions contained herein. It is published only for the exchange and stimulation of ideas.

TABLE OF CONTENTS

STAT

TABLE OF CONTENTS (Contd)

LIST OF ILLUSTRATIONS

STAT

STAT

LIST OF ILLUSTRATIONS (Contd)

LIST OF ILLUSTRATIONS (Contd)

STAT
STAT

LIST OF ILLUSTRATIONS (Contd)

LIST OF TABLES

LIST OF TABLES (Contd)

SECTION I

INTRODUCTION

This report is being submitted as a summary of the effort expended to date under Contract No. AF 33(616)-3339. The objectives of the investigation carried out during the present contract period are:

1. To develop ferrite materials for applications in the temperature range -65°C to +250°C.

2. To develop a narrow band, high frequency ferrite delay line, the delay of which can be varied by a biasing magnetic field.

Under objective 1 above, the specific types of materials to be considered are:

a. Materials for high power applications in the frequency range 20 kc to 1000 kc.

b. Materials for low signal applications with high μQ product, low temperature coefficient of permeability, and whose characteristics are not affected by prolonged exposure to high humidity.

c. Materials for magnetostrictive applications. Such materials are to be suitable for use in filters and oscillators over the frequency range 455 kc to 1000 kc, and have a maximum temperature coefficient of resonant frequency of 10 ppm per C° over the temperature range of interest.

Under objective 2, the present goal is to achieve a total delay of approximately 0.5 microseconds in a line of reasonable length (3 inches) and a change in delay of 0.1 microseconds at 30 mc.

Section II of this report covers the work on the development of materials for high power application. In this section, the processing and methods of compositional control are described for materials of this type. The choice of materials is governed by the high temperature requirements. The anticipated operating frequency range is such that a study of the dispersion in high signal permeability of these materials forms a basic aspect of the problem. Atmosphere conditions during firing are used as a compositional control agency. Superior transformer materials require a high degree of homogeneity throughout the volume of the material in a given configuration. Also, atmosphere firing conditions help determine the ultimate cation distribution and the valence state of the iron ions in the material. The percentage Fe^{2+} ions incorporated in the final composition determines to a great extent the shape of the hysteresis loop, the coercive force and the ultimate high signal permeability. Detailed discussion of

Manuscript released by the author 1 July 1957 for publication as a WADC Technical Report

STAT

STAT

these various aspects of the overall problem are given and recommendations are made for producing the most satisfactory material in the present ferrite system of interest.

Section III covers the work on the development of materials for low signal applications. The broad objectives of this program were such to give considerable latitude to the type of investigation. The results of this work indicate that a series of materials for low signal applications can be obtained with low loss and perform satisfactorily over the temperature range of interest, -65°C to +250°C. Data are presented which show the results of measurement at temperatures as low as -175°C. The significant successes of this broad development were: (1) The fabrication of materials with high μQ products, and (2) The development of materials with low temperature coefficient of permeability in the temperature interval -65°C to +25°C.

In the course of the current development, differential thermal analysis (DTA) was applied to the binder burnoff problem and carried into the temperature region of calcining and sintering.

A further important conclusion from this work resulted from observations made on ferrite systems in which various sources of iron oxide are used in the fabrication procedure. The difference in impurity content among these various sources of fron oxide affect the ultimate magnetic properties of these low fired, partially sintered materials. The results of these various investigations, the processing of the various significant compositions and the magnetic evaluation are presented in Section III.

Section IV of this report covers the work on the development of a modulated ferrite delay line. The initial objective of a 30 mc line with a ±0.1 variation in delay has not been achieved. However, a completely satisfactory 10 mc line has been developed which exhibits sufficient time delay variation for the intended application. The processing of the necessary materials and the method of line construction are described in detail in Section IV.

Section V contains the work performed in the investigation of ferrite materials for magnetostrictive applications. No large effort was expended on this project because of the overriding importance of other phases included in the total effort. However, the tentative conclusion is that the desired coefficient of resonant frequency, 10 parts per million per degree centigrade, cannot be obtained readily over the wide temperature interval, -65°C to +250°C.

In Section VI a review is given of the important conclusions and results derived from the investigations carried out in the areas of interest included in the scope of Contract No. AF 33(616)-3339.

SECTION II

MATERIALS FOR HIGH POWER APPLICATIONS

Objective

The purpose of this development is to provide ferrite materials having low losses at high flux density over the frequency range 20 kc to 1000 kc and over the temperature range -65°C to 250°C.

Approach

Previous work carried out at the Electronics Laboratory of the General Electric Company in the field of ferrite materials for high power applications led to the development of Composition 164, a 30-20 Ni-Zn ferrite. This work was described in WADC Technical Report TR-56-274, Part II.

The development of Composition 164 was an attempt to compromise the many conflicting demands on a high temperature, high saturation, low loss ferrite. This material consisted of 50 mol% Fe_2O_3, 30 mol% NiO, and 20 mol% ZnO, and represented a compromise among saturation magnetization, exchange energy, and magnetocrystalline anisotropy.

When a composition is chosen, saturation magnetization, magnetocrystalline anisotropy, exchange energy, and saturation magnetostriction are essentially fixed, give or take a few percent depending on small changes which vary with firing temperature and time, rate of cool, etc. These are the properties which determine the energy per unit area of domain walls, the density of magnetic poles at surfaces of magnetic discontinuity, the direction of preferred magnetization and the ease or difficulty of rotating the direction of magnetization away from the preferred direction. The grain size and shape, the density and size of defects such as inclusions, voids, lamellar precipitates, and the conditions of internal stress are the seats from which the above characteristics operate to determine magnetic response in the hysteresis loop.

In the development reported here, the proposed scheme included the introduction of magnetite into Composition 164 ferrite. This was attractive for many reasons. Magnetite is known to form solid solutions with nickel ferrite. It is reasonable to expect that magnetite will also be soluble in Composition 164. Magnetite has a higher saturation magnetization than nickel ferrite, so that the addition of magnetite to Composition 164 should increase the saturation magnetization. Since magnetite has a positive magnetostriction and Composition 164 a negative magnetostriction, the addition of magnetite should reduce the saturation magnetostriction of the solution and thus raise the permeability. It should be remembered, however, that magnetite has a much lower resistivity than nickel ferrite and therefore may be detrimental to magnetic performance at frequencies above 20 kc.

In proceeding with the planned approach, it was necessary to learn how to add magnetite to Composition 164. Merely adding Reagent Grade

STAT
STAT

magnetite to the other ingredients or to the calcine does not necessarily accomplish the desired result. On heating, magnetite converts to ferric oxide at about 500°C. Also, ferric oxide converts back to magnetite by losing oxygen at higher temperatures.

The range of temperatures for which ferric oxide converts to magnetite is lower than the sintering range of temperatures used in fabricating high power ferrites. As a result, magnetite additions to Composition 164 can be achieved by simply adding ferric oxide in excess of the amount needed to make the nickel-zinc portion of the solution. The problem does not end there. On cooling, the ferrite-magnetite solution accepts oxygen and precipitates ferric oxide. Two things can be done to prevent this. The solution can be cooled so quickly that the acceptance of oxygen and the resulting precipitation will not have time to occur; or, the solution can be protected from oxidation by a protective atmosphere such as nitrogen, argon, helium, carbon dioxide, or steam.

A preliminary experiment was carried out to determine the feasibility of introducing magnetite by the method described above. A new composition, Composition 690, was prepared containing

52.7 mol% Fe_2O_3
28.4 mol% NiO
18.9 mol% ZnO

which amounted to adding 5.4 mol% extra ferric oxide to Composition 164. When converted, 5.4 mol% Fe_2O_3 makes 3.6 mol% Fe_3O_4, magnetite.

Eight 1/4 inch cubes of this composition were placed in a tube furnace and heated at 94°C per hour to 1400°C for 3 hours. One cube was then withdrawn from the tube and quenched into water. The furnace was set to cool 100°C per hour. Cubes were pulled and water quenched at about 50°C intervals. These cubes were examined for precipitation of ferric oxide. None showed precipitation. The cubes were then crushed and analyzed for ferrous iron from which the magnetite content can be calculated. The results are shown in Table I.

TABLE I

MOL% Fe_3O_4 CALCULATED FROM FERROUS IRON ANALYSIS IN SOLUTION WITH COMPOSITION 164 FERRITE AT SEVERAL TEMPERATURES DURING COOLING FROM 1400°C at 100°C PER HOUR

Temperature from which quenched	Weight % Fe^{2+} by analysis	Mol% Fe_3O_4 calculated
1400°C	1.13	5.1
1350	1.13	5.1
1293	0.81	3.8
1250	0.81	3.8
1190	0.81	3.8
1150	1.19	5.4
1100	0.95	4.3
1045	0.91	4.1

The average for the series is 4.5 ±0.7 mol% Fe_3O_4. It is clear that this treatment produces the desired solution of magnetite in Composition 164. The control of the desired amount of magnetite leaves something to be desired in that aiming for 3.6 mol%, a value closer to 4.5 mol% was obtained. All the values are higher than anticipated. This was probably due to the presence of a greater effective amount of extra Fe_2O_3 than intended. It is not unlikely that ZnO is lost by volatilization during the heat treatments, which would lead to a proportional increase of excess iron.

Within the range of temperatures examined, there seemed to be no tendency to take on oxygen as confirmed by the absence of precipitated Fe_2O_3. Rapid cooling or atmosphere protection from 1000°C downward is adequate for maintaining solid solution in this ferrite. Thus, this preliminary experiment proved the feasibility of the method and served as a guide for preparation of the desired range of new compositions.

Compositions and Materials Preparation

Table II gives the ferrite compositions used in the course of the investigations.

TABLE II

DESCRIPTION OF COMPOSITIONS USED IN THE DEVELOPMENT OF HIGH POWER FERRITES.

Composition	Mol% Fe_2O_3	Mol% NiO	Mol% ZnO
164	50.0	30.0	20.0
690	52.7	28.4	18.9
704	54.6	27.2	18.2
716	57.5	25.5	17.0
723	50.0	30.0	20.0
724	50.0	35.0	15.0
737	53.6	27.9	18.5
730A	52.7	28.4	18.9
731	51.2	29.3	19.5

These materials were prepared in accordance with standard ceramic practice. The procedure in each case was as follows:

Reagent grade oxides were used. These materials satisfy the specifications set by the American Chemical Society for this classification.

The oxides were weighed with an accuracy of plus or minus 0.05 grams to make up a "batch" of total weight approximately equal to 2 kilograms.

The batch was ball milled for 16 hours in 3 liters of water in a 1 gallon size iron mill containing 10 pounds of 1" diameter steel balls and 15 pounds of 7/16" diameter steel balls. The slurry was separated from the balls by screening. No additional water was added to thin the slurry and

STAT
STAT

wash out the mill as the slurry when properly prepared did not separate into a liquid and solid portion. The slurry was dried in pyrex trays at 90°C, and the dry cake forced through a 10 mesh screen.

The entire batch was placed in a 2 x 5 x 10 inch mullite saggebox and calcined 3 hours at 900°C (variations in the calcine are indicated where appropriate in the body of the text.)

The calcined powder was ball milled for 16 hours in the same ball mill as before with 1 liter of water per kilogram of powder. (Water may be added after the milling operation to facilitate removing the slurry.) Drying then followed in pyrex trays at 90°C after which the dried cake was forced through a 10 mesh screen.

Polyvinyl alcohol was used as a binder being employed in a solution of 15 gm polyvinyl alcohol to 100 ml of water. The binder and powder were blended using a mortar and pestle. It was convenient to blend binder into at most 500 grams of powder at a time. Twenty milliliters of solution were used for 100 grams of powder.

The blended powder was then forced through a 40 mesh screen and pressed in toroid dies at 27,000 pounds per square inch pressure. The toroids were dried overnight at 80°C.

The toroids were set on mullite tile coated with 1/8 inch of Chemically Pure alumina powder. A typical sintering included a soak of 3 hours at 1400°C and a 129°C/hr rate of rise and rate of fall. The binder burned off satisfactorily at the above rate of rise.

This procedure achieved a fired density of 5.10 to 5.20 gm/cm3 with negligible surface porosity.

Magnetic Evaluation

Below are given the results of magnetic measurements for selected samples. Magnetization curves (B-H curves) are presented as functions of frequency and temperature. Core loss in Composition 704 as a function of maximum flux density and frequency is given for operation at 30°C.

Magnetization curves (B-H curves). Magnetization curves were obtained using the high frequency hysteresigraph developed under Contract No. AF 33(616)-2009 and reported in WADC Technical Report TR-56-274, Part VI. Figure 1 is a photograph of the hysteresigraph in operation. The sample for which the hysteresigram is shown on the oscilloscope is contained in the Dewar flask which houses a -65°C air chamber. The magnetization data at a given frequency were obtained by measuring the peak driving field for a given maximum flux density. These maximum values were read from the hysteresigraph display.

Magnetization curves are presented in Figures 2 through 13 for samples of Compositions 704, 690, 723, and 724. A typical set of curves with frequency of operation as parameter is shown in Figure 2 for toroid 704 F158-1SB (Composition 704). The data for Figure 2 were obtained with the sample in water at 30°C.

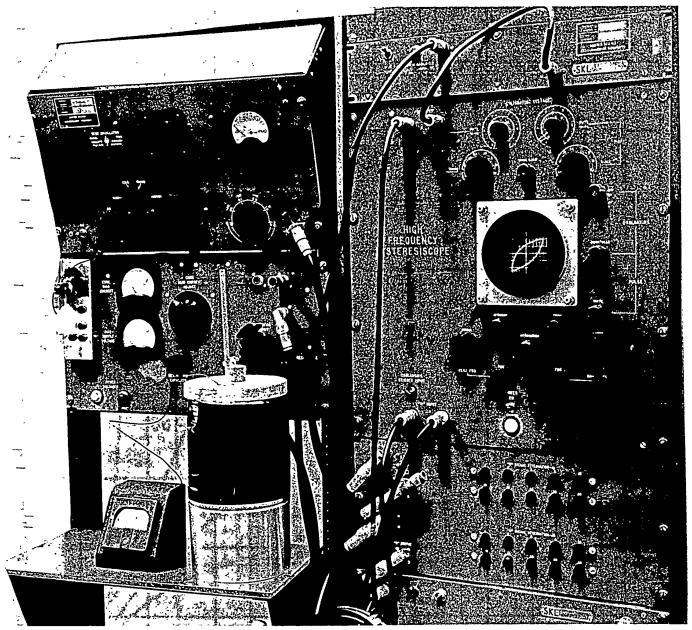

Figure 1. High Frequency Hysteresigraph

STAT

STAT

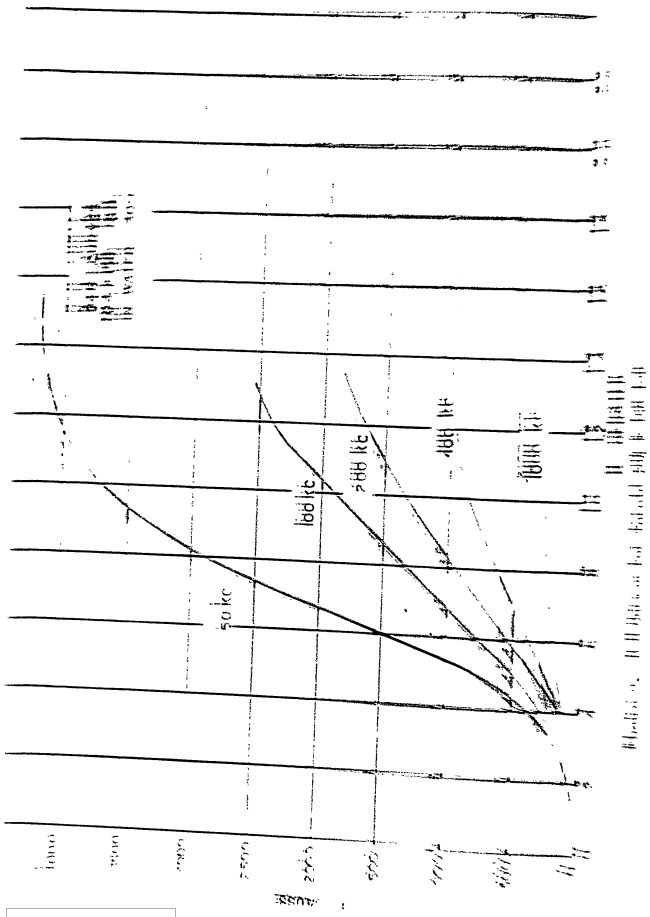

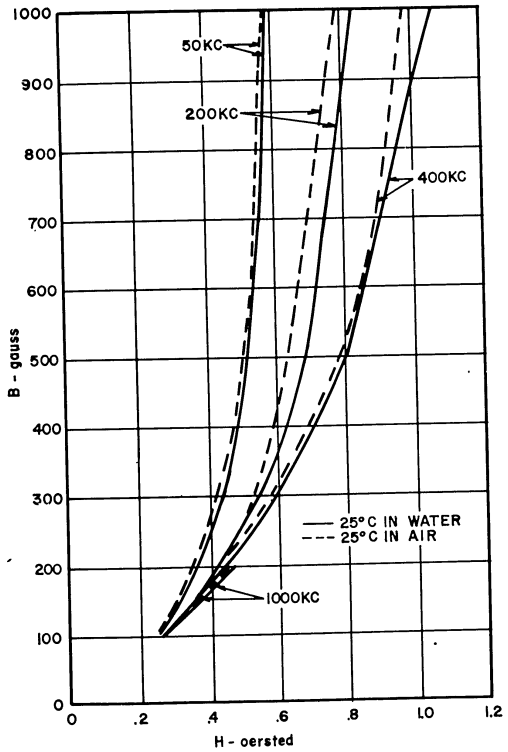

Figure 3. B-H Curves - Toroid 704 F 158-1SB 25°C in Water; 25°C in Air

STAT

STAT

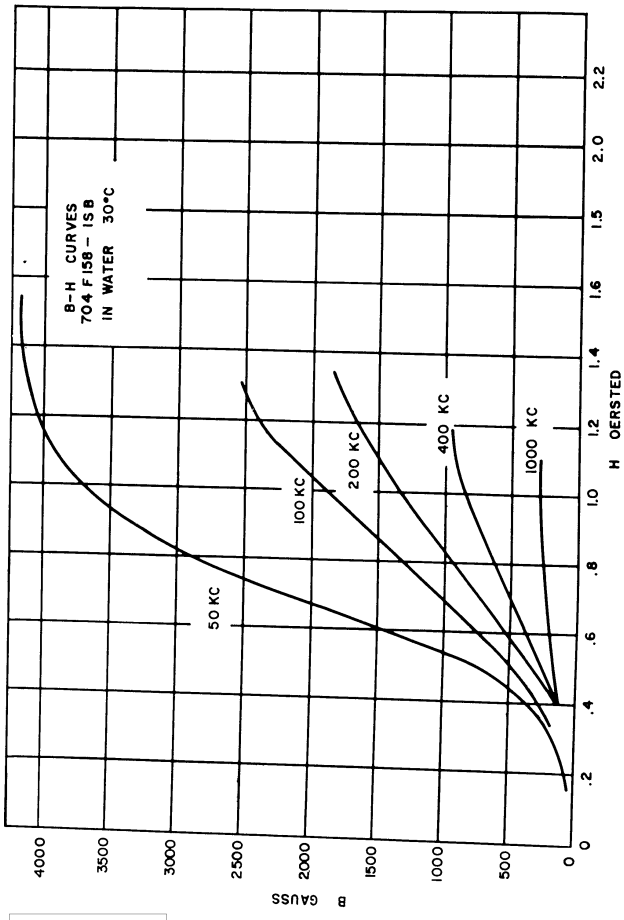

Figure 2. B-H Curves for Toroid 704 F 158-1SB

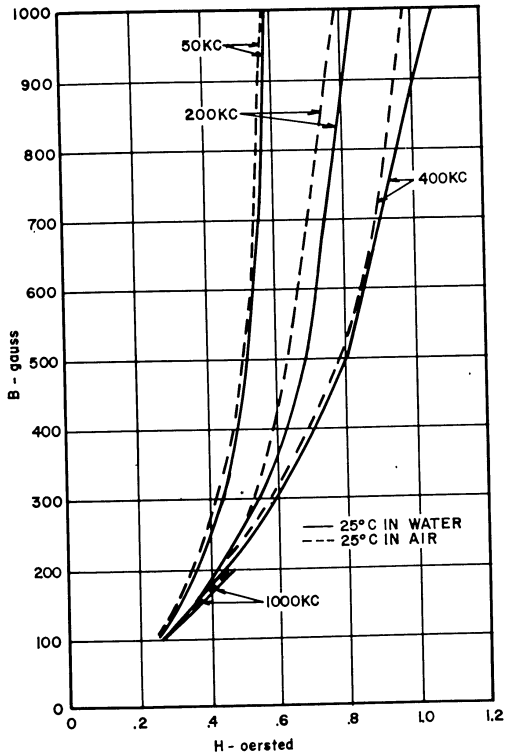

Figure 3. B-H Curves - Toroid 704 F 158-1SB 25°C in Water; 25°C in Air

STAT

STAT

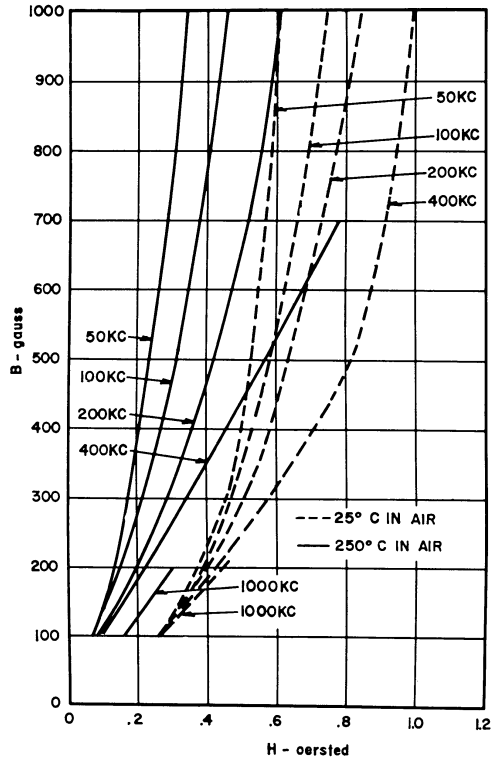

Figure 4. B-H Curves - Toroid 704 F 158-1SB 25°C in Air; 250°C in Air

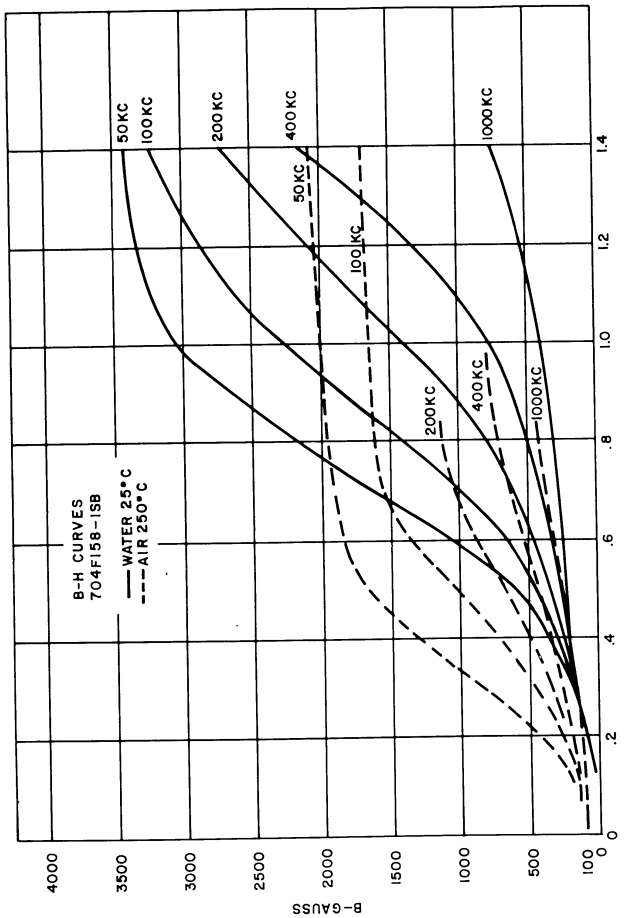

Figure 5. B-H Curves - Toroid 704 F 158-1SB 25°C in Water; 250°C in Air

STAT

STAT

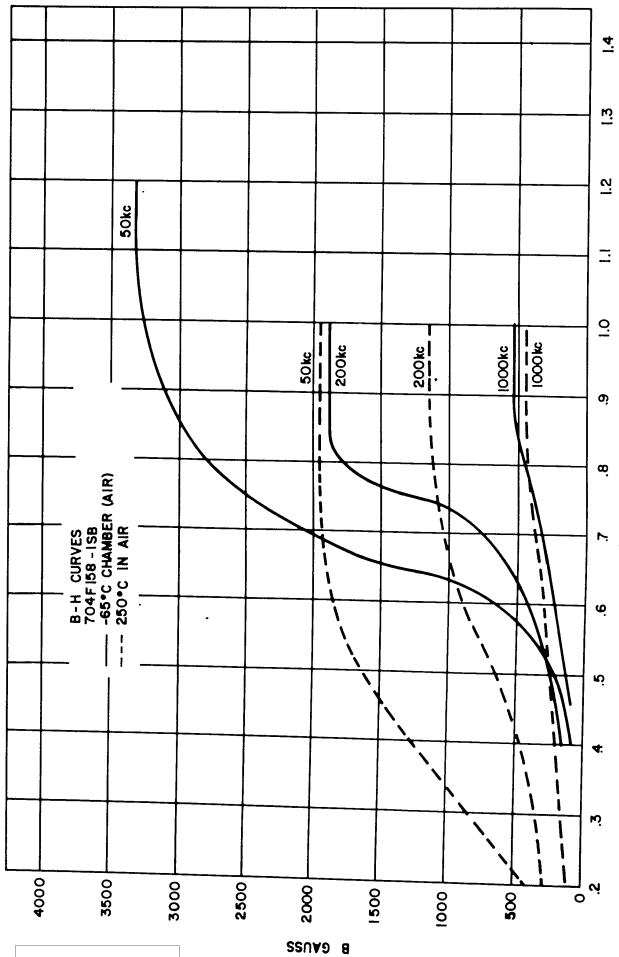

Figure 6. B-H Curves - Toroid 704 F 158-1SB -65°C in Air; 250°C in Air

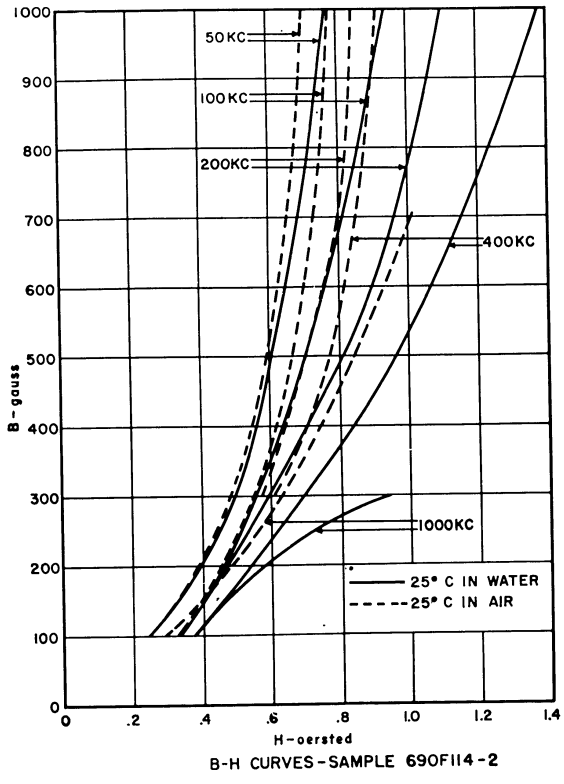

B-H CURVES-SAMPLE 690F114-2

Figure 7. B-H Curves - Toroid 690 F 114-2 250°C in Water; 25°C in Air

STAT

STAT

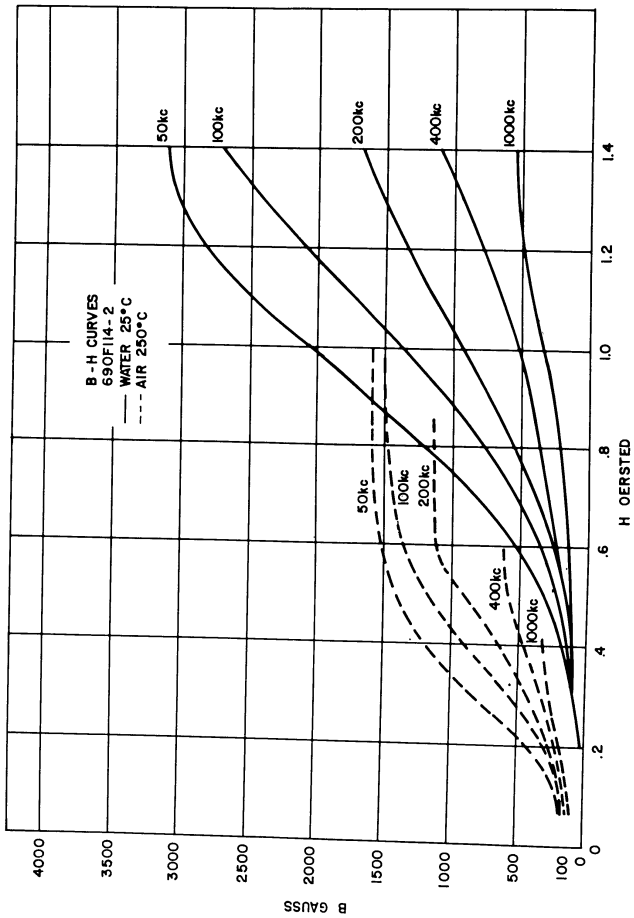

Figure 8. B-H Curves - Toroid 690 F 114-2 25°C in Water; 250°C in Air

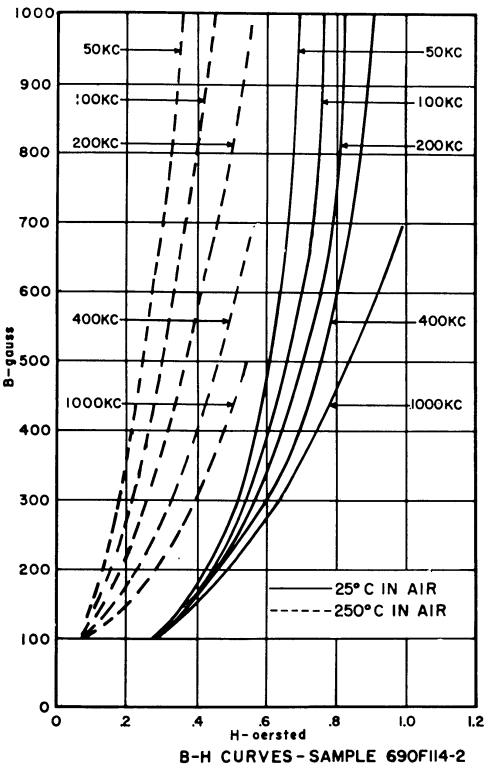

B-H CURVES - SAMPLE 690FII4-2

Figure 9. B-H Curves - Toroid 690 F 114-2 -65°C in Air; 250°C in Air

STAT
STAT

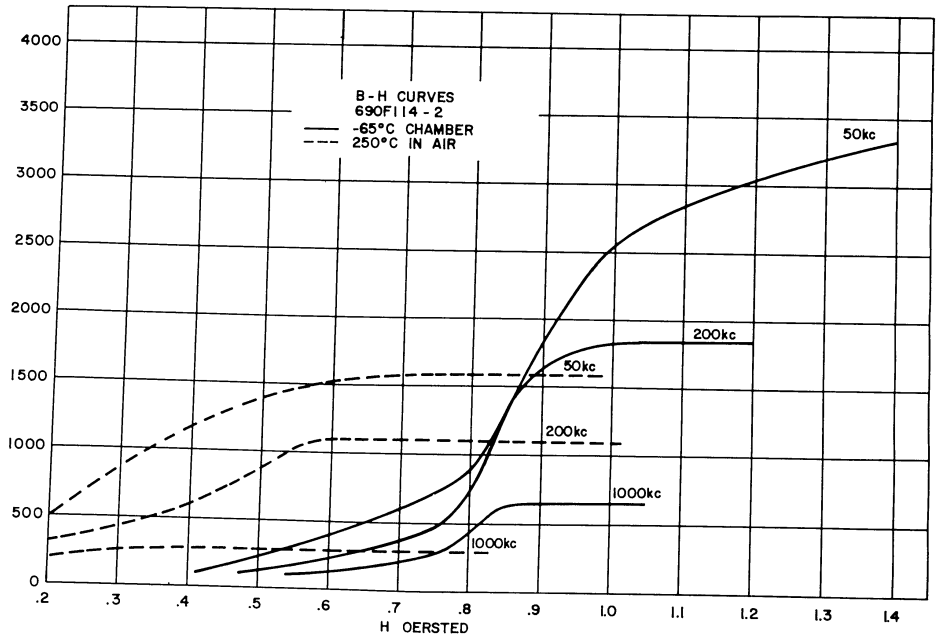

Figure 10. B-H Curves - Toroid 690 F 114-2 -65°C in Air; 250°C in Air

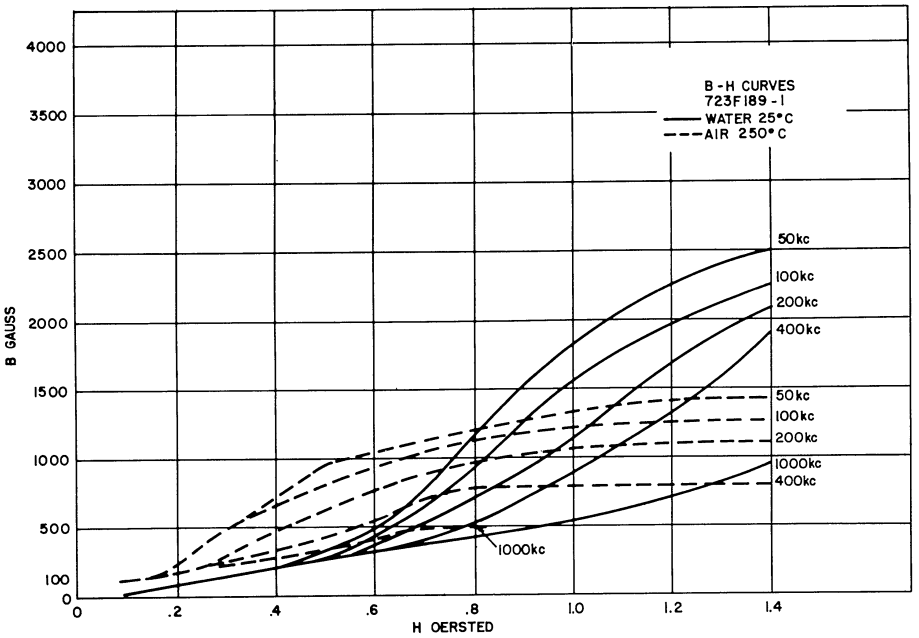

Figure 11. B-H Curves - Toroid 723 F 189-1 25°C in Water; 250°C in Air

Declassified in Part - Sanitized Copy Approved for Release @ 50-Yr 2014/02/05 : CIA-RDP81-01043R002800240003-8

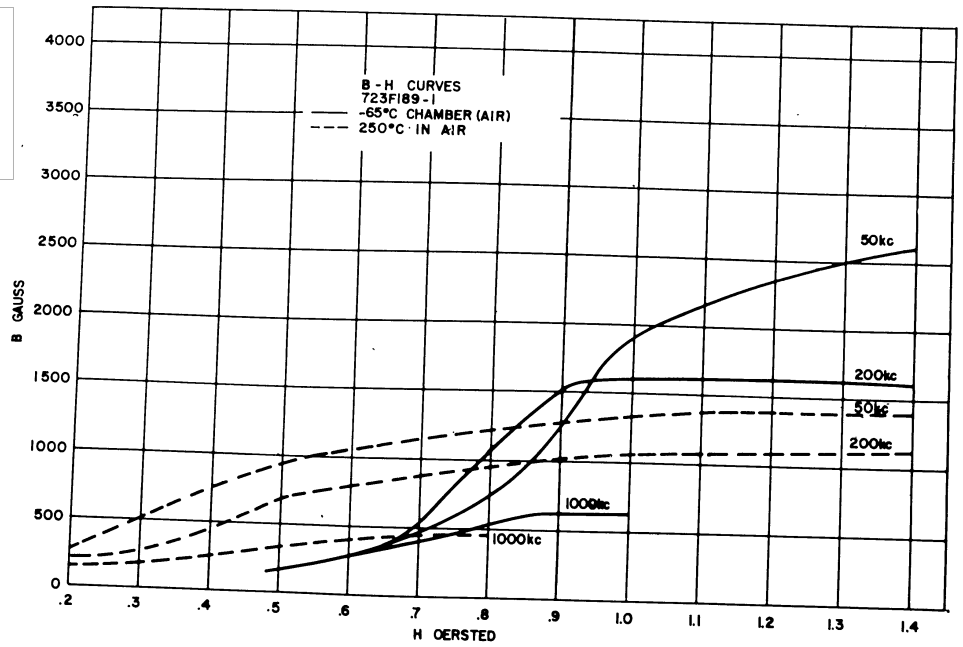

Figure 12. B-H Curves - Toroid 723 F 189-1 -65°C in Air; 250°C in Air

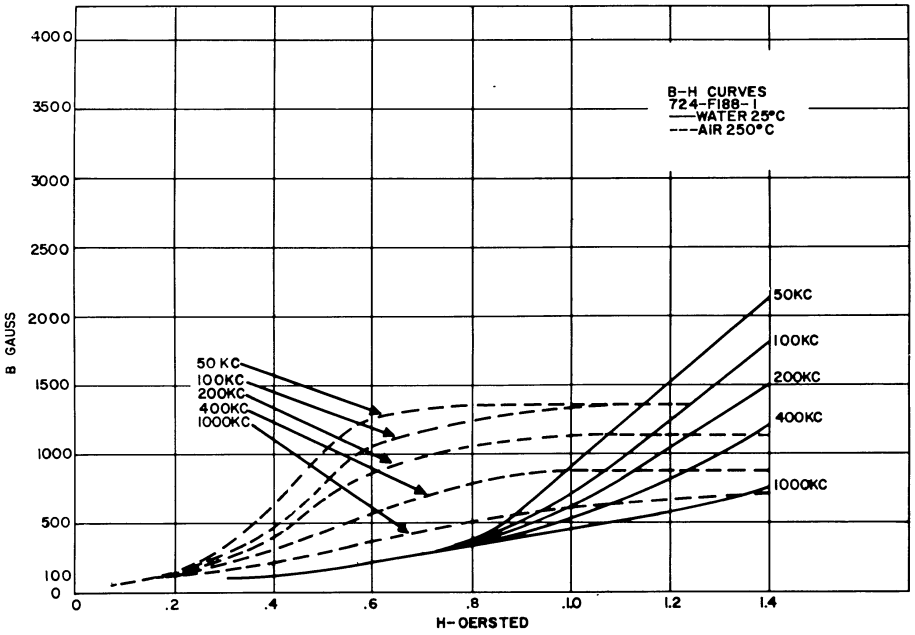

Figure 13. B-H Curves - Toroid 724 F 188-1 25°C in Water; 250°C in Air

STAT
STAT

The data shown in Figures 3 through 13 were obtained in a series of experiments carried out to determine the behavior of Compositions 690, 704, 723, and 724 which encompass a ZnO content from 15 mol% to 20 mol% and a Fe_2O_3 content from 50 mol% to 54.6 mol%. The curves were obtained by measuring the peak H values required to drive the test sample to peak B values of 100, 300, 500, 700 and 1000 gauss at five frequencies, 50, 100, 200, 400 and 1000 kc.

Four different temperature situations were employed: (1) the sample was immersed in water at 25°C in an effort to find the properties of the sample at 25°C; (2) the sample was suspended in still air at 25°C and allowed to reach a steady state temperature distribution in equilibrium with the air; (3) the sample was suspended in a tube furnace in still air at 250°C and allowed to reach steady state temperature distribution in equilibrium with the air. The temperature rise above ambient may have been as much as 100°C in the high loss situations; (4) the sample was suspended in still air at -65°C and allowed to reach a steady state.

Further comment should be made regarding the low temperature measurements. The low temperature chamber was a brass test tube immersed in a methyl alcohol bath, the temperature of which was adjusted to keep the temperature of the brass wall at -65°C ±2°C. The bath consisted of 1500 cc of methyl alcohol in a Dewar flask. The bath was cooled to the desired temperature with dry ice and had sufficient heat capacity to make adjustments about -65°C an easy task when the test samples were dissipating several watts. The magnetic samples were sealed in the brass tube (to avoid air circulation) about 4 inches below the bath liquid surface. A thermocouple was attached to the outside of the brass tube adjacent to the sample. The bath was stirred manually. In this arrangement, the temperature of the ferrite was permitted to rise until its heat loss to the walls reached steady state. At least one minute was allowed for this, although the observable changes were accomplished in 30 seconds.

Core loss measurements. Hysteresis energy loss per unit volume per cycle is defined by

$$\oint B \cdot dH$$

with H varying from $-H_{max}$ to $+H_{max}$ around the closed loop. The formula for computing the loss in watts per cubic centimeter is

$$P = (1/4\pi) f A B H \times 10^{-7} \qquad (1)$$

where

f = frequency of operation in cps
A = area of hysteresis loop in cm^2
B = scale factor, gauss/cm
H = scale factor, oersted/cm
p = loss in watts/cm^3

Figure 14 shows the loss in watts/cm^3 for toroid 704 F 158-1SB as a function of B_{max} and frequency. The data for Figure 14 were obtained with the sample immersed in water at 30°C. It is seen that the core losses reach the maximum power output capacity of the hysteresigraph driver.

It is also of interest to express the losses in ergs/cm^3 per cycle. This representation is shown in Figure 15. The dependence of loss on B ranges from $(B_{max})^{1.8}$ at 50 kc to $(B_{max})^{2.4}$ at 400 kc.

To obtain the frequency dependence of loss, data from Figure 15 are replotted in Figure 16. Figure 16 shows loss in ergs/cm^3 per cycle as a function of frequency with B_{max} as parameter. The frequency dependence is seen to be approximately $f^{0.35}$ at 100 gauss, $f^{0.55}$ at 300 gauss, and $f^{0.8}$ at 1000 gauss, considerably below an $f^{1.0}$ eddy current dependence.

Figure 17 is a graphic representation of several scattered experimental measurements made in air. The object of obtaining this information was to determine the range of permeabilities obtainable in selected frequency and flux density intervals. The data for Figure 17 were obtained with the core in air at 25°C ambient for a given frequency and flux level; the core was allowed to attain an equilibrium operating temperature. At 200 kc and a peak flux of 600 gauss, the resulting equilibrium core temperature lay between 80°C and 93°C. At the same frequency and a peak flux of 1055 gauss, a temperature between 149°C and 163°C was attained. Still at 200 kc but 1460 gauss, the temperature rose to the interval 288°C to 316°C.

It was further observed that at 100 kc and below, the core can be saturated without charring the magnet wire but, of course, the saturation value is lower than that observed under DC conditions at 25°C. The break even point with respect to charring and saturation occurs at about 200 kc. It may be further mentioned that the Formex wire used in these experiments begins to char at 200°C. Flux levels at 1000 kc above those shown resulted in charring of the formex wire.

Compositional Control

It was pointed out above that one objective to the approach governing the development of high power ferrites was the incorporation of magnetite in solid solution with the nickel-zinc ferrite. The amount of magnetite present is reflected by the Fe^{2+} content of a given sample, which is controlled by the oxygen concentration of the firing atmosphere.

A series of experiments was carried out for two purposes. These were: (1) to determine the effects of atmospheres of different oxygen concentration on the Fe^{2+} content; and (2) to produce a series of nickel-zinc-ferrous ferrite samples containing a wide range of Fe^{2+} contents. Compositions 690, 704, 737, 730A, and 731 were used in these experiments.

STAT

STAT

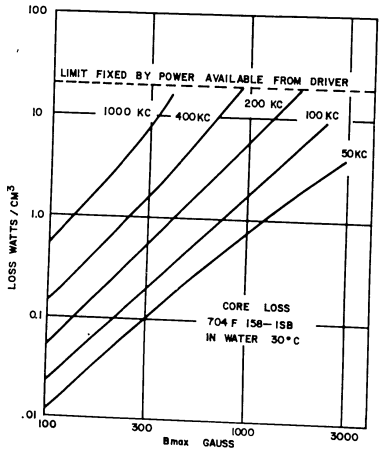

Figure 14. Core Loss in Watts/cm^3 for Toroid 704 F 158-1SB as Function of B_{max} with Frequency as Parameter

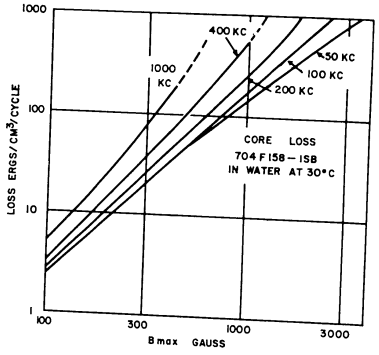

Figure 15. Core Loss in Ergs/cm per Cycle for Toroid 704 F 158-1SB as Function of B_{max} with Frequency as Parameter

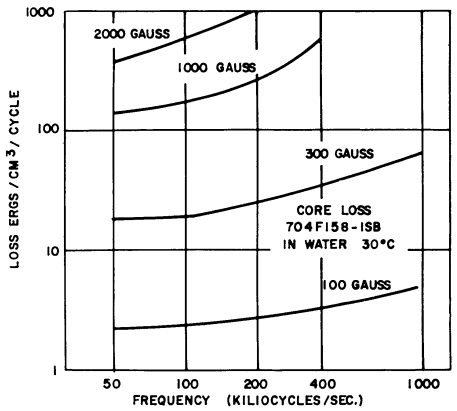

Figure 16. Core Loss in Ergs/cm^3 per Cycle for Toroid 704 F 158-1SB as Function of Frequency with B_{max} as Parameter

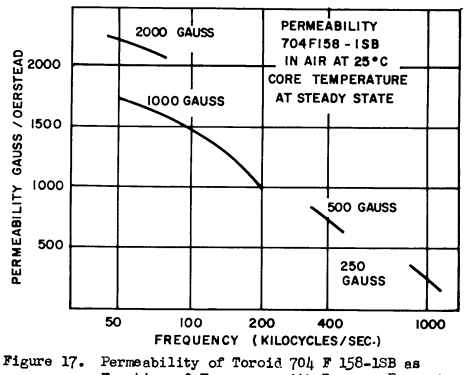

Figure 17. Permeability of Toroid 704 F 158-1SB as Function of Frequency with B_{max} as Parameter

STAT

STAT

Experiment 690 F 144. Five 1/4 x 1/4 x 1/2 inch slugs of Composition 690 were fired in a tube furnace. The rate of rise was 46°C/hr in flowing oxygen. The samples were held at 1507°C for 1 hour in flowing oxygen. At the end of 1 hour, sample number 1 was quenched into water. With the temperature still at 1507°C, the atmosphere was changed to flowing air for 1 hour at which time sample number 2 was quenched into water. The atmosphere was then changed to a 97.4% argon - 2.6% oxygen mixture for one hour at which time sample number 3 was quenched into water. Sample number 4 had an additional hour in 0.24% oxygen. Sample number 5, besides all that had gone before, had an additional hour in 0.042% oxygen. Analysis for Fe^{2+} yielded the following results:

Sample	$\%O_2$	Wt% Fe^{2+}
No. 1	100	1.26
No. 2	20	1.08
No. 3	2.6	1.73
No. 4	0.24	1.97
No. 5	0.024	1.82

The expected result in this experiment is to have the weight % Fe^{2+} increase steadily from sample number 1 through sample number 5. There is a trend toward such behavior and on a plot of weight % Fe^{2+} vs. percent oxygen a line of positive slope could be fitted to these points. Actually, the Fe^{2+} content overshot the mark. The weight % Fe^{2+} for all the excess iron converted to magnetite is 1.68% for this composition. Three of the five samples exceed this value. In ferrite systems with which we are familiar the presence of Fe^{2+} in excess of the stoichiometric amount is accompanied by a second solid phase. The surface appearance of these samples did not arouse any suspicion of a second phase so were not examined under the microscope. Whether or not another phase was present is not known.

The deviation of values from the expected increase probably arises in part from the heating cycle. The heating rate was slow and the firing temperature high. It is possible that even before the samples reached the high temperature soak, their density was near maximum and their porosity very small. At the end of the high temperature soak, their Fe^{2+} content was about 1.2%. There probably was a scatter of a few tenths of a percent in the Fe^{2+} content of the five samples at this point, presumably due to variations in density and porosity. In the course of the experiment, each successive decrease in the oxygen content of the furnace atmosphere increased the net rate of escape of oxygen from the samples. However, this rate of escape may also have been determined largely by variations in density and porosity. This same condition is encountered in all the experiments which will be described below.

Experiment 690 F 143. Five slugs of Composition 690 were fired in oxygen with a rise rate of 79°C/hr, soaked at 1415°C for 3 hours. Sample number 1 was quenched into water. Then a schedule of gas changes, similar to those of the experiment described above but with 2 hour treatments at each change of gas was carried out with the following results:

Sample	$\%O_2$	Wt% Fe^{2+}
No. 1	100	1.22
No. 2	20	1.39
No. 3	2.8	1.47
No. 4	0.28	1.35
No. 5	0.028	1.81

The Fe^{2+} values encountered here are subject to the same variability as those of the previous experiment. Except for the number 3 sample, they show the expected trend.

Experiment 690 F 145. Four slugs of Composition 690 were fired in air at 96°C/hr rate of rise, soaked at 1405°C for 4 hours, then cooled in about 30 minutes to 1205°C at which temperature they were held for 3 hours. Sample number 1 was quenched into water then a schedule of gas changes was begun. The amount of time for each gas was much longer than in the experiments above since it was anticipated that a much longer time would be required for diffusion processes to achieve equilibrium at this lower temperature. The times used are indicated below:

Sample	$\%O_2$	Duration	Wt% Fe^{2+}
No. 1	20	3 hours	1.05
No. 2	2.0	3	1.06
No. 3	0.20	2 1/2	0.73
No. 4	0.02	4	1.04

In this experiment, there is less scatter of results than in the previous one, but one is forced to conclude that the different treatments made negligible difference in Fe^{2+} content. The fact seems to be that for samples which have been fired to 1400°C and above the response to different values of oxygen content in the furnace atmosphere are sluggish and erratic.

Experiments 704 F 143 and 704 F 144. Similar sluggish and erratic response was found using slugs of Composition 704. The gas changes were identical to those used in the 690 experiments.

STAT

STAT

Sample	%O_2	Wt% Fe^{2+} at 1507°C	Wt% Fe^{2+} at 1405°C
No. 1	100		1.41
No. 2	20	1.45	1.48
No. 3	2.0	1.03	1.60
No. 4	0.20	1.55	1.44
No. 5	0.02	1.71	1.94

The weight percent Fe^{2+} for all the excess iron converted to magnetite is 2.81%. This was not exceeded in these experiments. A possible explanation is that temperatures higher than were used here are required to drive off enough oxygen to convert all the excess iron to magnetite. If this is the case, for this composition, the densification process can take place at a temperature further removed from the temperature at which substantial amounts of oxygen are driven off. This, in turn, makes the formation of Fe^{2+} an even slower process than in Composition 690. Keeping in mind that there will be a scatter of values due to variations in density from sample to sample, we must conclude that in this series of treatments, Composition 704 has failed to respond to different values of oxygen content in the furnace atmosphere out to 0.20% O_2.

Permeability and Fe^{2+} content. Although the sluggish response of the Fe^{2+} content of these ferrites has thus far prevented the preparation of magnetic test samples by a method that will give an accurately predicted value of Fe^{2+} content, some data relating magnetic properties and Fe^{2+} content have been collected. Seven samples of Composition 704 were selected (because of their high B values at H = 1 oersted with direct current) from seven separate firings. The differences between firings were trivial, consisting of small differences in soak temperature or soak time. The samples were analyzed for Fe^{2+} content for the purpose of determining whether or not this collection of superior samples occurred at any particular content of Fe^{2+}. Thus, results of these analyses are plotted against B values in Figure 18. They occupy a relatively narrow band of Fe^{2+} contents. The lowest B of the set lies at the low Fe^{2+} edge of the series. If there is a trend, it seems to be that the higher B values go with the higher Fe^{2+} values.

Domain Wall Relaxation and Dispersion

From Figures 2 through 13 above, it is seen that the effective large signal permeability for a given ferrite decreases with increasing frequency. This dispersion in the large signal permeability is due to domain wall relaxation.

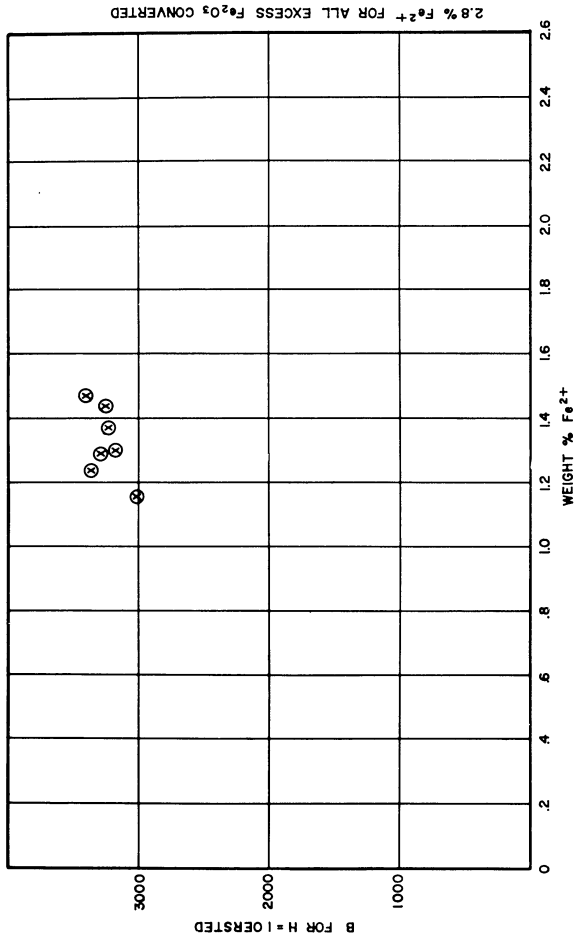

Figure 18. Composition 704. B for H = 1 Oersted vs. Fe^{2+} Content by Analysis

STAT

STAT

The domain wall relaxation phenomenon can be described as follows. When a core is being driven around a hysteresis loop and a condition of dynamic equilibrium has been achieved, the same pattern of domain wall creation and motion takes place during each cycle. Wall motion in a given direction must be accomplished during the time occupied by half of the cycle. At very low frequencies, the progress of a domain wall in sweeping out its assigned volume depends upon the magnitude of the magnetizing field effective in the volume occupied by the wall, and upon the "height" of the barriers currently impeding the motion of the wall. A wall once over a barrier moves to the next barrier in a time short compared with the time for half a cycle. In this situation, B reaches its maximum at the same time as H reaches its maximum.

At sufficiently high frequencies a different situation obtains. A wall once freed from a barrier may not advance to the next barrier in a time small compared with the time required for half a cycle. A wall may continue to move in the same direction after the value of H has passed through its maximum value. In this case, B reaches its maximum value after H has reached its maximum value and the hysteresis loop assumes an elliptical shape. When the frequency is so high that many walls fail to reach barriers for lack of time, the maximum value of B associated with a driving field of a given maximum value begins to decline. At sufficiently high frequencies, the walls may move practically not at all. Rotation of the magnetization of whole domains may in comparison with domain wall motion be the easier process for changing the direction of magnetization.

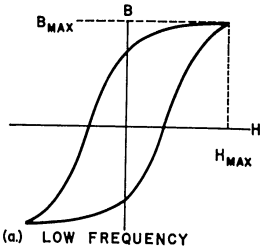

(a.) LOW FREQUENCY

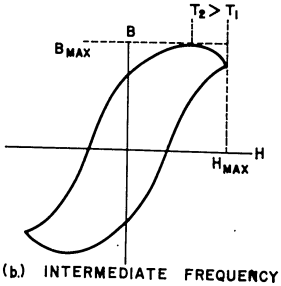

(b.) INTERMEDIATE FREQUENCY

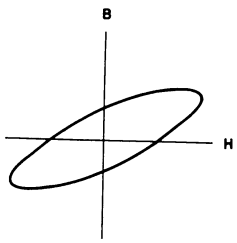

(c.) HIGH FREQUENCY

The situation is schematically represented in the accompanying set of diagrams. Diagram (a) corresponds to the low frequency case with B_{max} and H_{max} occurring at the same time.

In diagram (b) the frequency is intermediate, B_{max} occurs at a later time in comparison with H_{max} and some ellipticity in the loop has been introduced. At sufficiently high frequencies, diagram (c), the loop is essentially elliptical and the permeability is considerably reduced.

Additional experiments were performed to determine the dispersion of the large signal permeability in high temperature transformer ferrites. In these experiments, Compositions 704, 737, 730A, and 731 were used.

The test specimens were toroids of OD = 0.75 inch, ID = 0.50 inch, ht = 0.20 inch before firing.

In order to have the critical parts of the firing take place during the working day so that they could be observed, the following firing procedure was used: The samples were loaded in a tube furnace at the end of the day and the furnace temperature was programmed to arrive at 982°C at 8 a.m. During this rise, the samples were in flowing air. The gas or gas mixture to be used was then set flowing through the tube containing the samples. Since these compositions will precipitate a hematite second phase if cooled in oxygen or gases containing appreciable oxygen, it was necessary to switch to argon for atmosphere protection during the fall. However, if argon is admitted too soon, the ferrite is damaged. To minimize the danger, 0.01% oxygen mixture was used from 1100°C to 982°C and argon from 982°C to room temperature.

The rate of rise from 982°C to the soak was 123°C/hr, our maximum controlled rate, and the rate of fall after soak, 371°C/hr. These rates allowed the process to fit into a working day.

The magnetic evaluation had to be kept as brief as possible because of the large number of samples involved, nearly 100. For a first screening, measurements of B were made for two values of H, 0.7 oersteds and 1.4 oersteds. The B values were obtained at D.C. (ballistic galvanometer), 50 kc, and 1000 kc. Based on these data, ten samples were chosen which represented a wide variety of dispersion behavior. These were then measured in more detail between 50 kc and 1000 kc to determine the shapes of the dispersion curves.

Magnetic evaluation. An introduction to the dispersion of large signal permeability can best be obtained from the curves for the ten selected samples shown in Figure 19. These samples were measured carefully to determine the shapes of the curves between 50 kc and 1000 kc. The dashed

STAT

STAT

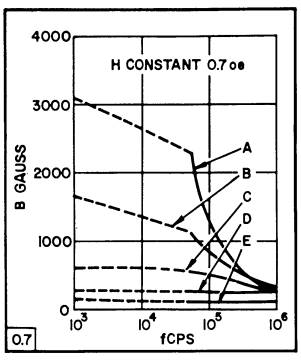

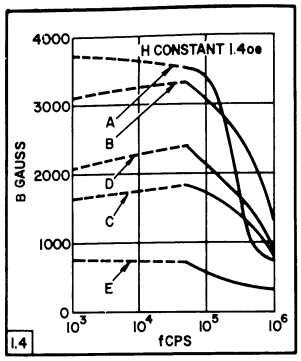

	COMP	FIRED	ATMOSPHERE
A	704	2730F 1HR.	100% O_2
B	704	2530F 3 HR.	0.2% O_2
C	704	2730F 1HR.	0.2% O_2
D	704	2430F 2 1/2HR.	0.2% O_2
E	704	2430F 2 1/2HR.	4.0% O_2

	COMP	FIRED	ATMOSPHERE
F	731	2730 1HR.	100%
G	731	2610 1HR.	100% O_2
H	730A	2530 3HR.	0.2% O_2
J	731	2530 3HR.	0.2% O_2
K	730	2610 2HR.	0.01% O_2

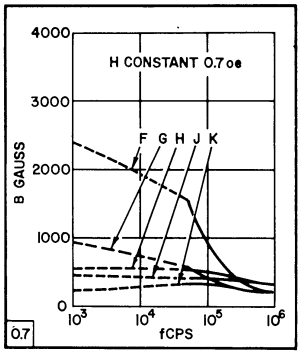

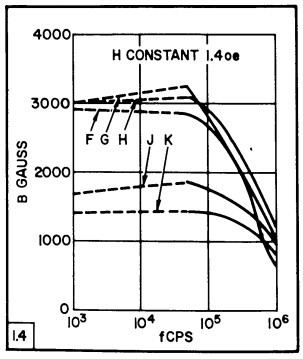

Figure 19. Typical Dispersion Curves at Two Values of H

part of each curve connects the 50 kc value to the D.C. value which has arbitrarily been placed at 1 kc. This is a way of indicating where the curve ultimaterly should terminate.

Composition numbers and firing conditions are shown on the figure.

There are some general features to be noted. When H = 0.7 oersteds, the curves are concave upward if B is greater than 1000 gauss at 50 kc. The curves have an inflection point after which they are concave downward if B is less than 1000 gauss at 50 kc.

When H = 1.4 oersteds, nine of the ten curves are concave downward at 50 kc, two curves, A and F, have inflection points. Curves A and F are examples in which a large part of the dispersion takes place between 50 kc and 1000 kc. The shapes of the other curves can be understood when it is realized that only portions of curves are seen the shapes of which are similar to those of A and F.

Examined from this point of view, the concave upward curves obtained at H = 0.7 oersteds are the "high frequency" part of dispersion curves. The concave downward curves obtained at H = 1.4 oersteds are the "low frequency" part of dispersion curves. The curves which have inflection points are exhibiting the middle frequencies of their dispersion curves.

These curves illustrate how the relaxation is shifted to higher frequencies when the driving field is increased. The steep part of the dispersion curve occurs at those frequencies which are beginning to allow insufficient time for a domain wall to sweep through the same volume that was traversed at lower frequencies. Within certain limits, increasing the driving field will increase the domain wall velocity and consequently move the steep part of the dispersion curve to higher frequencies.

Figures 20, 21, 22, 23 show additional results. Each figure presents data for samples fired in one atmosphere beginning with 100% oxygen in Figure 20, through 0.01% oxygen in Figure 23. The shapes of the dispersion curves have been assumed to be similar to those shown in Figure 19 and were obtained by joining the 50 kc and 1000 kc points with an appropriate curve chosen from Figure 19.

Consider the 50 kc properties first. The highest permeabilities are obtained by firing at the highest temperature, 1500°C in 100% oxygen. The individual compositions rate in the order of the amount of extra Fe_2O_3 they contain. Composition 704 contains the most excess Fe_2O_3. The peak in low frequency permeability shifts to lower firing temperatures as the oxygen content of the gas is decreased.

High permeability at 1000 kc is obtained most reliably by firing at the lower temperatures and low percent oxygen such as 1390°C in 0.2% oxygen or 1330°C in 0.01% oxygen.

STAT

STAT

Dispersion curves were extended to lower frequencies for samples of Compositions 704 and 730A. The entire set of characteristic curves for these specimens are shown in Figures 24 and 25. From these results, it is seen that the relaxation frequency associated with Composition 730A is greater than that for Composition 702. The high relaxation frequency of Composition 730A accounts for the superior behavior at 1000 kc of this material over Composition 704 with respect to permeability.

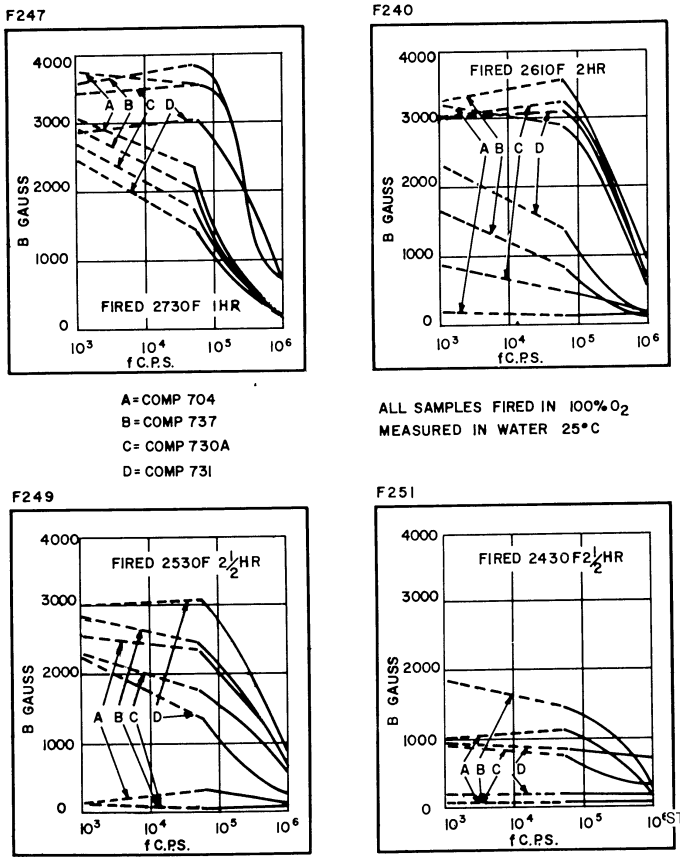

Figure 20. Dispersion Curves at H 0.7 Oersteds and H = 1.4 Oersteds

STAT

F-242

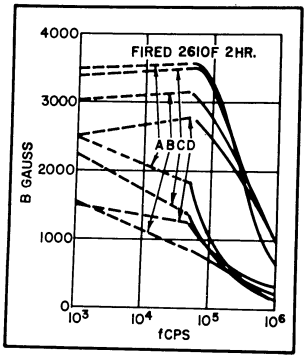

A= COMP. 704
B= COMP. 737
C= COMP. 730A
D= COMP. 731

ALL SAMPLE FIRED IN 4% O_2
AT TEMPERATURES INDICATED
MEASURED IN WATER 25°C

F-253

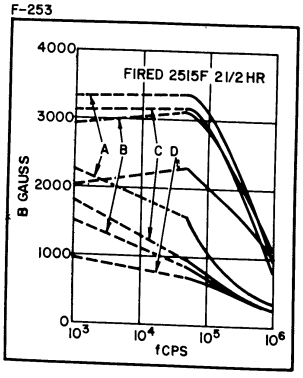

F-249

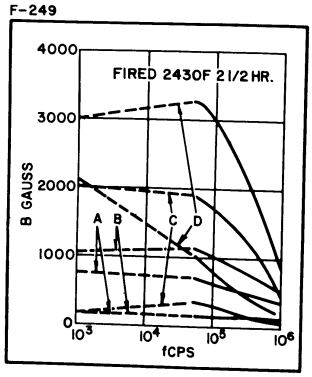

Figure 21. Dispersion Curves at H = 0.7 Oersteds and H = 1.4 Oersteds

F-248

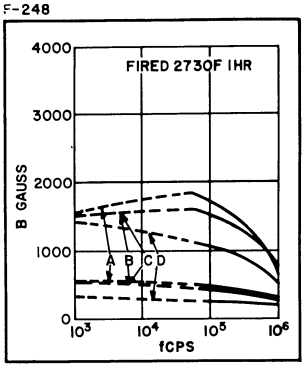

A = COMP. 704
B = COMP. 737
C = COMP. 730A
D = COMP. 731

F-241

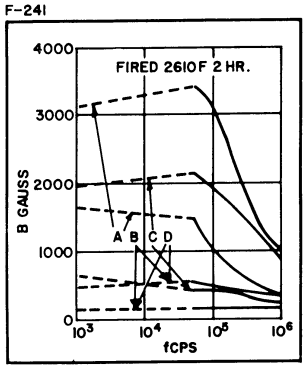

ALL SAMPLES FIRED IN 0.2% O
MEASURED IN WATER 25°C

F-245

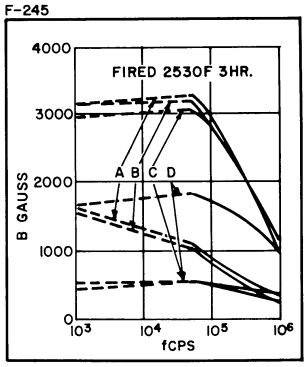

F-250

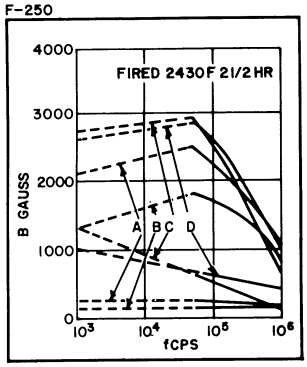

Figure 22. Dispersion Curves at H = 0.7 Oersteds and H = 1.4 Oersteds

STAT
STAT

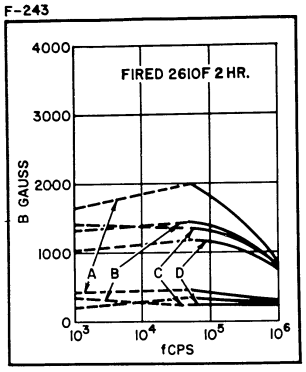

A = COMP. 704
B = COMP. 737
C = COMP. 730A
D = COMP. 731

ALL SAMPLES FIRED IN 0.01% O_2
MEASURED IN WATER 25°C

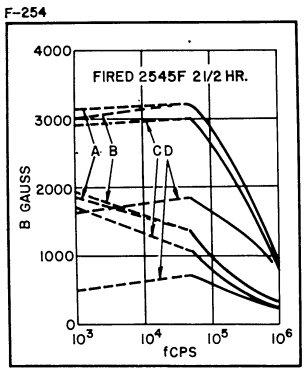

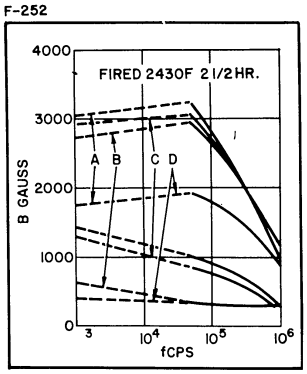

Figure 23. Dispersion Curves at H = 0.7 Oersteds and H = 1.4 Oersteds

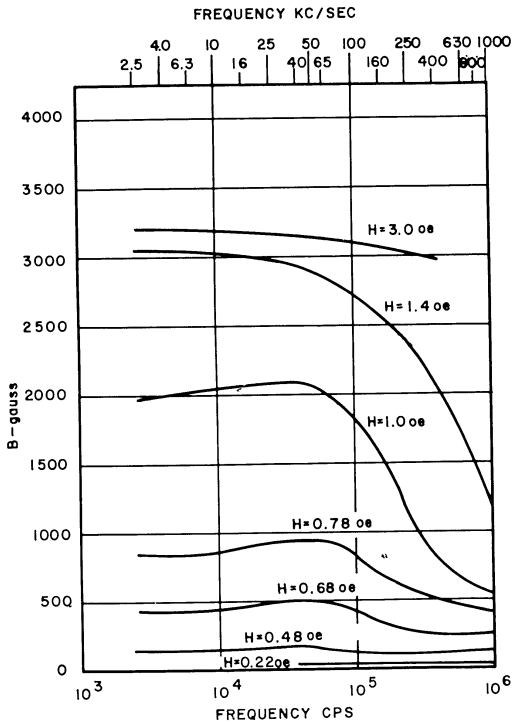

Figure 24. Dispersion Curves for Toroid 704 F 158-1SB in Water at 25°C

STAT

STAT

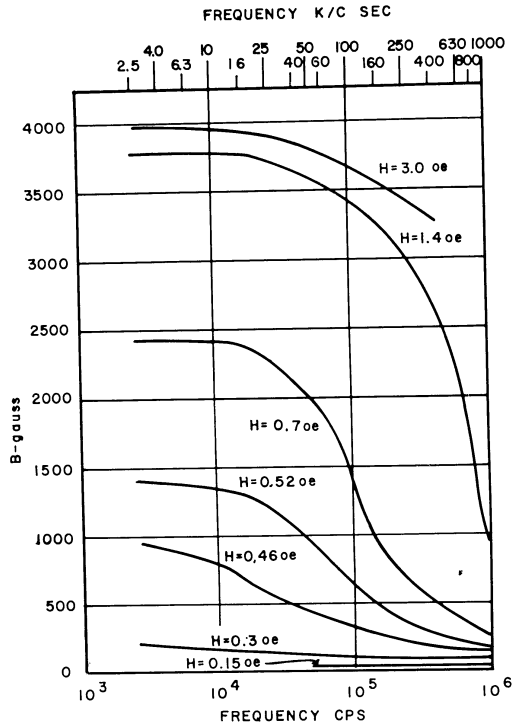

Figure 25. Dispersion Curves for Toroid 730A F 245-1 in Water at 25°C

Conclusions and Recommendations

The utility of a high temperature transformer ferrite depends upon its intended application. The magnetization curves given in the body of the text may be considered as characteristics for design use. However, from the point of view of large signal permeability definite recommendations can be made as a result of the investigations carried out during the period covered by this report.

For operation at frequencies up to 200 kc in an ambient temperature range -65°C to +250°C, Composition 704 is recommended for high large signal permeability. The proper firing schedule is 1480°C for 2 hours in 100% oxygen. This material must be cooled in a protective atmosphere such as argon.

For operation at frequencies between 200 kc and 1000 kc in an ambient temperature range -65°C to +250°C, Composition 731 is recommended for high large signal permeability. The characteristics of Composition 731 are similar to those of Composition 730A but are more reproducible. The proper firing schedule is 1370°C for 3 hours in 0.2% oxygen, and cooled in the same atmosphere.

A measure of the large signal permeability can be obtained by considering the flux in the core when the driving field is 1.0 oersted. Thus, below 200 kc the permeability of Composition 704 lies between 3000 and 1500, the decrease occurring monotonically with frequency. For frequencies between 200 kc and 1000 kc, the large signal permeability of Composition 731 varies between 1500 and 600.

It is also recommended that work in this area of ferrite materials development be terminated until the present materials are evaluated in a specific application. After this evaluation, further effort may be fruitful in tailoring specific properties to the needs of a given device.

STAT

STAT

SECTION III

MATERIALS FOR LOW SIGNAL APPLICATIONS

Objective

The objective of this work is to produce ferrite materials having a high μQ product and low temperature coefficient of permeability. It is desired that the characteristics of developmental samples be relatively unaffected by prolonged exposure to high humidity, and suitable for operation over the temperature range -65°C to +250°C.

Approach

The approach taken in this effort is to determine the processing conditions and compositions necessary to yield the above combination of properties. It is well known that for a given composition, specimens fired at low temperature and for short times (low heat work) generally exhibit lower loss than samples fired at high temperature for long times (high heat work). Typical data showing this trend are given in Table III. All aspects of the preparation and treatment of the samples listed in Table III were equivalent except the final firing. It should be stressed that the aspect of preparation concerned with here is that of firing temperature and time. The comparison in Table III is given only to illustrate that particular processing parameter. It should not be inferred that this is the only parameter which controls the low loss characteristics in low signal materials. Pressing pressure, particle size, heating and cooling rates, and specific composition, as well as the effects of impurities and additives strongly influence the ultimate low loss characteristics.

TABLE III

EFFECT OF FIRING TIME AND TEMPERATURE ON MAGNETIC Q.
COMPOSITION: 48 MOL% Fe_2O_3, 25 MOL% ZnO, 26.5 MOL% NiO, 0.5 MOL% V_2O_5.

Sintering Temp.	Sintering Time	Q at 1 mc	Q at 4 mc
1139°C	30 min.	60	47
1266	240 min.	21	5

The firing cycle should be such as to discourage the formation of ferrous iron as this is known to reduce the resistivity in ferrites giving rise to appreciable eddy current losses at high frequencies.

The nickel zinc ferrites with small additions of vanadium pentoxide present a promising system in which to work. Nickel zinc ferrites have been studied extensively and processing variations permit a wide latitude of properties.

Compositions of interest to this study must contain less than 18 mol% ZnO in order that the Curie temperature be sufficiently high (above 350°C). The temperature coefficient of initial permeability then can be expected to remain low up to 250°C. The temperature coefficient generally increases strongly in the neighborhood of the Curie temperature.

Ferrite Compositions

The range of compositions investigated during the phase covered by this report is given in Table IV.

TABLE IV

DESCRIPTION OF FERRITE COMPOSITIONS
FOR LOW SIGNAL APPLICATIONS

Comp. No.	Mol% Fe_2O_3	Mol% NiO	Mol% ZnO	Mol% V_2O_5	NiO/ZnO
67	50.0	34.5	15.0	0.5	2.30
69	56.0	28.5	15.0	0.5	1.90
73	48.0	36.5	15.0	0.5	2.43
75	50.0	32.4	17.1	0.5	1.90
76	48.0	33.7	17.8	0.5	1.90
77	49.9	34.4	15.0	0.7	2.30
78	49.9	32.3	17.1	0.7	1.90
79	47.9	33.6	17.8	0.7	1.90
80	55.9	28.4	15.0	0.7	1.90
81	50.1	32.5	17.1	0.3	1.90
82	48.1	33.8	17.8	0.3	1.90
83	56.1	28.6	15.0	0.3	1.90
84	49.7	32.6	17.1	0.5	1.90
85	49.5	32.8	17.2	0.5	1.90
86	50.1	34.6	15.0	0.3	2.30
285	50.0	42.0	7.5	0.5	5.60

STAT
STAT

Of the compositions listed in Table IV, three were shown to be of particular interest, Compositions 67, 84, and 285. The low signal properties of these materials are such to cover a range of initial permeability from 12 to 120, exhibit low loss, and possess a low temperature coefficient of permeability over the temperature interval -65°C to +250°C. Also, these low signal properties are not affected by prolonged exposure to high humidity.

Standard ceramic fabrication procedures have been followed in the processing of these compositions. Usual practice has been to weigh out approximately 1 kg total batch on a large (2 kg) analytical balance. The resultant mixture is ball milled overnight for about 16 hours in a one gallon iron mill with steel balls, in the presence of about 1 1/2 liter deionized water. This process both mixes and grinds. The slurry is then placed in glass drying pans and brought to dryness in standard ovens. The next step in the process is to run the dried powder through a pulverizer for sizing.

Binder is added as 8% by weight Hyform emulsion containing 30% wax. The resulting slurry is again ball-milled for 15 hours, after which it is dried at a low temperature (less than 60°C). The cake is then broken and pelletized through a 60 mesh sieve.

Some initial experiments included the preparation of Composition 285 in pellet sizes: (a) -20, material retained on No. 20 sieve; (b) 20-40, material passing No. 20 sieve retained on No. 40 sieve; (c) +20, all material passing No. 20 sieve; (d) +80, all material passing No. 80 sieve. The results of these early evaluations indicated that small pellets yield a greater densification and better quality ceramic when fired at low temperature and short time. Thus, the procedure was standardized using the 60 mesh sieve. (60 mesh pellets are easier to handle than 80 mesh and this sorting is preferred from a manufacturing point of view.)

Results of Magnetic Evaluation

The primary results of magnetic evaluation of the various compositions of interest are given below.

Humidity effects. Under proper conditions a saturated solution of lead nitrate will maintain a relative humidity of 98% at 20°C in a closed chamber. Wound toroids of Composition 67, 84, and 285 were placed in this environment for 350 hours (approximately 15 days) and measurements of permeability and Q were made at intervals at a frequency of 1.5 mc.

Data for Compositions 67 and 84 are given in Table V. For Composition 285 the sample used had a permeability of 14 which remained constant over the entire time interval. The intrinsic loss in the 285 sample was so low that after the correction for wire loss was made the associated Q values were infinite within the limits of experimental error. This was the case for measurements made over the entire time interval of 350 hours. As a result, the data for composition 285 are not given in Table V.

Although Q values appear somewhat erratic, it is safe to conclude that if loss increases with exposure to high humidity, Q decreases no more than 10% over the period considered here. It is seen from Table V that permeabilities remain constant.

TABLE V

EFFECT OF HIGH HUMIDITY ON μ_o AND Q
FOR COMPOSITIONS 67 AND 84
(RELATIVE HUMIDITY - 98%)

Comp.	Firing	Time	μ_o	Q
67	1100°C-10 min.	0 hrs.	75	240
	Pereny furnace	25	75	255
		75	75	208
		170	75	240
		350	75	223
84	1152°C-11 min.	0	125	221
	Pereny furnace	25	125	278
		75	125	178
		170	125	212
		350	125	205

In addition to the results presented in Table V, further measurements were made on a selected toroid of Composition 84 (toroid 84.11). Determination of permeability and Q were made over a period of 215 hours. The lata are presented in Table VI.

The results obtained here are essentially the same as observed previously. The permeability is unaffected by prolonged exposure and a slight increase in loss is observed with increasing time of exposure. Apparently, the entire decrease in Q, about 10%, takes place during the first 120 hours.

STAT
STAT

TABLE VI

EFFECT OF HIGH HUMIDITY ON
PERMEABILITY AND Q OF TOROID 84.11

Time	μo	Q	Temp.
0 hours	110	235	24°C
1	110	235	24
20	110	223	24
45	110	225	24
120	110	220	25
140	110	218	24
170	110	218	26
190	110	223	25
215	110	220	23

Permeability, Q, and μQ product. In Figures 26 through 30 permeability, magnetic Q and the μQ product as functions of temperature are shown for several samples. The measurements were made at a frequency of 1.5 mc.

Table VII below lists the toroids for which the data in Figures 26 through 30 were obtained.

TABLE VII

DESCRIPTION OF COMPOSITIONS

Comp. No.	Toroid No.	Heat Treatment
67	67.24	uncalcined Fired 1100°C - 20 min.
67	67.52	calcined (750°C - 3 hrs.) Fired 1100°C - 15 min.
67	67.54	uncalcined Fired 1100°C - 15 min.
84	84.7	uncalcined Fired 1050°C - 10 min.
84	84.11	uncalcined Fired 1152°C - 11 min.

From Figure 26, it can be seen that the major effect of calcination is to increase significantly the temperature coefficient of initial permeability.

Figures 27 and 28 give the results for selected samples of Composition 67 which has a larger NiO/ZnO ratio than Composition 84. The data for Composition 84 are given in Figures 29 and 30.

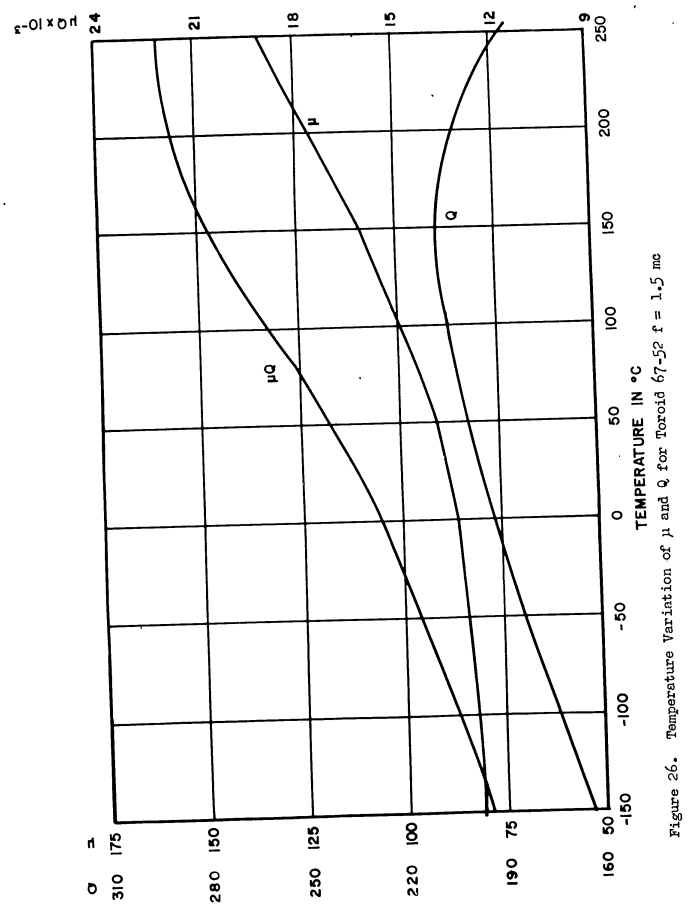

Figure 26. Temperature Variation of μ and Q for Toroid 67-52 f = 1.5 mc

STAT

STAT

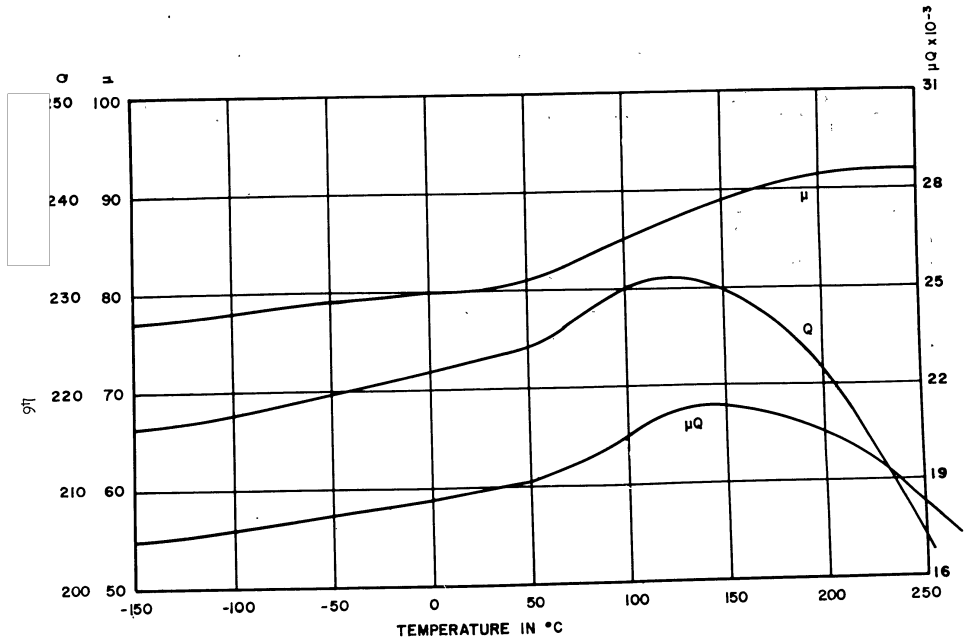

Figure 27. Temperature Variation of μ and Q for Toroid 67.24 f = 1.5 mc

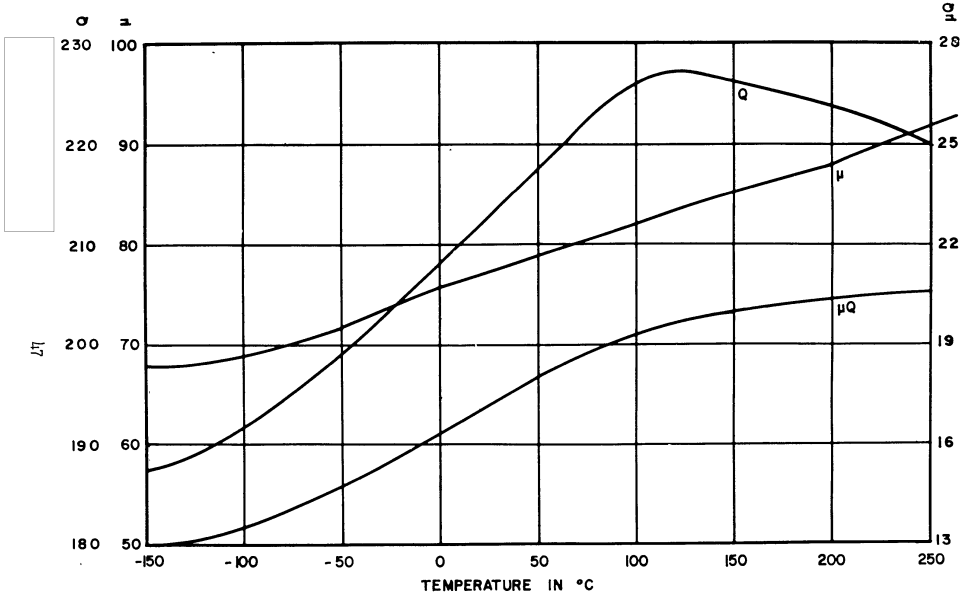

Figure 28. Temperature Variation of μ and Q for Toroid 67.54 f = 1.5 mc

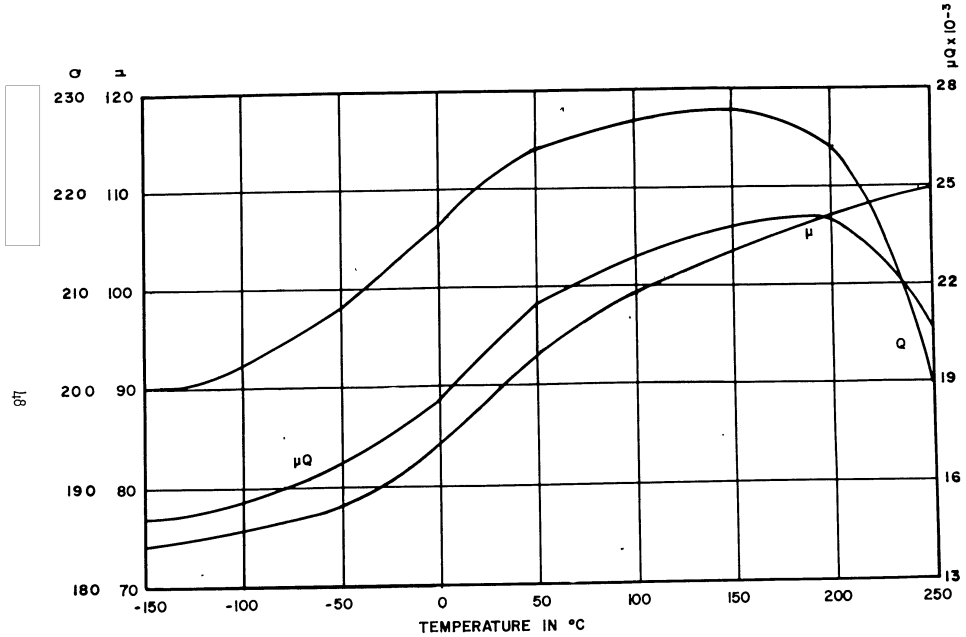

Figure 29. Temperature Variation of μ and Q for Toroid 84.7 f = 1.5 mc

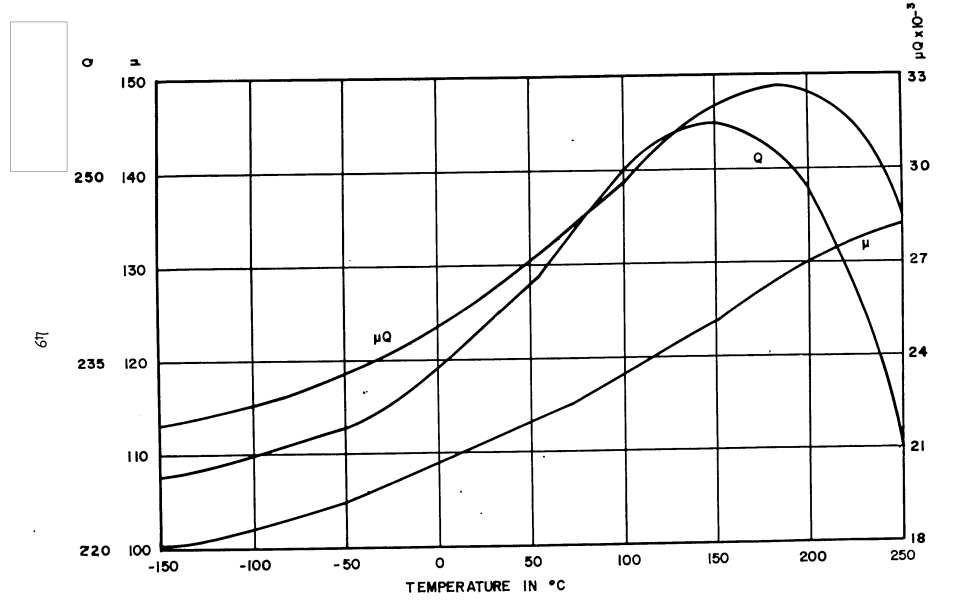

Figure 30. Temperature Variation of μ and Q for Toroid 84.11 f = 1.5 mc

STAT
STAT

Declassified in Part - Sanitized Copy Approved for Release @ 50-Yr 2014/02/05 : CIA-RDP81-01043R002800240003-8

It is well known that the measured values of permeability and Q depend upon the amplitude of the driving signal. The true low signal values of these parameters are obtained by extrapolating the measured values to zero field. Figure 31 shows the results obtained for a selected sample of Composition 84. In Figure 31, μ_o and Q are shown as functions of driving field, and it is clear that these parameters are essentially independent of drive over the range considered. The constancy of Q indicates a very low value of hysteresis coefficient for this material.

A General Radio Twin-T bridge was used to obtain the spectrum of the low signal parameters over the frequency range 1 to 30 mc. Seven test bodies were examined, six of Composition 84 and one of Composition 285. Table VIII gives the data on the firing of these samples.

Figure 32 shows Q as a function of frequency for the seven samples referred to above. From Figure 32, it is seen that the Q of Composition 285 (Sample 7) is considerably higher than that for Composition 84 (Samples 1-6) at frequencies above 10 mc. Of course, the initial permeability of Sample 7 is only about 1/2 to 1/3 that of the Composition 84 bodies.

Figure 33 shows the frequency response of μ_o for Sample 3. In this material, μ_o is approximately independent of frequency over the investigated range. For Composition 285, μ_o increases slightly with increasing frequency to 30 mc.

Figure 34 shows the μQ product as a function of frequency for Composition 84 and 285. Again, it is seen that Composition 285 holds up better at high frequencies, but this material has a lower μQ product than Composition 84 below 7 mc.

TABLE VIII

PROCESSING OF TEST BODIES FOR LOW SIGNAL APPLICATIONS

Sample No.	Comp.	Brand of iron oxide	Soak temp.	Soak time	Rise rate	Ramming pressure
1	84	Baker	1105°C	20 min.	575°C/hr.	14,700 psi
2	84	Map. 110-2	1105	20	575	18,800
3	84	Baker	1056	20	1300	14,700
4	84	Baker	1100	20	slow	14,700
5	84	Map. 110-2	1100	20	200	4,200
6	84	Map. 477	1055	20	1300	14,700
7	285	Baker	1154	20	580	14,700

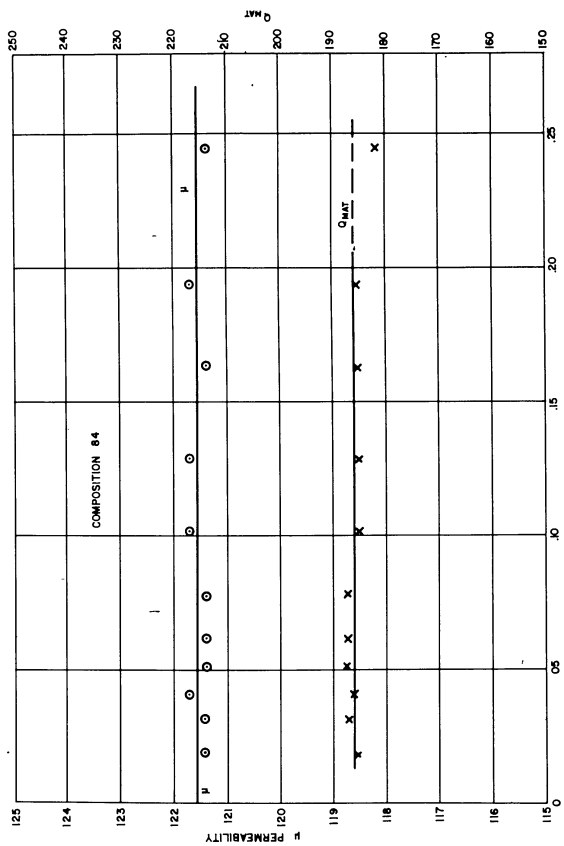

Figure 31. Dependence of Permeability and Material Q on Driving Field

STATT

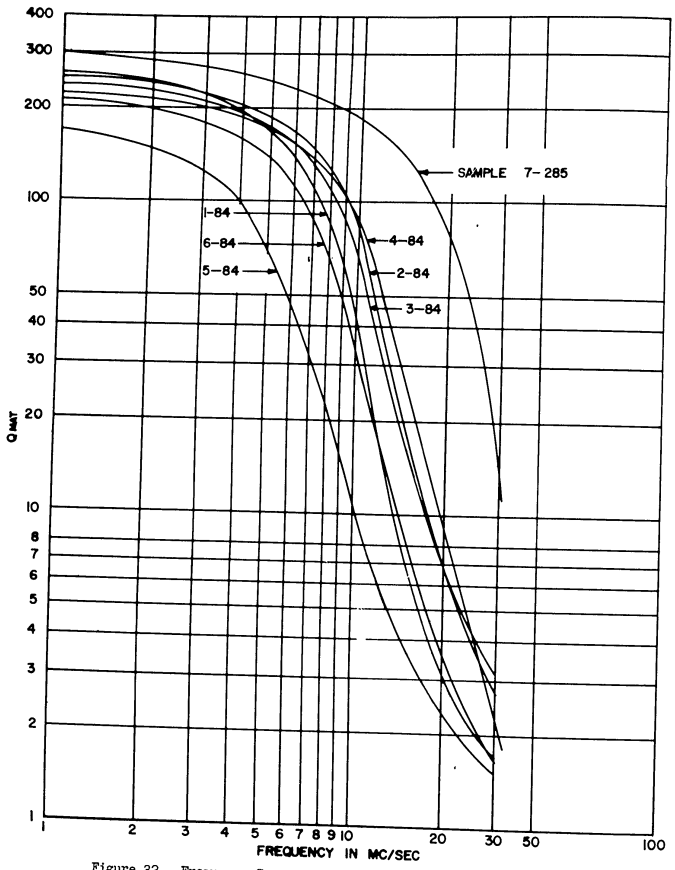

Figure 32. Frequency Spectrum of Q_{mat} for Selected Samples

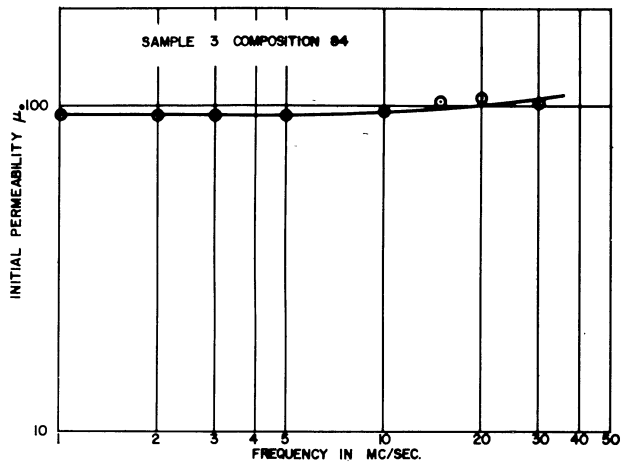

Figure 33. Frequency Spectrum of Initial Permeability

STAT

STAT

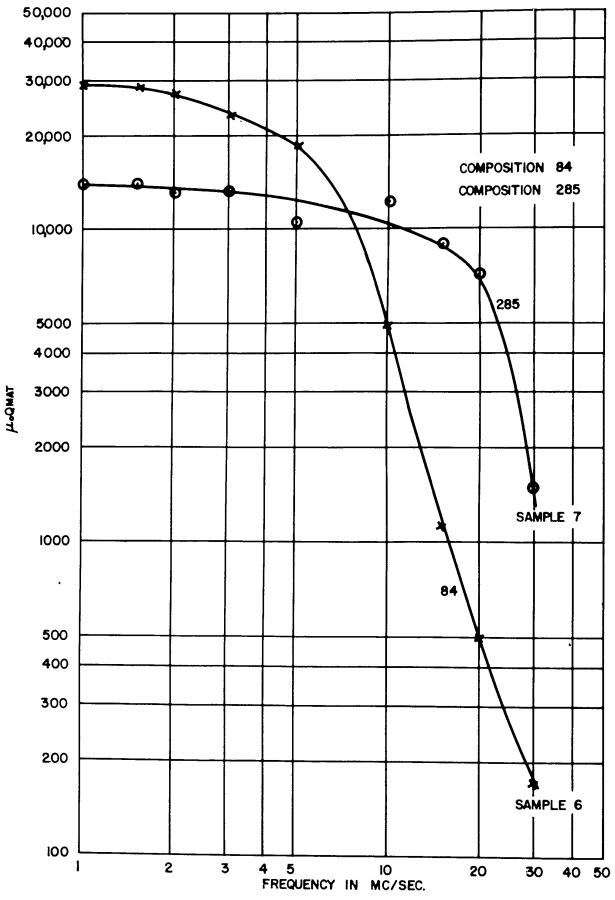

Figure 34. Frequency Spectrum of $\mu_o Q_{mat}$ for Two Selected Samples

Processing of Low Loss, Low Signal Ferrites

Below the results are given for a series of investigations designed to determine the effects of various processing techniques on the low signal properties of the ferrites of interest in the present development. These include the effects of calcine, the addition of V_2O_5, the effects observed when compositions are prepared using different sources of Fe_2O_3, the effects of rise rate, the effects of ramming pressure, and the effects of oxygen firing.

Effect of calcine. In the preparation of ferrites for low signal applications, the general practice is to press samples for firing using raw oxides rather than calcined material. It is known that bodies prepared from pre-reacted powder of a given composition will generally exhibit higher loss and permeability than bodies fired from raw oxides, particularly for low heat work. However, an optimum may exist for the μQ product in considering the competition between the increase in μ and the decrease in Q. Composition 67 was chosen for the calcination experiments.

Composition 67 was calcined for three hours in oxygen at various temperatures in a tube furnace. Toroids were then pressed in the usual manner with the exception that no binder was used. After firing for 10 minutes at 1100°C, permeability, Q and shrinkage were measured. Data are given in Figure 35 and Table IX. It is evident that calcination at 650°C gives the highest μQ product among the temperatures tried. A temperature of about 900°C appears to be a critical one for this composition. The data given in Table IX for the 900°C calcine include measurements made on samples prepared from powder located at different positions in the furnace during calcine.

TABLE IX

EFFECT OF CALCINATION TEMPERATURE ON SHRINKAGE, μ_o, AND Q
TOROIDS FIRED AT 1100°C FOR 10 MINUTES

Calcine Temp.	% Shrinkage	μ_o	Q at 1.5 mc	$\mu_o Q$
Uncalcined	14.5	84.0	256.	21,500
650°C	18.7	106.	240.	25,400
750°C	17.4	107.	225.	24,100
870°C	16.9	113.	200.	22,600
"900°C"-front portion	14.7	108.	131.	14,200
"900°C"-center portion	5.7	81.7	162.	13,300
"900°C"-end portion	3.6	88.8	138.	12,200

STAT

STAT

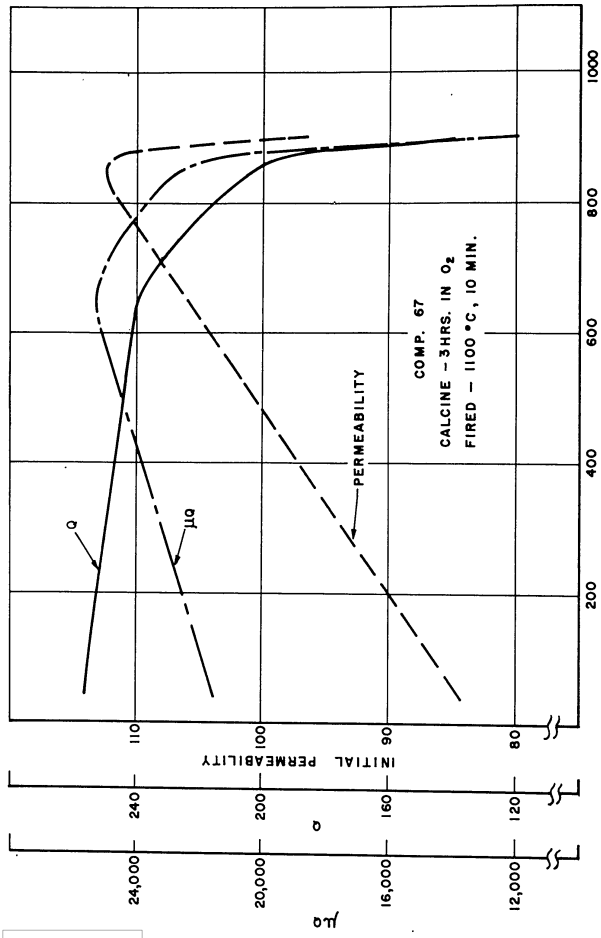

Figure 25. Initial Permeability, Q, and μQ vs. Calcine Temperature for Composition 67

Even though the expected optimum was observed for the μQ product (650°C calcine), further measurements, Figure 26, showed that the temperature coefficient of permeability was increased significantly as a result of the calcine. Thus, no calcination was included in subsequent body preparation.

Addition of V_2O_5. The primary effect of introducing vanadium pentoxide in small quantities, less than 1.0 mol%, is to increase shrinkage during firing. Thus for a given low heat work cycle the presence of V_2O_5 allows an increase in ceramic curing over that which would be experienced when this additive is omitted. Though conclusive evidence is lacking, it is felt that the favorable results obtained under exposure to high humidity for materials prepared using V_2O_5 is attributable to the inclusion of this additive.

Illustrative data which indicate the primary effect of V_2O_5 addition are shown in Table X.

TABLE X

EFFECT OF 0.5 MOL% VANADIUM PENTOXIDE FOR 10 MINUTE FIRING AT 1100°C

Comp.	Description	% Shrinkage	μ_o	Q at 1.5 mc
67	50 Mol% Fe_2O_3 with V_2O_5	14.4	76.	250.
68	50 Mol% Fe_2O_3; V_2O_5 omitted	4.7	15.	High
69	Excess Fe_2O_3 with V_2O_5	17.1	125.	90.
70	Excess Fe_2O_3; V_2O_5 omitted	8.1	23.	160.

Comparison of different brands of iron oxide. It has been pointed out that low signal ferrite materials are fabricated using a heat treatment cycle that includes short time firing at relatively low temperature. Thus the impurity content of the various commercial iron oxides can alter the ceramic curing rate for bodies which are only partially sintered. As a result, sample preparation and evaluation has been carried out utilizing several brands of iron oxide.

Only Composition 84 was used to evaluate the effects arising from the use of different sources of iron oxide. Results are given in Tables XI, XII, and XIII. Close study of Table XI shows, first, that the brand of ferric oxide consistently makes a great difference in permeability and Q. The highest Q is consistently obtained using the C.P. ferric oxide of the J. T. Baker Co. In general, Columbian Carbon Co. High Purity produces the highest μ; however, for this work, we are primarily interested in a high μQ product, and this brand does not give as high a product as the others.

STAT

STAT

It is also clear from Table XI that the rise rate upon heating is of more importance than the actual soak temperature. Note that the sets in Table XI are arranged according to increasing rise rates toward the bottom, and the Q for a particular brand follows the trend of increasing rates. No such agreement with sintering temperature is found.

Table XII presents somewhat similar results for a repeat study. All firings were made at the same temperature for 20 minutes. Table XII also shows the effect of cooling rate.

As before, J. T. Baker iron oxide is the preferred one for high Q properties, although Mapico 110-2 is also very good, and available in commercial quantities. Columbian Carbon Co. H.P. and C.K. Williams 5098 are somewhat equivalent showing higher permeability and lower Q. But, for this type of firing the Columbian Carbon Co. H.P. iron oxide shows consistently higher initial permeability than any of the others.

This study (Table XII) also shows the same increase in Q at higher rise rates, the sintering temperature being held constant. No clear trend in permeability is evident.

Table XII also presents the results of a simple experiment to determine the effect of cooling rate. Although this suffers from insufficient data due to broken cores, the data show a general increase in permeability for the slower furnace cooled samples. Q does not show a clear trend.

In Table XIII, the effects of pressure on μ_o and Q are given. All samples were fired for 20 minutes at the soak temperature, but the tempera tures measured with an optical pyrometer did not turn out exactly the same. Results are inconclusive. The μQ product does appear to peak at 12,500 psi, but the effect is not large. The effect upon Q is even less clear although one is tempted to see a trend toward higher Q at lower pressure.

Effects of rise rate. Some information on the effects of rise rate on the low signal properties were reported above. This work was extended to cover a wider range of rise rate variable. The results are shown in Figure 36 and Table XIV. Here again, an increase in μQ product is realized as the rise rate increases, but only up to a point -- about 700°C/hr. The improvement is realized almost entirely through increase in Q. This can readily be seen by inspection of Table XIV.

Pressure studies. **Table XIII gives the results obtained from ramming** pressure experiments made on bodies prepared from Mapico 110-2 and J.T. Baker ferric oxides. These experiments were extended and the results shown in Figures 37 and 38.

In Figure 37, initial permeabilities and the μQ products are presented for samples made with J.T. Baker and Mapico 110-2 ferric oxide. The effect of increasing pressure shows up differently for samples made with the different iron oxides. Samples made with Mapico 110-2 iron oxide increase in permeability and μQ product with increasing pressure, while those made with J.T. Baker do exactly the opposite. Thus, no generalization can be made on the effect of pressure except that a series of experiments may be required to find the optimum.

TABLE XI

MAGNETIC PROPERTIES OF COMPOSITION NO. 84 PREPARED WITH DIFFERENT IRON OXIDES (3/4 IN. TOROIDS PRESSED 8000 PSI, ALL FIRING TIMES 20 MINUTES)

Brand of Fe_2O_3	Sint. Temp.	Rise Rate	μ (1.5mc)	Q (1.5mc)	μQ
Columbian Carbon Co. H.P.	1150°C	200°C/Hr.	191	48	9200
Mapico 110-2	"	"	152	47	7200
J. T. Baker C.P.	"	"	120	120	14400
Columbian Carbon Co. H.P.	1090°C	300°C/Hr.	180	57	10300
Mapico 110-2	"	"	133	72	9600
J. T. Baker, C.P.	"	"	92	214	19700
Columbian Carbon Co. H.P.	1050°C	300°C/Hr.	180	75	13500
Mapico 110-2	"	"	123	115	14100
J. T. Baker, C.P.	"	"	96	266	25400
Columbian Carbon Co. H.P.	1115°C	400°C/Hr.	198	73	14500
Mapico 110-2	"	"	114	125	14200
J. T. Baker, C.P.	"	"	93	215	20000
Columbian Carbon Co. H.P.	1100°C	625°C/Hr.	160	75	12000
Mapico 110-2	"	"	115	337	39000
J. T. Baker, C.P.	"	"	112	347	39000

TABLE XII

COMPARISON OF BRANDS AND EFFECTS OF HEATING AND COOLING RATES ON COMPOSITION NO. 84 TOROIDS PRESSED AT 4200 PSI AND FIRED 1100°C - 20 MIN.

IRON OXIDE	RISE RATE	COOLING RATE	μ_o (1.5 mc)	Q_m (1.5 mc)	μQ
Col. Carb. H.P.	100°C/Hr.	Quench 3 min.	158	75	11900
Mapico 110-2	"	" " "	122	65	7900
Baker C.P.	"	" " "	79	340	26800
CKW No. 5098	"	" " "	150	41	6200
Col. Carb. N.P.	100°C/Hr.	Furnace Cool	165	63	10400
Mapico 110-2	"	" "	176	92	16200
Baker C.P.	"	" "	109	262	28600
CKW No. 5098	"	" "			Cracked
Col. Carb. H.P.	200°C/Hr.	Quench 3 min.	178	79	14100
Mapico 110-2	"	" " "	110	98	10800
Baker CP	"	" " "	86	325	28000
CKW No. 5098	"	" " "	173	40	6900
Col. Carb. H.P.	200°C/Hr.	Furnace Cool	178	87	15500
Mapico 110-2	"	" "	193	305	40500
Baker CP	"	" "			Broken
CKW No. 5098	"	" "			Broken
Col. Carb. H.P.	350°C/Hr.	Quench 3 min.	144	194	28000
Mapico 110-2	"	" " "	82	455	37300
Baker CP	"	" " "	74	436	32200
CKW No. 5098	"	" " "	111	148	16400
Col. Carb. H.P.	350°C/Hr.	Furnace Cool	113	8	
Mapico 110-2	"	" "	152	18	
Baker CP	"	" "	97	230	22300
CKW No. 5098	"	" "	107	172	18400

Col. Carb. H.P. = Columbian Carbon Co. High Purity

TABLE XIII

EFFECT OF RAMMING PRESSURE ON μ_o AND Q

Pres lb/in	Sint. Temp.	Sint. Time	Rise Rate	μ 1.5 mc	Q 1.5 mc	μQ
		Mapico 110-2 Ferric Oxide				
4700	1059°C	20 min.	350°C/Hr.	40	253	10100
6300	1059	20 min.	350°C/Hr.	39	261	10200
9400	1074	20 min.	350°C/Hr.	51	292	14900
12500	1074	20 min.	350°C/Hr.	50	286	14300
		J. T. Baker Ferric Oxide				
4700	1053°C	20 min.	350°C/Hr.	73	317	23000
6300	1053	20 min.	350°C/Hr.	79	315	24900
9400	1068	20 min.	350°C/Hr.	71	378	26800
12500	1069	20 min.	350°C/Hr.	77	305	23500
14700	1069	20 min.	350°C/Hr.	81	300	24300

TABLE XIV

EFFECT OF RISE RATES ON μ_o AND Q

ALL SAMPLES PREPARED WITH MAPICO 477 IRON OXIDE
1 1/8 IN TOROIDS PRESSED AT 14700 PSI
ALL MEASURED AT 1.5 MC - G.R. TWIN-T BRIDGE

Rise °C/Hr.	(Opt. Pyr.)	μ_o	Q_{mat}	μQ
100	1048°C	204	26	5300
200	1051	139	88	12200
300	1049	111	107	11900
400	- - Cracked - -			
500	1057	144	183	26300
600	1057	138	189	26100
700	1056	149	211	31400
1000	1054	154	207	30000
1300	1055	132	255	33600
1700	1057	147	205	30200

STAT

STAT

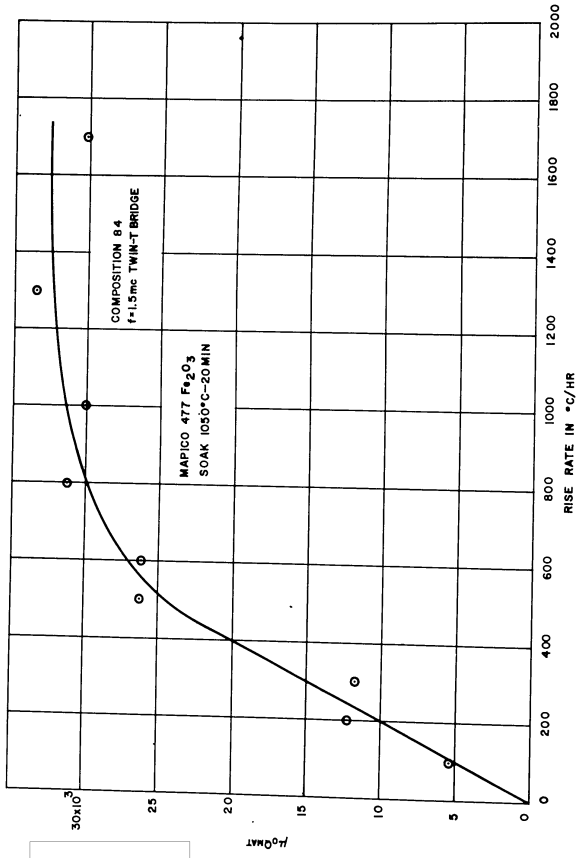

Figure 36. $\mu_o Q_{mat}$ vs. Rise Rate

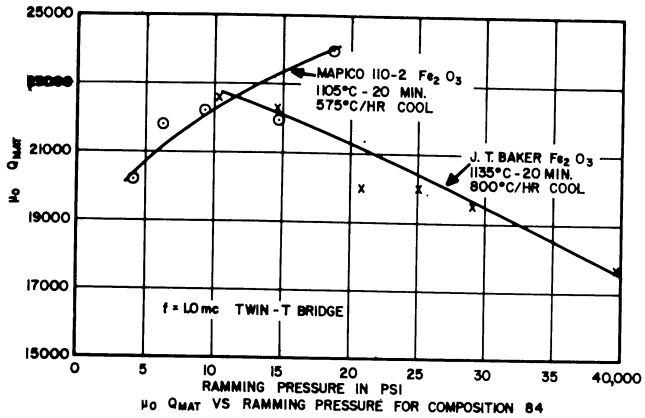

$\mu_o Q_{MAT}$ VS RAMMING PRESSURE FOR COMPOSITION 84

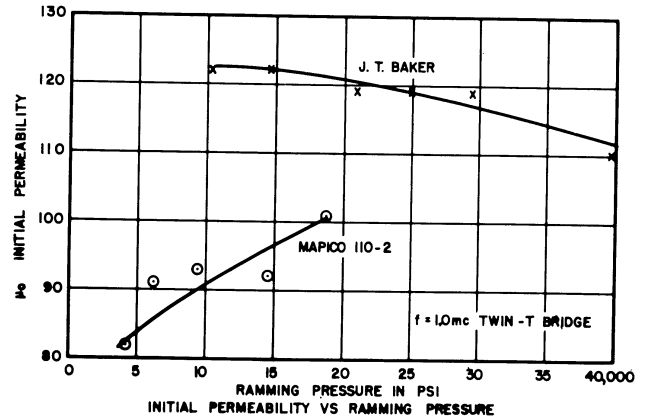

INITIAL PERMEABILITY VS RAMMING PRESSURE

Figure 37. μQ and μ vs. Ramming Pressure for Composition 84

STAT

STAT

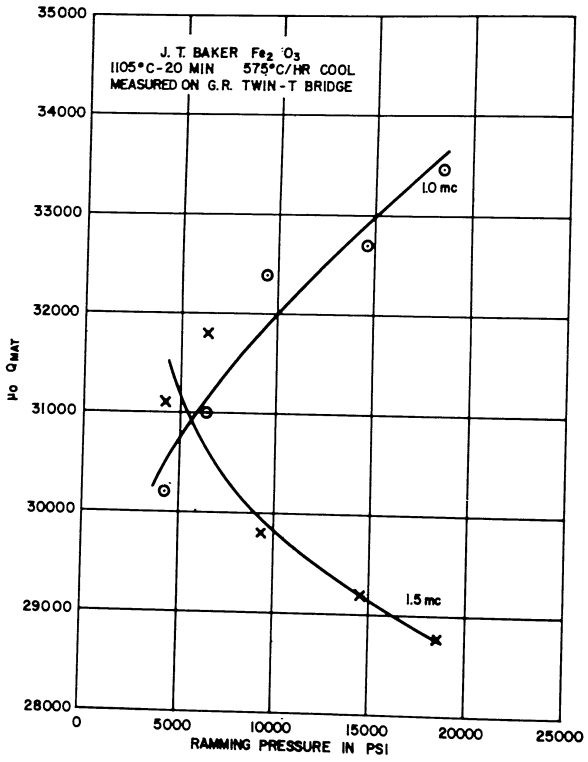

Figure 38. μQ vs. Ramming Pressure for Composition 84

Somewhat more interesting results are presented in Figure 38 where the μQ products at different pressures are given, but at two different frequencies. These curves indicate that higher μQ products at higher frequencies should be obtained by lower ramming pressures.

Atmosphere firings. As part of the development program on Composition 84, a comparison series of samples was fired, two toroids at a time in a double tube furnace, one sample in air, the other in pure oxygen. Hence, rise rates and soak times were identical, and soak temperatures also were very nearly the same. The air and oxygen were supplied as a steady stream to each tube at 2 liters/min throughout rise, soak and fall.

In all, twenty-four comparison firings were made and the test toroids (1 1/8 inches O.D.) were measured on a G. R. Twin-T bridge. The values are reported in Table XV. Oxygen treatment during firing consistently improved the permeability although not uniformly. Greatest improvement was gained at lowest rise rates. Q also was generally increased slightly by oxygen treatment although there are a few exceptions. As a result of this study, it is clear that oxygen firing is desirable in order to develop the optimum permeability and Q. A moderate rise rate is also indicated.

Low Temperature Evaluation

For the development of low signal level ferrite materials, applicable properties of these materials must be studied throughout the temperature range -65°C to 250°C. For the low end of this temperature range, it was decided to study these properties under the best and most reproducible conditions - namely with a vacuum cryostat.

Using such equipment, residual water which might be trapped on the surface or in the interior of highly porous samples can largely be eliminated and hence icing which has been a problem is no longer troublesome here.

Description of equipment. While the vacuum cryostat used in this study is not of a new design, it will be worth while to point out its salient features. Figure 39 shows a block diagram of the cryostat.

The cryostat consists essentially of a liquid nitrogen container placed in the vacuum chamber. At the base of this, and inside the vacuum, is connected a copper rod around which heater windings have been applied. At the extremity of the end of this heater rod is screwed a copper chamber inside of which the sample is contained. Hence, the basic operation of this system is clear. Good thermal contact between sample and liquid nitrogen container allows temperatures of -170°C at the sample to be readily obtained. Upon the application of power to the heater windings temperatures up to near 0°C can be achieved. For temperatures from that of room to about 100°C, just the heater windings are used without any coolant such as liquid N_2.

The sample chamber which screws on tightly to the heater rod to maintain good thermal contact is made of copper and is large enough so that there is essentially no thermal gradient along it when no power is applied to the windings.

STAT

STAT

TABLE XV

COMPARISON OF AIR AND OXYGEN ATMOSPHERE FIRINGS
μ_o AND Q AT 1.5 MC FROM G.R. 821-A BRIDGE

Rise °C/Hr.	Atm.	Firing Temp.	μ_o	Q_{mat}	μQ
		Mapico 110-2 Iron Oxide			
300	Air	1094°C	79	247	19500
	O_2	1087	117	267	31200
600	Air	1112	80	242	19400
	O_2	1096	107	289	30400
1400	Air	1106	81	239	19400
	O_2	1099	93	264	24600
300	Air	1147	103	253	26100
	O_2	1150	139	199	27700
600	Air	1166	94	250	23500
	O_2	1147	106	256	27100
1200	Air	1162	95	186	17700
	O_2	1142	117	250	29200
		J. T. Baker Iron Oxide			
300	Air	1094	78	232	18100
	O_2	1087	107	238	25500
600	Air	1112	88	232	20400
	O_2	1096	105	254	26700
1400	Air	1106	113	211	23900
	O_2	1099	130	158	20500
300	Air	1147	117	169	19800
	O_2	1150	140	143	20000
600	Air	1166	111	189	21000
	O_2	1147	131	142	18600
1200	Air	1162	123	158	19400
	O_2	1142	135	108	14600

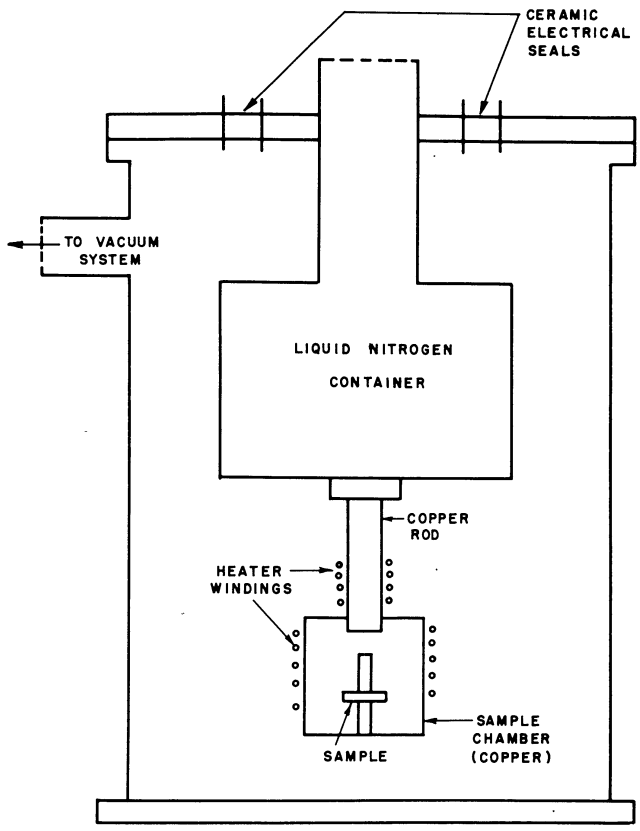

Figure 39. Block Diagram of Cryostat

Several Cu - Constantan thermocouples are provided to measure temperatures in various locations within the cryostat. These thermocouples as well as sample leads and the power leads of the heater windings are soldered to ceramic vacuum-tight lead through insulators.

It has been possible by proper thermal design to minimize loss of liquid N_2 after the liquid N_2 chamber has been sufficiently cooled. The coolant will remain in the chamber for over 2 hours if no power is supplied to the heater windings; if the heater is used, as during a run, this storage time for liquid N_2 is somewhat reduced.

The entire liquid nitrogen container-heater rod-sample chamber assembly is soldered to the top flange of the cryostat with an "O" ring providing the vacuum seal between the top flange and the flange of the body of the cryostat. This type of demountable design has worked exceedingly well.

The cryostat is evacuated by means of a side port connected directly to the main glass vacuum line through a "Sylphon" bellows and a Kovar-glass seal.

The vacuum system used is a conventional one. A Welch 1405-B DuoSeal mechanical forepump is used in conjunction with a low vacuum ballast, an H.I.T. mercury diffusion pump and a liquid nitrogen condensing trap. An NRC 501 thermocouple gauge reads the pressure between the forepump and ballast while a Philips-type cold cathode ionization gauge reads the pressure on the high vacuum side, i.e. on the main line to the cryostat. For convenience of operation there is a roughing line to the high vacuum side of the line. Under good operation of the cryostat, it has been possible to obtain vacuum of the order of 6×10^{-6} mm Hg as measured with the Philips gauge.

Figure 40 shows an external view of the cryostat connected to the main vacuum line. The potentiometer pictured is a Leeds and Northrup Model 8657-C and is used to measure the thermal emf's.

To measure μ and Q of the samples, a radio frequency bridge is used. The signal is supplied from a Marconi Instruments Ltd. Standard Signal Generator Model TF 867. This particular generator is rated from 15 kc to 440 mc. A National HRO-50T1 receiver is used as the detector. An internal modulator allows an audio output to be displayed on an oscilloscope.

Figure 41 shows the general setup of the equipment used in conjunction with the cryostat.

Method of measurement. A block diagram of the circuit used to measure μ_o, the initial permeability, and Q_{mag}, the material quality factor of the toroidal cores is shown in Figure 42.

A typical toroid is prepared for measurement by winding it with 30 turns of number 31 wire (about 20 inches). After placing the sample in the cryostat, its inductance and resistance are measured on a radio frequency bridge. Generally it is necessary to correct the results because of lead capacitance, inductance and resistance. The bridge measures the equivalent

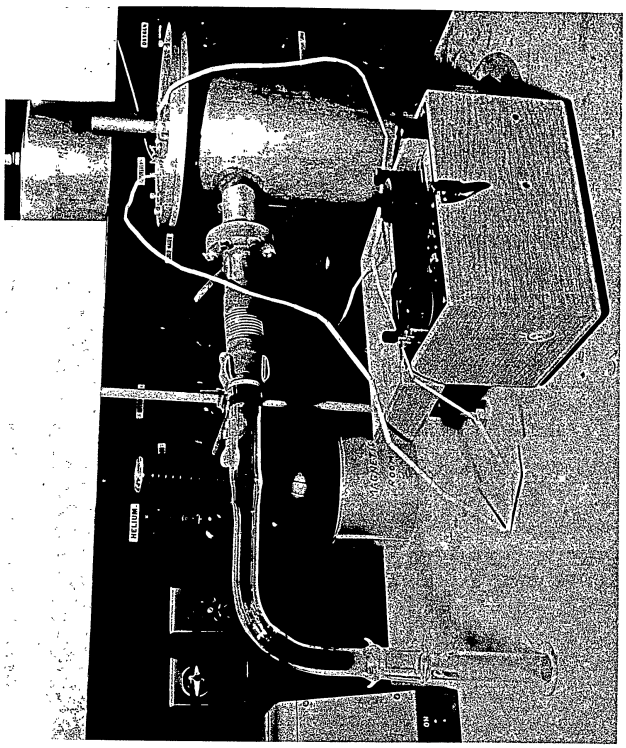

Figure 40. Photograph of Cryostat

STAT

STAT

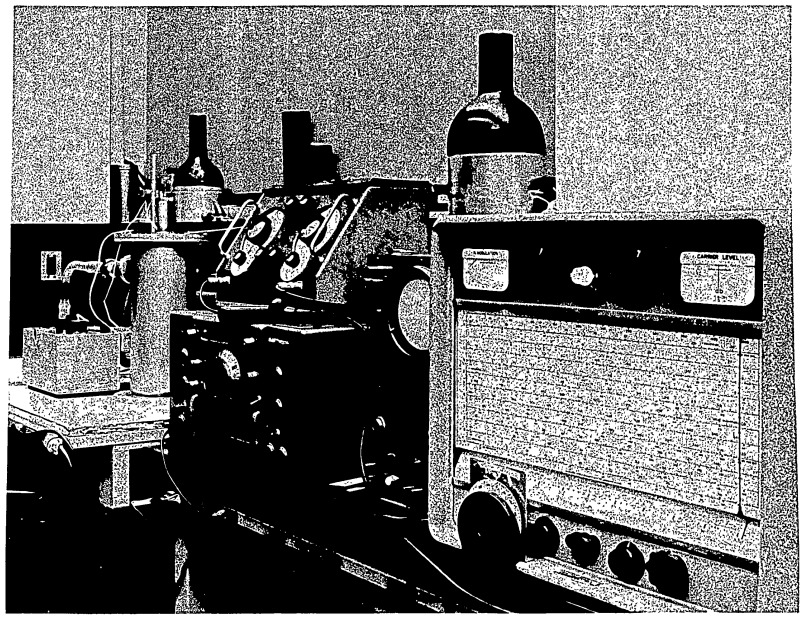

Figure 41. Photograph of Equipment Used in Conjunction with Cryostat

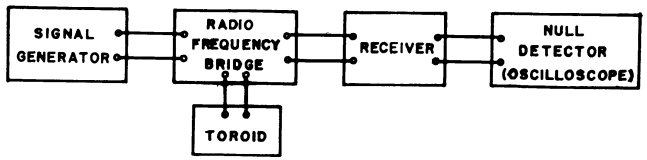

Figure 42. Block Diagram of Circuit Used to Determine Initial Permeability and Q

Declassified in Part - Sanitized Copy Approved for Release @ 50-Yr 2014/02/05 : CIA-RDP81-01043R002800240003-8

parallel inductance and resistance between its terminals which is easily converted to the actual series inductance and resistance of the toroid and leads provided lead capacitance does not have to be considered. See Figure 43.

Some initial measurements of μ_e as a function of temperature are presented in Figure 44 for a sample of Composition 67, toroid .75HQ67.23. Composition 67 is described in Section III. Toroid .75HQ67.23 was sintered at 1100°C for 20 minutes. Figure 44 shows that the initial permeability increases .07% per degree Centigrade over the temperature range -170°C to 25°C. Q_{mag} did not vary appreciably over this range.

One additional remark should be made regarding the low temperature behavior of the nickel-zinc ferrites investigated during this program. In the course of permeability measurements in the temperature range -50°C to -25°C, an indication of a "thermal arrest" was observed in the heating curve, which may be indicative of an ionic ordering taking place somewhere in this temperature interval. Time did not permit a detailed investigation of this effect so no significant data are available. However, close scrutiny of the behavior of properties in this temperature range should be made in any future work on this ferrite system.

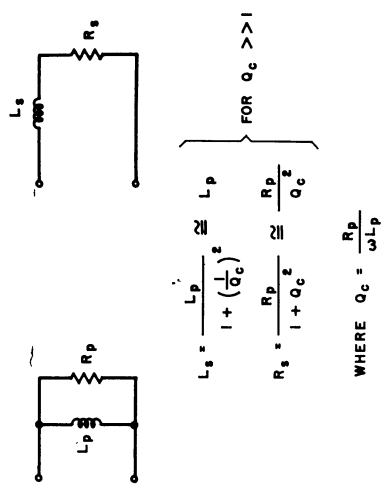

Figure 43. Series and Parallel Equivalent Circuits of Coil

STAT

STAT

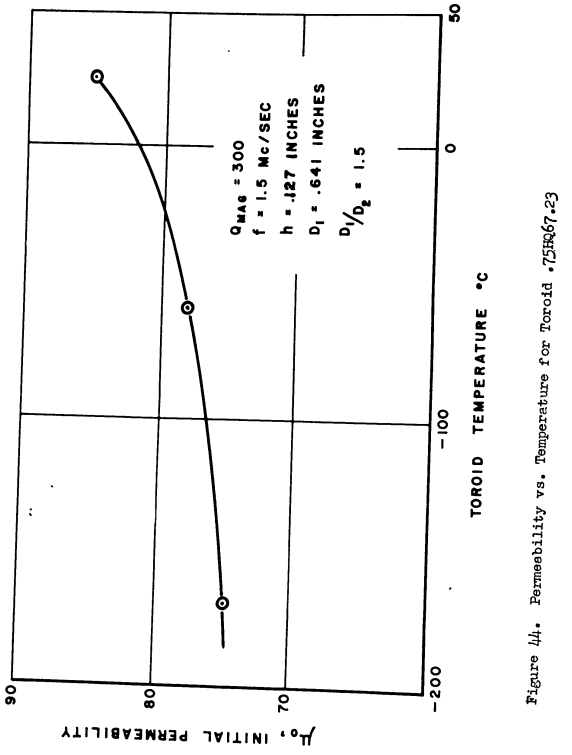

Figure 44. Permeability vs. Temperature for Toroid #75H67-23

Differential Thermal Analysis

Fabricating high quality ferrite pieces is beset by many difficulties for which no good evaluation procedure is available. A finished test piece of ferrite material is no better than the weakest link in the chain of steps leading to the finished specimen. But the situation may be even worse. Failure to produce a high performance specimen is frequently a matter of severe failure of one operation or process rather than a summation of partial failures in many steps. And without good evaluation procedures for individual unit processes, it is difficult, in fact almost impossible, to exert the vigilance required to produce ferrites of the highest quality.

One of these difficult processes is "binder burnoff". Although in small pieces it does not cause much trouble, it becomes more and more serious as the size of the pressed piece increases. The difficulties also mount with increasing binder content particularly for large pieces heavily loaded with binders and lubricants.

For extrusion, large concentrations of binder are used to achieve uniformity during ejection. But during the subsequent drying and binder elimination strains and even cracks can be introduced.

Careful and complete binder elimination before high temperature firing is also important for developing maximum permeability and saturation as in the nickel zinc ferrites for large signal use. Binder burnoff is also a problem of some consequence in preparation of the low loss materials for low signal applications.

For best pressing or extrusion characteristics ferrite powders are mixed with binders, powder lubricants and other conditioning agents. The elimination of these materials proceeds by several different processes, such as (a) volatilization, (b) cracking followed by vaporization and, (c) combustion of carbonaceous materials.

Practice varies considerably on kind of binder, some favoring polyvinyl alcohol (PVA) types with others preferring wax base emulsions. This makes considerable difference in the processes by which they are eliminated. PVA can be eliminated largely by depolymerization at lower temperatures to volatile products, while wax types must be largely burned off. Actually on rising temperature the hydrocarbon waxes first give off volatiles, an endothermic process, then they start to crack, also endothermic; then the new volatile components start to burn, and finally the tarry residue begins to burn, the latter both exothermic processes. In addition starchy materials also break down in a somewhat similar manner leaving hard carbon residues which must be removed by oxidation at fairly high temperatures.

Since some of these processes are endothermic while others are exothermic, their study can be profitably pursued by differential thermal analysis (DTA). Methods of approach other than DTA have been applied to this problem, e.g. use of a recording thermobalance, but it is difficult to interpret the data. Since the DTA will give a different type information

STAT

STAT

we hope to get a better understanding of the mechanism of the physical and chemical processes in binder elimination. For this purpose a special small furnace was constructed which was adapted from the design of Borschardt[1]. A somewhat schematic diagram of the furnace is given in Figure 45. Test material and reference material are supplied as powder (0.1 g) into the tubes marked Sample in Figure 45. Both loosely piled powders as well as tamped specimens have been tried. Packed samples were generally preferred.

After early troubles with the aluminum block furnace described above, it was redesigned to reduce heat loss by removing some of the aluminum in the flange and then rewound and again placed in service. With these improvements, we were able to pursue the differential thermal analyses to 500°C many times. At this temperature the aluminum blocks had a tendency to weld together, making it extremely difficult to separate the parts of the furnace.

However, sufficient data were obtained to indicate that still higher temperatures would be desirable. A special fire brick door (Figure 46) was designed to fit into a small standard muffle furnace (Tempco 1400 watts). The furnace is controlled by the same Leeds Northrup cam program control, amplifier and X-Y recorder used on the previous furnace. This apparatus with this second furnace was proved out to 800°C several times and was adequate for use in binder studies.

The special fire brick door carrying the sample holders shown in Figure 46 was made up by cementing fire brick together after channels (tubes) for the thermocouples were provided. Thermocouples (Pt - 13% Rh) are cemented in the protection tubing which projects 1/4 inch above the brick. Three thermocouple junctions are shown, two differential junctions ΔT_1 and ΔT_2, and a third T_3, which measures the sample temperature. This latter tube can also be supplied with a metal tube and unknown powder to measure the temperature of the sample by substitution.

The bosses carrying the thermocouple junctions provide the seats for the thin walled metal tubes which are pushed down upon them making easily demountable crucibles. We use stainless steel tubes 1/4 inch in diameter by 1/2 inch high with 6 mil wall. These tubes have withstood temperatures up to 1000°C without severe oxidation and are quite satisfactory, but platinum tubes would be more suitable for higher temperatures. To clean the setup, the tubes are removed and the powdered sample brushed off from the thermocouples and bosses, after which it is ready for a repeat analysis.

Although this furnace setup is satisfactory for binder-burnoff studies, it is limited to about 800°C because it does not have sufficient electrical power capacity to maintain the constant rise rate above this temperature. For studies of calcination phenomena, a higher temperature and higher power furnace has been provided and is described later.

1. H. J. Borschardt, J. Chem. Educ. 33, 103 (1956)

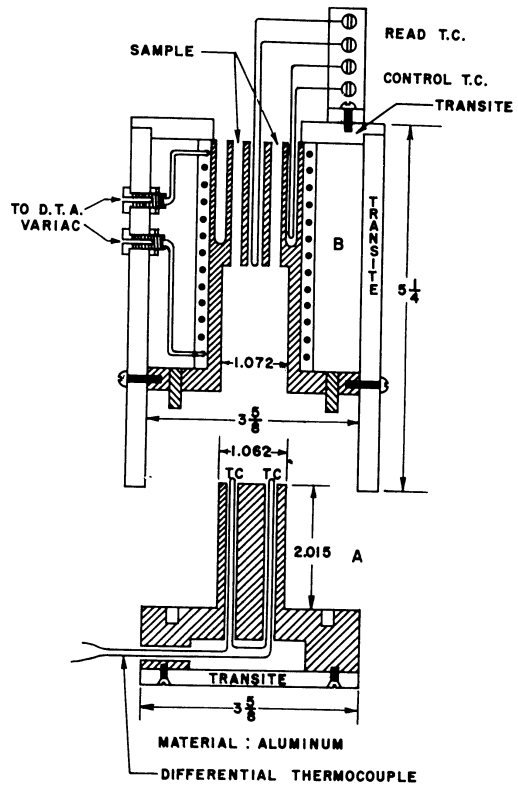

Figure 45. D.T.A. Furnace

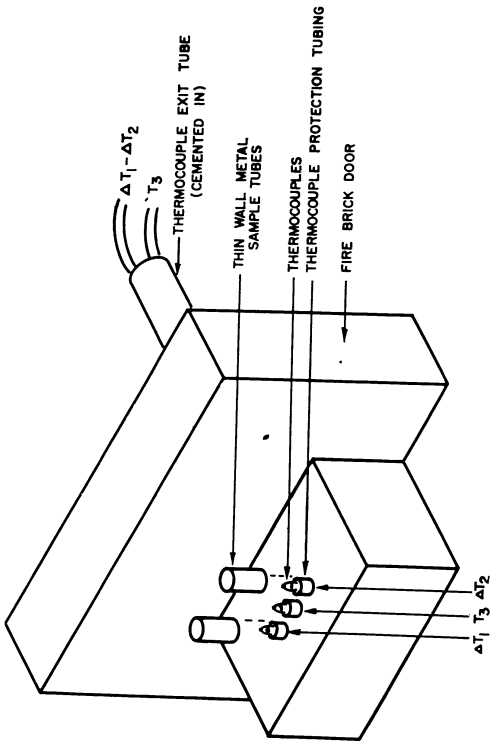

Figure 46. Fire-Brick Door Carrying Sample Holders

Results of burnoff studies in furnaces No. 1 and No. 2. None of the nickel ferrites under study in this contract was available with a wax binder already mixed in. And since several magnesium manganese ferrites were immediately available with Hyform binder (wax), several differential thermal analyses were made on these materials. However, thermograms of the materials with polyvinyl alcohol (PVA) and methylmethacrylate (MMA) were made on nickel zinc ferrites.

Many different experimental procedures have been tried but no completely standard procedure evolved. In general, it was found that 0.1 g. samples accurately weighed give very satisfactory sensitivity. Instead of using powdered Al_2O_3 as the standard material as is common in DTA, our practice was to use powdered ferrite with binder in one tube and the same ferrite without binder in the other. This discounts most effects except that of the binder. A powder at least as fine as minus 60 mesh is used and lightly tamped. Before we began to tamp the samples, the resulting differential thermograms were quite variable. Mostly, a heating rate of 3°C per minute has been used, primarily because it was not easy to alter.

Although nearly two dozen differential thermograms have been made, only a few representative examples are shown in Figure 47. Sample temperature is plotted on the x-axis and the difference temperature (ΔT) on the y axis. Exothermic reactions show a positive deviation ($+\Delta T$) and endothermic negative ($-\Delta T$). The largest ΔT shown is about 15°C, and all differential thermograms given are plotted on the same scale.

In order to prove that the apparatus was working properly and was capable of resolution of fine detail a differential thermogram of copper sulfate decahydrate was prepared and appears at the top of the group. It agrees quite well with that published by Borschardt[1] except that it shows detail beyond his high temperature limit. Presumably these peaks are due to decomposition of the anhydrous sulfate.

The next four curves are all of calcined ferrite material incorporating a wax type binder (Hyform). The top one contains 16% by weight of Hyform emulsion (4.8% by weight, wax), 3/4% by weight of Flocgel (starch) and 3/4% by weight of magnesium stearate. The other three have 8% of Hyform emulsion only (2.4% wax).

All of the thermograms of samples containing wax cover about the same range of temperature and show large differential heat effects in the range from about 200°C to 450°C. The maximum varies somewhat but generally occurs from 300° - 340°C. However, as a generalization, one might say that exothermic reaction begins very early on heating, accelerates very rapidly around 200° - 250°C and starts to fall off at 350°C and is practically over at 420°C. But the final stages of combustion of the carbonaceous matter are not complete until 500°C.

In spite of the general agreement among the thermograms of the samples containing wax there are differences among them that seem understandable. All three of the samples containing 8% Hyform emulsion (2.4% wax in sample) show structure in the combustion peak. Note that the finer powder (-140 mesh) shows substantially the same behavior as the others.

STAT

STAT

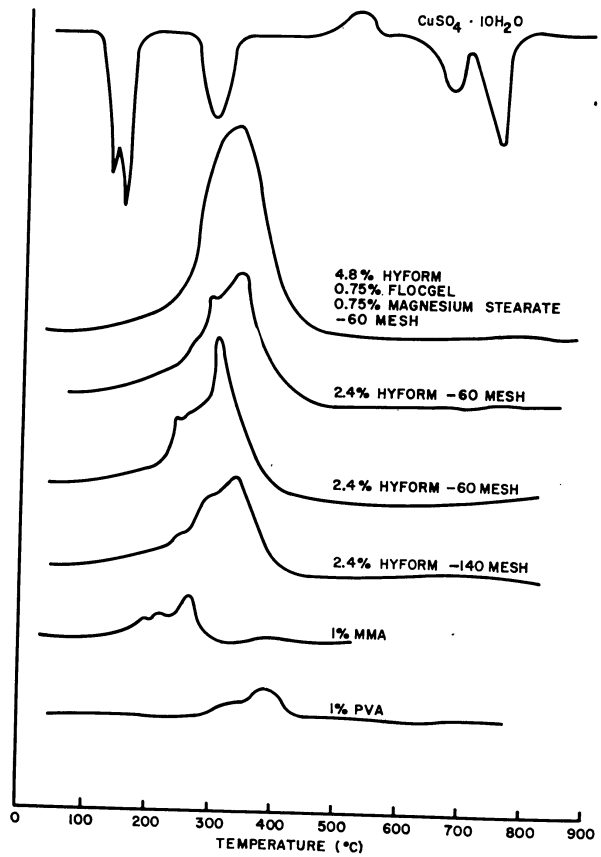

Figure 47. Differential Thermograms

On the other hand, the one containing 1% Hyform, 3/4% Flocgel and 3/4% magnesium stearate (top) shows a larger and smoother peak. With twice as much binder more heat would be expected. And with several combustible binder components one would expect better packing and smearing of the combustion curve, just what is found.

Polyvinyl alcohol and methyl methacrylate are also eliminated by exothermic reaction. Methyl methacrylate begins to leave the sample at 100°C and is entirely gone before 300°C is reached. On the other hand, polyvinyl alcohol begins to go at about 300°C and is all gone by 440°C. The total net heat evolved in the process is much less than with the wax. However, it should be pointed out that the total weight of binder is less in these two cases, 1% by weight.

Although the present work is by no means conclusive, it does point to need for great care in the "binder burn-off heating cycle". With temperature differences as large as 15°C between the unknown and standard specimens in a small 1/4 in. x 1/8 in. lightly packed sample, one would expect large temperature differences in a large densely rammed production piece. On the basis of these differential thermograms, it appears that the most sensitive temperature zone for wax (Hyform) burnoff is 200° - 325°C. From the peak at 325°C an increasing rate could be used up to 450°C.

High temperature DTA in sintering range. A new furnace was provided to pursue the differential thermal analysis up in temperature to include the sintering range, 1100°C to 1200°C. For a variety of reasons, a wire wound furnace was preferred to one using Globars. None of the commercially available furnaces seemed appropriate, so one was built to suit the needs of the present program.

Furnace No. 3 is a tube type, 12 inches long by 12 inches overall outside diameter, and is shown in Figure 48. The tube muffle is 2 inches inside diameter and grooved outside to carry the wire, Kanthal A-1 which allows operating temperatures to 1350°C. The winding consists of twenty-three feet of B and S Gage No. 20 wire (0.85 ohms/ft) giving a cold resistance of 10 ohms for the furnace; a center tap allows the net magnetic field due to current in the winding to be reduced to zero at the sample position. Before assembly, the heating element was cemented to the muffle with a cement specifically designed for use with Kanthal wire.

K-30 high temperature insulating fire brick was cut to shape to fill the space between the wire wound muffle and the stainless steel can making up the shell of the furnace. The ends of the shell are also stainless steel and fitted with handles so that the furnace can be carried easily or used in the vertical position. The furnace is used in the vertical position, mounted on an angle iron stand which holds the furnace 9 inches above the bench top.

The furnace has been tested to 1300°C and has sufficient reserve power to maintain a rise rate of 6°C/min or greater up to that temperature.

STAT
STAT

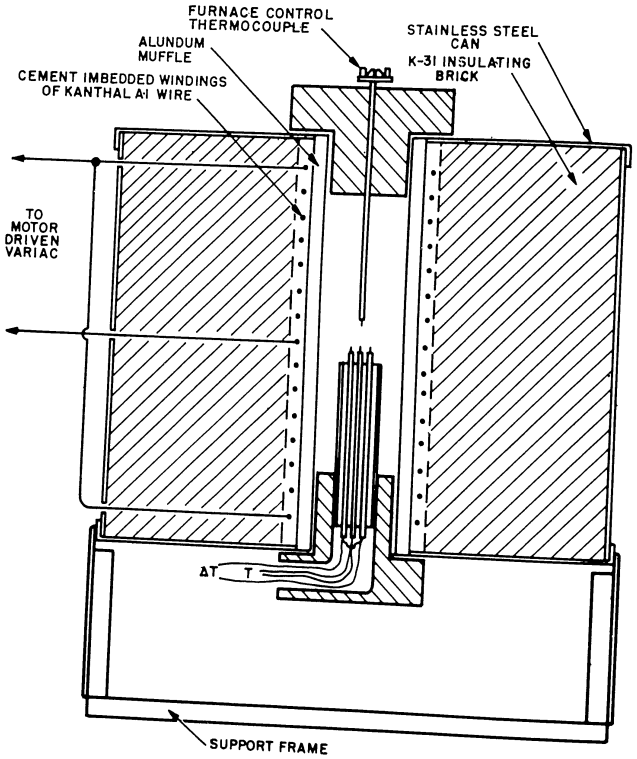

Figure 48. Schematic Diagram of DTA Furnace No. 3

In the previous DTA furnaces, the samples were contained in stainless steel tubing, slipped onto the thermocouple protection tubing to make demountable crucibles. That system worked well and has been incorporated in the third design. However, there is always some possibility of reaction with the metal container. Therefore, pressed pellets of material were substituted as shown in Figure 49 rather than powdered samples.

A special small die was constructed to press the pellet sample (3/16 inch O.D.) with a small hole to allow the sample to sit upon the thermocouple junction. Mechanically, this works fine. It also gives a sufficient T for measurement. As yet, it is not clear that use of pellets is superior to powder in crucibles, but the pellet technique is much cleaner and simpler.

Unfortunately, even before this furnace (No. 3) was built, trouble was encountered with noise in the electronic circuits of the measuring equipment, i.e. the X-Y recorder. This has been continually getting worse. Since the third furnace has been in use, noise and erratic behavior of the control and measuring equipment have hampered progress considerably. Shielding of the thermocouple lines and grounding of amplifier chasses did not remove the trouble. A complete metal tubular shield inside of the furnace surrounding the samples and thermocouple leads was tried and showed promise.

In order to obtain measurements at high temperature, independent of the difficulties encountered in the electronic circuitry, the X-Y recorder was replaced by two thermocouple potentiometers and a firing was carried out to 1300°C. No erratic behavior was apparent in this setup. The results are shown in Figure 50. From Figure 50, it appears that the binder burnoff accounts for the major part of the response but that the heat effects in the sintering range are very small, only two or three microvolts as recorded by the differential potentiometer. If desired, the deflection could be magnified through the use of a sensitive galvanometer but it appears that the X-Y recorder would not be sufficiently sensitive to make investigations in the sintering range fruitful.

Figures 51 and 52 are photographs showing the DTA furnace and the temperature and differential temperature recorders. Further work in differential thermal analysis should be extended to calcination studies with and without additives and sintering studies with and without additives. However, it appears that the best method should include exploratory measurements using point by point potentiometric methods. After this initial work, an indication will have been obtained of the required sensitivity. The final analysis would then be made using a galvanometer with the appropriate sensitivity. These recommendations are based upon the results shown in Figure 50.

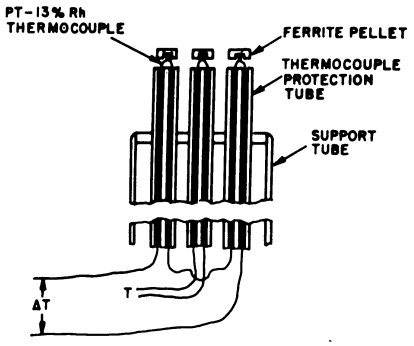

Figure 49. DTA Test Sample Arrangement

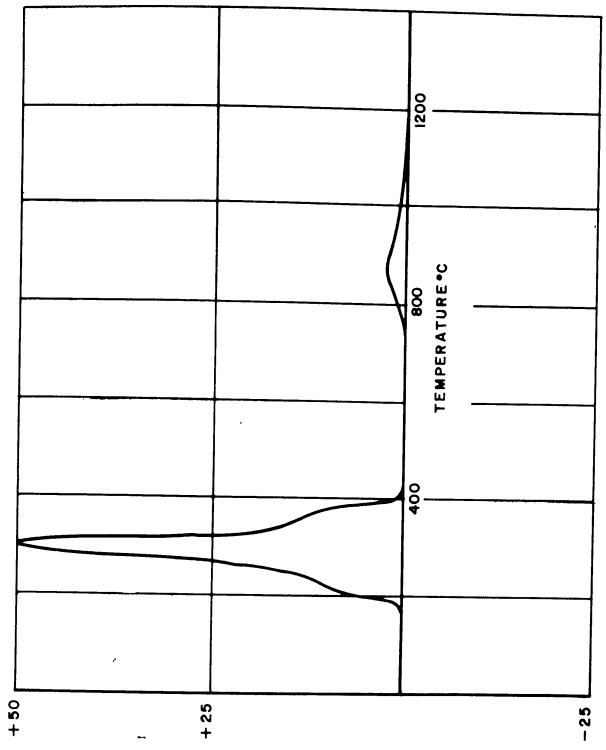

Figure 50. DTA Composition 84 vs. Al_2O_3

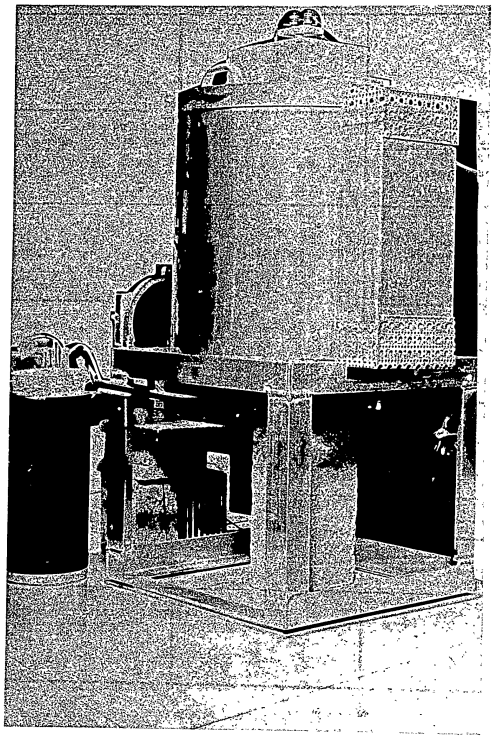

Figure 51. DTA Furnace Assembly

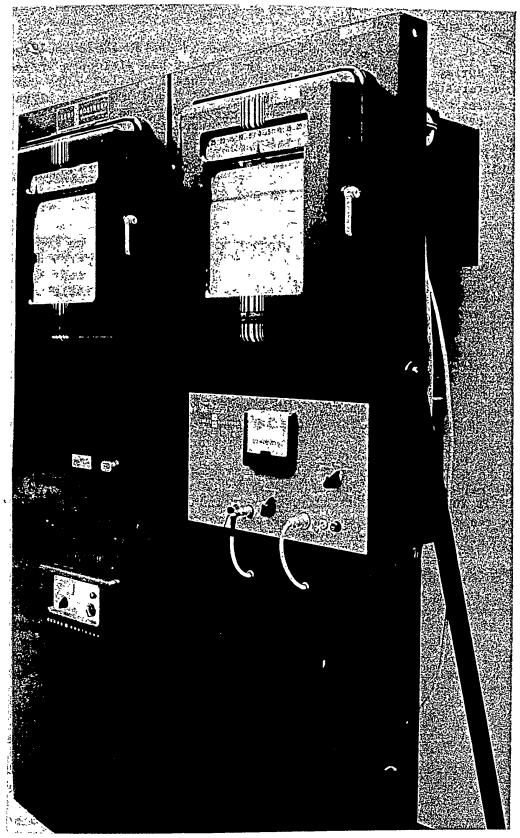

Figure 52. Temperature and Differential Temperature Recorders for DTA

STAT

STAT

Conclusions and Recommendations

The effort expended on the development of low loss, low signal ferrites during the period covered by this report has yielded a series of high Q materials with permeabilities in the range 12 to 120. The Curie temperatures of these materials lie between 385°C and 500°C and high Q behavior persists over the temperature interval -65°C to +250°C. In addition, the low signal properties of these materials have been shown to be relatively unaffected by prolonged exposure to high humidity. Of particular importance is the low temperature coefficient of permeability exhibited in the range -65°C to +25°C. In this critical temperature interval, the variation in Compositions 84 and 67 is less than 0.1% per degree C.

The variation of the μQ product with frequency is an important design characteristic. Composition 84 bodies have been prepared which exhibit μQ products greater than 10,000 at 7 mc. For applications which require operation above 7 mc, Composition 285 bodies are available with μQ products in the range 10,000 to 7,000 between 7 mc and 20 mc; at 30 mc, the μQ product is still as large as 1500.

Much useful information was gained from the investigation of the effects of processing techniques, the investigation of the effects of different brands of iron oxide, and the results of differential thermal analysis. Knowledge of this type is necessary to assure reproducibility of developmental samples for future large quantity use.

Thus, the broad objectives of the low signal materials program have been achieved. Future work in the development of low signal ferrites should include further study of sintering control in these partially cured materials in the hope that the μQ product can be increased in the frequency range 10 to 30 mc and that better control can be exercised over the temperature coefficient of permeability, particularly at low temperatures. Also, broad objectives, which applied in the phase of effort currently completed, should be narrowed to stipulate specific low signal parameter values.

SECTION IV

HIGH FREQUENCY NARROW BAND MODULATED DELAY LINES

Introduction

The use of delay lines has become an integral part of a large variety of electronic systems. Radar, color television, correlators, and computers are but a few of the many applications utilizing delay lines. The specifications for a particular line are of course a function of the needs of the specific application. However, one can classify delay lines in terms of the range of delay times that are required. Very short delays of the order of 0.1 of a microsecond are conveniently achieved with lumped constant elements. Delay times of the order of one microsecond to several microseconds are usually accomplished with lumped constant or distributed parameter systems. Finally, delays of the order of tens or hundreds of microseconds are usually obtained by some form of sonic element. However, in each of these groups the objectives are very similar.

An adequate delay line must be capable of passing a band of frequencies with a constant time delay and constant attenuation for each frequency component in the pass band. Though there may be many solutions to these two problems, one is usually compelled to compromise with other factors such as overall size, ease of fabrication, cost, accuracy of time delay adjustment, temperature stability, and the impedance level that is desired.

The present report is concerned with the development of a narrow band, high frequency ferrite delay line, the delay of which can be varied by a biasing magnetic field, thus yielding a component which can be used for phase modulation.

Of the many ways by which one can produce phase modulation, the use of a controllable delay line appears most attractive. The usual procedure for the production of a phase modulated carrier is to generate a low frequency carrier to which the modulation is applied and the final carrier is generated through a series of multiplications. The modulation itself is usually produced by some form of reactance tube. In order to decrease the overall size and power consumption during the modulation process, it would be more desirable to perform the modulation function at the actual transmitted frequency or at a stage which reduces the number of multiplications required. A delay line whose time delay could be varied with an electrical signal would meet such requirements.

Objective

The objective of this phase is to produce a ferrite delay line whose delay can be adjusted by the application of a biasing magnetic field. The present goal is to achieve a total delay of approximately 0.5 microseconds and a variable delay of 0.1 microsecond at 30 mc.

STAT
STAT

General Considerations

A phase modulation element operating at 30 mc with a modulation of 30 - 3000 cps is desired. However, it was decided to work in the 10 mc region at the start of the project and progress toward the 30 mc region in determining the feasibility of the device. Since the delay of a distributed constant line is equal to $\sqrt{(LC)}$, where L is a function of the permeability of the medium, the delay can be modulated by changing the permeability. In a ferrite, the permeability is a function of the applied magnetic field. A ferrite delay line can therefore be modulated by establishing a magnetic field in the line with the modulation signal. The delay line must also have reasonable attenuation and a fairly high order of time delay, with respect to the change in delay desired. Moreover, it must be fairly small if the input modulation power is to be minimized. While the line must operate at the carrier frequency, it need not have a flat time delay characteristic, since it will operate about a fixed carrier frequency. A line having a total time delay of 0.5 microseconds at 10 mc in three inches length would be acceptable, if a variation of ±0.1 microseconds can be effected. The delay line output could be peaked at 10 mc to obtain lower attenuation, if desired.

The design of the lines discussed below, including choice of dimensions, was governed by the analytical development presented in WADC Technical Report TR 56-274, Part V. In this analysis, the time delay vs. frequency characteristic for a given permeability of rod and sleeve was presented. The important feature of this curve is a flat portion which persists until a critical frequency is reached. At this critical frequency the delay decreases sharply with frequency. In the present development, this is of no real concern except that sufficient magnitude of delay must be available so that the appropriate changes in delay can be effected by application of a biasing field.

Materials Preparation and Initial Evaluation

The initial phase entailed the measurement of ferrites in order to determine the variations of permeability with bias obtainable at high frequencies. The circuit arrangement shown in Figure 53 was used for the measurement of μ vs. bias. A National Electronics Laboratories Radio Frequency Permeameter was modified slightly by drilling two small holes through the main body. This permitted the insertion of a wound toroid whose leads could be brought through the permeameter to a d.c. supply. The tuned circuit was inserted so that the power supply would not load down the permeameter. The use of a Q-meter in conjunction with the permeameter allowed for a rapid determination of μ vs. bias field. The number of turns, n, that are wound on the core is determined by two factors. It is desirable that n be as large as possible in order to reduce the amount of current required. On the other hand, n must be reduced far enough so that the self-resonant frequency is sufficiently far above the test frequency. In most cases, this required about 15 turns on a half-inch toroid.

A sample of Composition 84 (toroid .75HQ84.10) was evaluated using the modified National Electronics Laboratories Radio Frequency

Permeameter by the technique outlined above. The results are shown in Figure 54. In Figure 54, the low signal permeability decreased by a factor of 13 from zero field to a field of 19 oersteds for the initially unmagnetized sample. The change in permeability observed from remanence to saturation is shown by dotted line and the return solid line.

Other materials, Compositions 67 and 285, were similarly evaluated at 10 mc but it was immediately obvious that the necessary change in permeability could not be obtained in these materials.

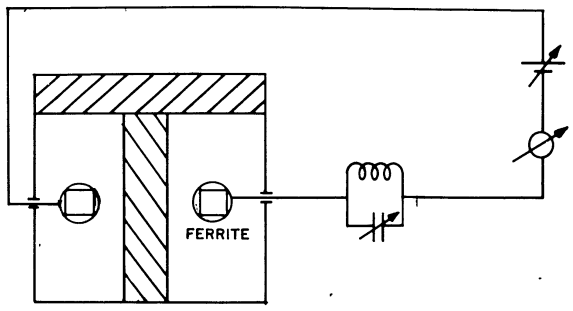

Figure 53. Permeameter Schematic for μ vs. Bias

STATT

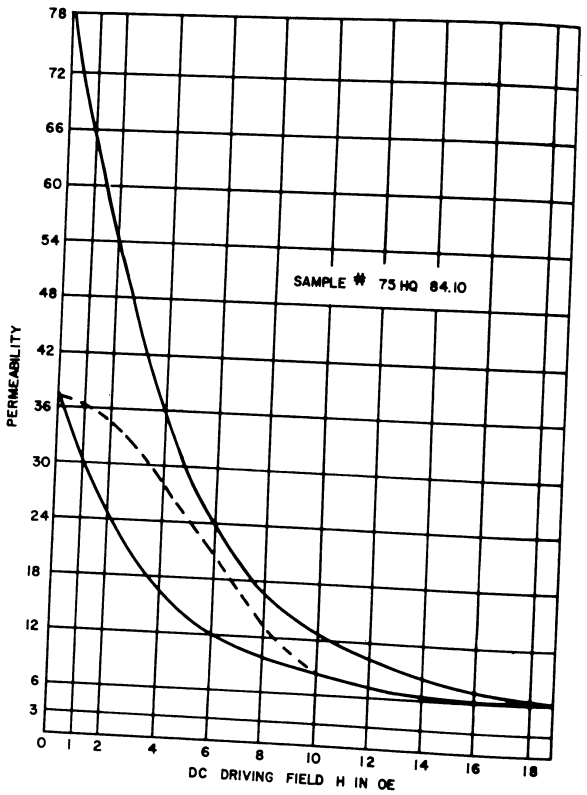

Figure 54. Permeability vs. Driving Field for Sample .75HQ84.10

Having established that sufficient permeability variation can be obtained using Composition 84, rods and tubes were extruded for the fabrication of delay lines. It will be recalled that Composition 84 consists of 66.96 wt% Fe_2O_3, 20.53 wt% NiO, 11.74 wt% ZnO and 0.77 wt% V_2O_5.

Standard ceramic fabrication procedures were followed in the processing of this composition. Usual practice is to weigh out approximately 1 kg total batch on a large (2 kg) analytical balance. The resultant mixture is ball milled overnight for about 16 hours in a one gallon iron mill with steel balls, in the presence of about 1 1/2 liter deionized water. This process both mixes and grinds. The slurry is then placed in glass drying pans and brought to dryness in standard ovens. The next step in the process is to run the dried powder through a pulverizer for sizing.

DuPont No. 7005 polyvinyl alcohol (PVA) is used as a binder for the extrusion in the extent of about 4 1/2 wt%. The PVA is made up fresh each time in a 17% water solution. Homogenizing and mixing were done in a Lancaster mixer.

Rods and tubes of Composition 84 were extruded. One set of extrusion samples consisted of rods 0.250" in diameter, tubes with an O.D. of 0.375" and an I.D. of 0.255", and tubes with an O.D. of 0.500" and an I.D. of 0.255". Another extrusion yielded rods 0.094" in diameter and tubes with an O.D. of 0.157". The dimensions given are for samples in the "green state".

Five different firings were made. These firings consisted of a 20 minute soak with a fast rise rate of the order of 600°C/hr after the binder had been burned off. Soak temperatures of 1175°C, 1160°C, 1140°C, 1125°C and 1100°C were used with an optimum, as determined by desirable end results in the finished delay line, occurring at about 1140°C to 1150°C.

More specifically, for the firings of 1175°C for 20 minutes, the permeability of the material as measured on the prototype line was excellent while the Q or attenuation was rated good. Firing at 1160°C for 20 minutes still maintained an excellent μ while the Q or attenuation improved. Essentially, the same thing was true for the firing at 1140°C for 20 minutes. The firing at 1125°C for 20 minutes resulted in a good permeability but only fair Q while the firing at 1100°C produced lines which had both a low μ and poor attenuation. The exact values of permeability and Q were not directly obtainable, but were inferred from the resulting delay line performance.

Testing of Delay Lines

In order to establish modulation techniques and testing procedures, initial experiments were performed on lines constructed using rods and tubes of ferrite Composition 205. Composition 205 was developed under Contract No. AF 33(616)-2009 for application in a video delay line. The oxidic constituents are 48 mol% Fe_2O_3, 26.5 mol% NiO, 25.0 mol% ZnO, and 0.5 mol% V_2O_5.

STAT

STAT

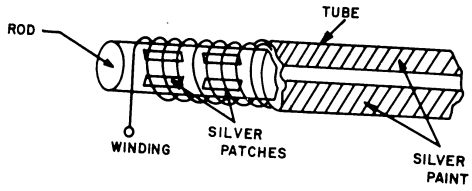

Figure 55. Ferrite Delay Line

The processing of this material and the subsequent video delay line fabrication is described in full in WADC TR 56-274, Part V. The particular Composition 205 ferrite used here is of no significant interest. However, it was a simple matter to test evaluation methods with materials immediately at hand. The prior development showed that the rods and tubes of Composition 205 were of sufficient attenuation that usable delay lines could be produced. However, Composition 205 cannot be operated at frequencies above 8 mc so that this material does not satisfy the needs of the present program.

A rod of Composition 205 5.1 cm long having one continuous silver stripe and three notched ones was wound with No. 42 HF FORMEX wire. (Figure 55). The tube had a silver coating which was of the same material as that used on the rod (DuPont 4916 lacquer). Two unsilvered stripes were left on the tube to reduce any possible eddy current losses. The silvered areas were grounded at the output and the entire line placed in a ferrite "C" core magnetic yoke wound with 1000 turns of number 38 QF wire. Silver paint was used to isolate the line from the yoke structure (Figure 56).

The line was left open circuited and an R.F. signal applied while the magnet windings of the yoke were excited with a direct current (Figure 57). The time delay, T_d, could then be measured by noting the current maxima on the vacuum tube voltmeter, V_1. Since the admittance of an open circuited transmission line will be a maximum when the line length is an odd number of quarter wavelengths, and since the total delay, T_d, is the ratio of length to velocity of propagation, then $T_d = n/(4f)$ where f is the frequency in cps and n an odd integer. Therefore, by noting those frequencies at which V_1 peaks we may find the time delay of the line. By applying D.C. signals to the yoke the family of curves of Figure 58 may be obtained.

At one megacycle $T_d = 0.65$ microseconds with a variation of 0.35 microseconds with the application of 200 ampere turns and an attenuation of 9db.

A further experiment in modulation techniques used a similar ferrite yoke having 5000 turns of number 38 QF wire. A line was constructed and wound with number 42 H.F. formex wire on a rod having eight silver patches arranged in three stripes. The line was terminated in its characteristic impedance of 6.5K. The input and output wave-forms were viewed simultaneously on a Tektronix type 535 oscilloscope with a type 53C dual trace preamp triggered by the input waveform (Figure 59). The change in delay without a ferrite tube as noted on the oscilloscope = 0.08 microseconds with an applied field of 1250 ampere-turns. With the tube, which was unsilvered, the change in delay = 0.6 microseconds. Clearly, the ferrite tube extended the usable time delay in this region.

Before proceeding to lines constructed using Composition 84, Compositions 67 and 75 were used in further establishing proper fabrication techniques. (Compositions 67 and 75 are described in Section III of this report.) Tables XVI and XVII indicate the physical characteristics and magnetic evaluation of various lines constructed from a variety of materials, including Compositions 205, 67, 75 and 84.

The data given in Tables XVI and XVII for lines I and II are self-explanatory. Lines III and IV were fabricated to investigate the use of indium-amalgam[6] in place of DuPont type 4916 silver bearing lacquer as a conducting coating for capacitive patching on rods and ground planes on tubes. It is evident from the information of Tables VI and VII, and Figures 60 and 61 that the indium-amalgam is a better conductor on a ferrite surface.

STAT

STAT

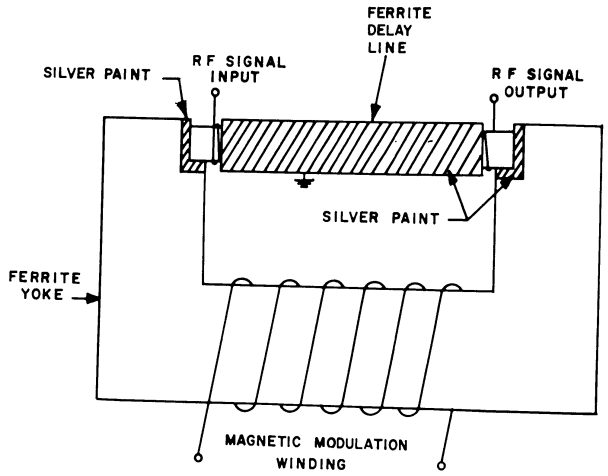

Figure 56. Ferrite Delay Line Mounted in Ferrite Yoke

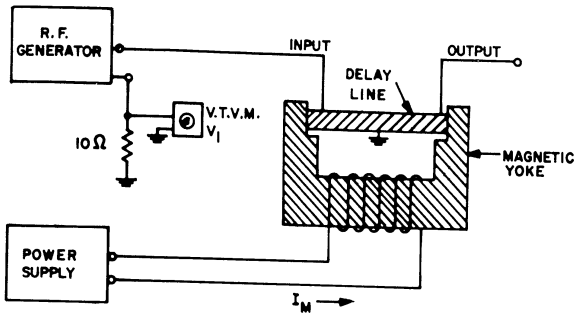

Figure 57. Block Diagram for Modulated Delay Evaluation

STAT

STAT

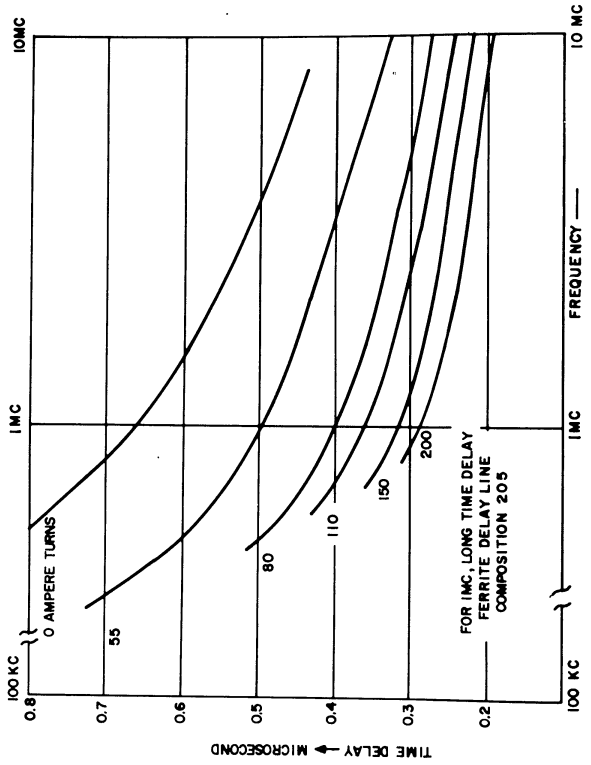

Figure 58. Time Delay vs. Frequency for Ferrite Delay Line with Various Biasing Fields

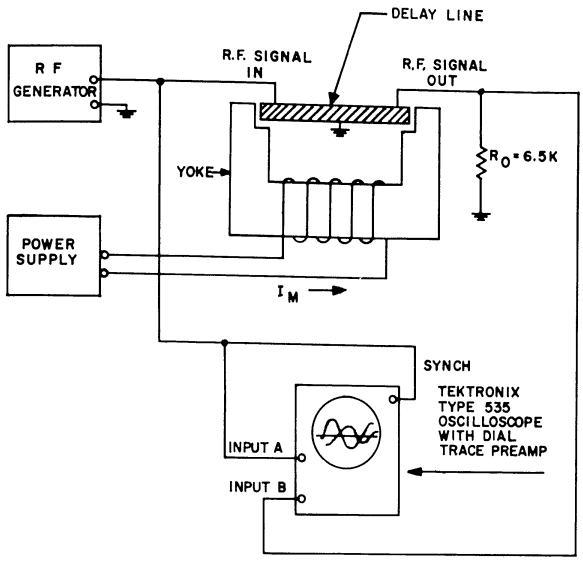

Figure 59. Block Diagram for Visual Presentation

STAT

TABLE XVI

PHYSICAL CHARACTERISTICS OF DELAY LINES

Line No.	Material	Length inches	Diam.*	Wire Size	Modulation Structure**	Description of Line
I	205	2	L	42HF	Y	Rod and tube silvered with DuPont 4916 lacquer.
IIa	67.8	2	L	42HF	Y	Patched rod, 3 patches in 3 stripes; without tube.
IIb	67.8	2	L	42HF	Y	Patched rod, 3 patches in 3 stripes; unsilvered tube.
IIIa	75	2	S	42HF	Y	Rod and tube patched with 8 patches; DuPont 4916 lacquer.
IIIb	75	2	S	42HF	Y	Tube had 2 nonconducting stripes; indium-amalgam.
IV	75	2	L	42HF	Y	Rod and tube patched with 10 patches; indium-amalgam. Tube had 2 nonconducting stripes.
V	84	2	S	42F	Y and C	Tube patched with indium-amalgam with one nonconducting stripe. Rod not patched. When the number of nonconducting stripes on the tube was increased to six progressively, no change in output characteristics could be noted.
VI	84	2	L	42F	Y	Rod and tube patched with indium-amalgam.
VII	84	3.85	S	42F	C	Tube patched with indium-amalgam in one nonconducting stripe. Rod not patched.
VIII	84	2	S	42F	C	Temperature check, line operated at ambient temperatures of -44°C to +110°C.

* Diameter refers to large (L) tube or rod diameters or small (S)
Large: Tube O.D. = 0.29 inches Small: Tube = 0.122 inches
Rod O.D. = 0.193 inches Rod = 0.078 inches

** Refers to ferrite yoke (Y) or concentric coil (C)

TABLE XVII

MAGNETIC AND ELECTRICAL EVALUATION OF DELAY LINES

Line	(at 1 kc) Z_o kilohms	(at 1 kc) T_{do} (μsec)	f (mc)	attenuation db	T_d (μsec)	Change of T_d (μsec)	Modulating field in T_d	Comments
I	2.2	0.54	1	9	.6	.35	200 a.t.	
IIa	7.1	.56	1	6		.08	1250 a.t.	Ferrite tube necessary for large change in delay at high freq.
IIb			1	10		.60		
IIIa	6.5	.34	see Figure					Line with indium-amalgam patching exhibited peaking, other did not.
b	6.5	.47						
IV	5.1	.56	see Figure					Peaking shifted up in frequency as patching and diameter increased.
V	7.5	.43	10	10		.12	300 Oe.	Modulation power so low that yoke dispensed with. Feed-through at 10 mc occurred when the rod was patched.
			20	20		.06		
			see Figure					
VI			10	20		.01	600 Oe.	Large cross section line not as effective.
VII	8.5	.70	10	20*		.1	60 gauss 0.35 watts driving power	* Can be peaked to 5 db. (see discussion)
			see Figures		and			
VIII			see Figure					

STAT

STAT

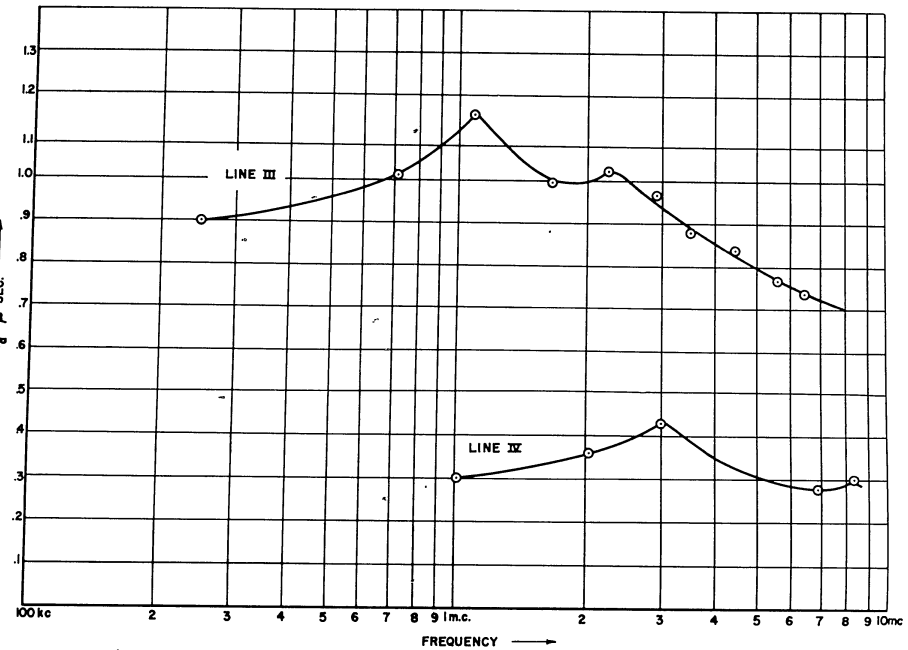

Figure 60. Time Delay vs. Frequency for Delay Lines Patched with Indium-Amalgam. Lines III and IV

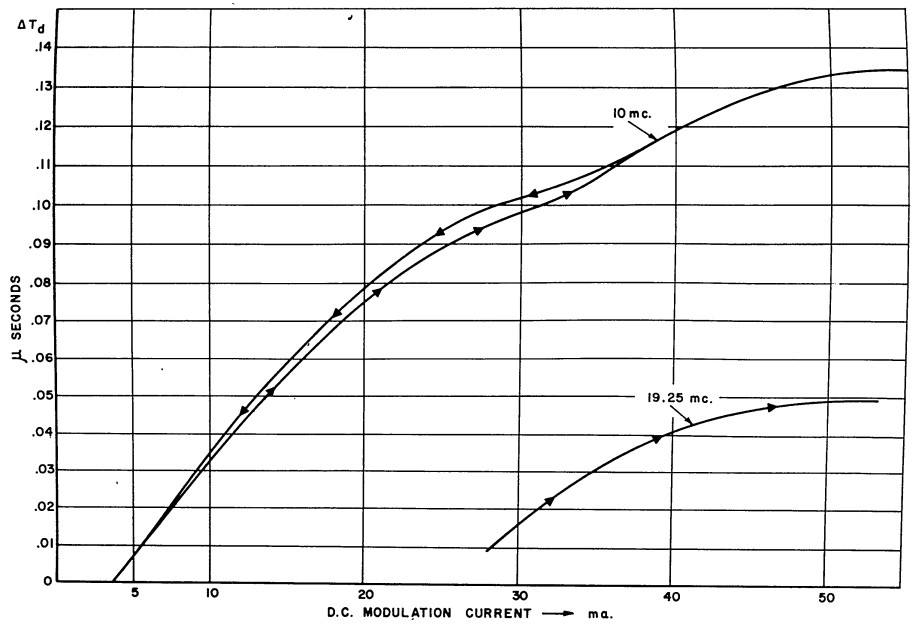

Figure 61. Change in Delay vs. D. C. Modulation Current. Line V

Declassified in Part - Sanitized Copy Approved for Release @ 50-Yr 2014/02/05 : CIA-RDP81-01043R002800240003-8

The amalgam undoubtedly adheres better to the ferrite surface. The peaking displayed in Figure 60 could not be observed with the silver lacquer. In line IV the peaking has been extended to a higher frequency by using a large cross section line which has less distributed capacitance.

When line V was first constructed, the rod was not patched since only a cross-check on the permeameter reading on Composition 84 was desired. The line exhibited excellent characteristics and was operable at 20 megacycles (Figure 61). Its modulation requirements were so moderate that the ferrite yoke structure was replaced by a simple solenoidal winding. This procedure eliminated some feed-through problems, since the yoke structure had represented an alternate low resistance path to the incoming signal. However, when the rod was patched, feed-through of the input waveform became the dominant factor at the output. It was found that this feedthrough was due to the capacitive link formed by these patches. The patches could not be reduced in size to the point where the effect would be tolerable, and had to be abandoned. At 10 mc the impedance presented by the stray capacitance was considerably less than that offered by the ferrite to the solenoidal wave. Peaking could be accomplished only through the geometry of the line and the output load.

Line VI established that a larger cross sectional area was not as effective as the smaller cross section. The product of the frequency, f, time delay, T_d, and diameter of the line D is equal to the line inductance, L_1. That is, $fT_dD = L_1$. A given delay will occur at a higher frequency if D is kept small. Also, less flux will be necessary to saturate a line of smaller cross section. This, of course, will result in smaller modulating power requirements.

Line VII clearly established the feasibility of the modulated delay line. Although its attenuation is somewhat high it can be peaked with a proper resonant load. At 10 megacycles, with a 10 microhenry inductor shunting an 8 μμf Textronix oscilloscope probe, the attenuation was reduced to 5db, and a comparatively linear time delay-modulating current characteristic resulted to 0.1 microseconds change in delay (Figure 62). The hysteresis effect noted in Figure 62 is of the order of 5% which is within the distortion limits of the best reactance tube methods. The time delay vs. modulation current relation, of course, becomes nonlinear if operation is pursued into the saturation region. Longer lines would tend to avoid this problem as would materials of still higher permeability, by presenting a greater initial delay.

It will be noted from Figure 63 that the point at which the time delay-modulation current relation becomes nonlinear coincides with the point at which the output amplitude increases drastically. This evidently occurs because the line is approaching saturation and behaves like an air core line with low loss. This region is not valuable, however, because of the large nonlinearity.

The modulation winding of line VII was a solenoid wound upon a form concentric with the rod and tube. No attempt was made to get a close fit as the isolation afforded by the separation precluded any coupling between the carrier RF signal and the audio or DC modulation current. Although

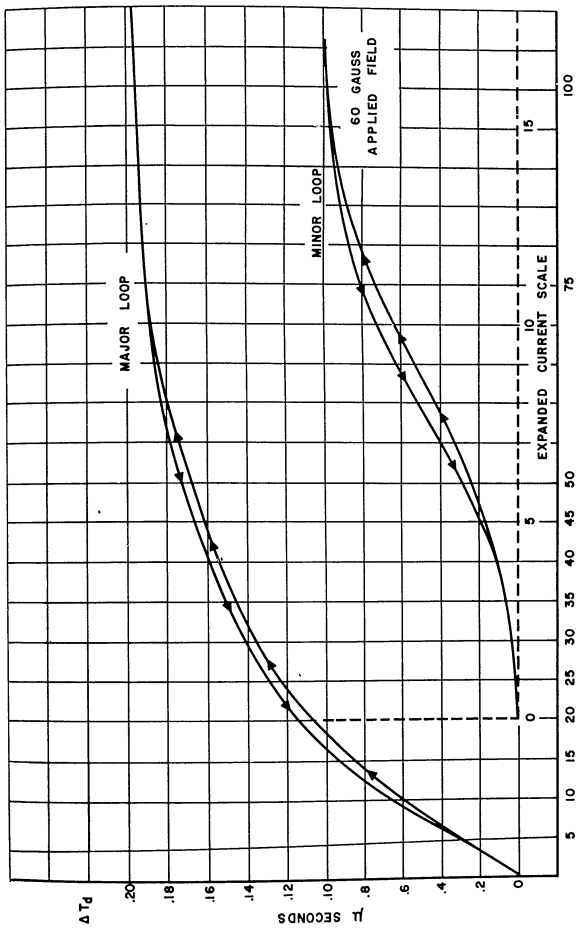

Figure 62. Change in Delay vs. D.C. Modulation Current at 10 mc Line VII

STAT

STAT

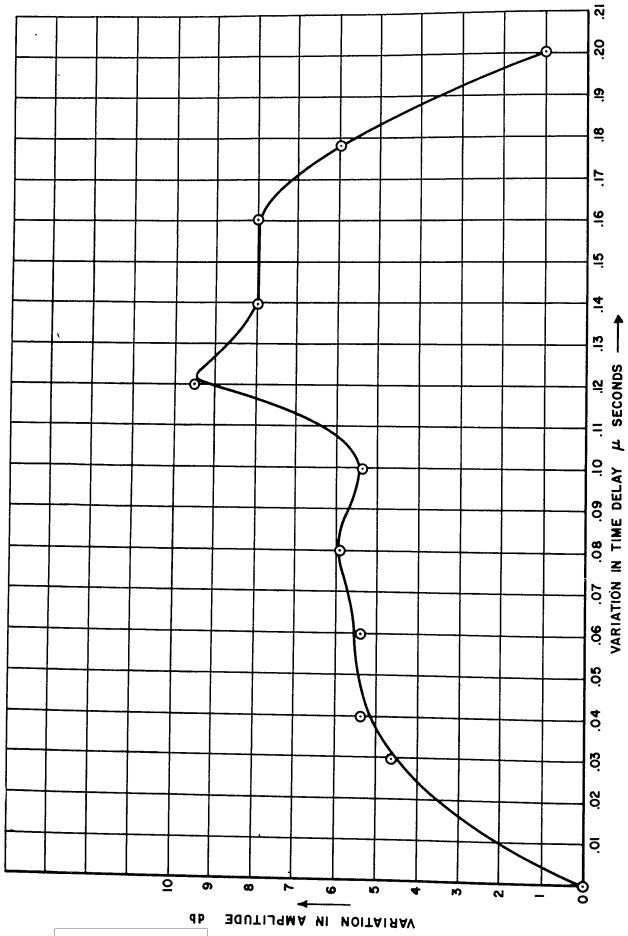

Figure 63. Variation in RF Output Amplitude vs. Variation in Time Delay at 10 mc Line VII

the modulation signal could have been applied to the same winding as the RF carrier, the additional winding afforded a means of isolating the two signals and gave a flexible four terminal network where the impedance of the modulation circuit could be adjusted to that of its drive circuitry.

The DC modulation characteristics noted demonstrate the practicality of the delay line phase modulator. The impedance of line VII at 10 megacycles was found to have a magnitude of about 750 ohms. The delay line cannot be loaded, however, since it still has a rather high series impedance. The unpeaked attenuation of line VII was 20 db. The attenuation may, however, be reduced to 6 db, if the line is matched into a class A_1 amplifier and its output peaked. In a typical communications transmitter, at least three stages could be eliminated by the 10 megacycle delay line. Line VIII was the basis of a determination of the effects of temperature on the variation in time delay with DC modulation current. The results are shown in Figure 64. It is evident that the device is stable through the range of -44°C to 110°C.

Additional lines were fabricated and the change in delay available determined as a function of D.C. modulation current. Table XIX is a summary of the firing and winding conditions for each line. The corresponding curves of change in time delay vs. bias are shown in Figures 65 and 66. It is apparent that line No. 10A is the superior one of this group.

Further tests were made with line No. 10A in a commercial frequency modulating equipment. A summary of the results are shown in Table XVIII.

TABLE XVIII

TEST INFORMATION FOR LINE NO. 10A

Modulation freq.	1000 cps
Carrier freq.	10 mc
Final freq.	30 mc
Freq. deviation at 30 mc	± 7.5 kc (± .1 μs)
Audio power required	0.3 watt
% RETMA distortion	5.2%

Similar tests taken at 30 mc on line No. 10C, indicated a change in time delay of ± .01 μs, in the linear range. Systematic testing at 30 mc has not been possible until very recently. With the acquisition of a calibrated 30 mc receiver, it now is possible to determine whether the basic limitations are produced by the line geometry or the material characteristics. The tentative conclusion at present is that the original goal

STAT

STAT

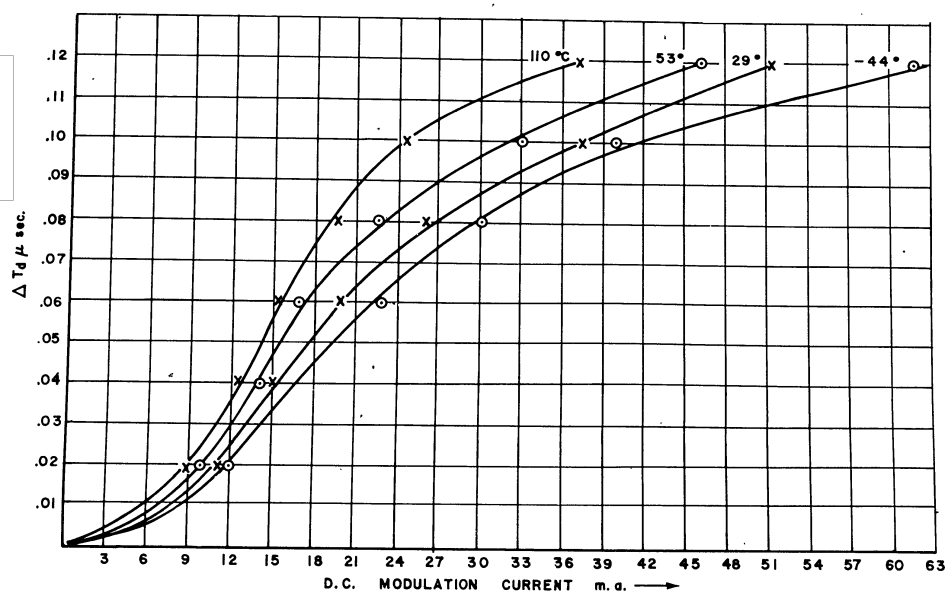

Figure 64. Change in Delay vs. D.C. Modulation Current with Temperature as Parameter Line VIII

TABLE XIX

DELAY LINE FABRICATION DATA

Line No.	Line Length	Soak Temp. °C	Soak Time (min.)	Rise Rate °C/hr.	Fall Rate	(ohms) Resistance of Modulation Winding
4A	2"	1140	20	500	Furnace Cool	800
5	2"	1125	20	500	" "	750
6	2"	1100	20	500	" "	950
7A	3 7/8"	1150	20	400	" "	1850
7B	3 3/4"	1150	20	400	" "	2250
9	2 3/4"	1135	20	800	" "	1650
10A	4 3/4"	1160	20	600	Slow Cool (100°C/hr.)	1850
10B	3 1/2"	1160	20	600	Slow Cool (100°C/hr.)	2000
10C	2 1/4"	1160	20	600	Slow Cool (100°C/hr.)	800

A, B, and C, for a given designation, refer to different lines fabricated from a particular firing.

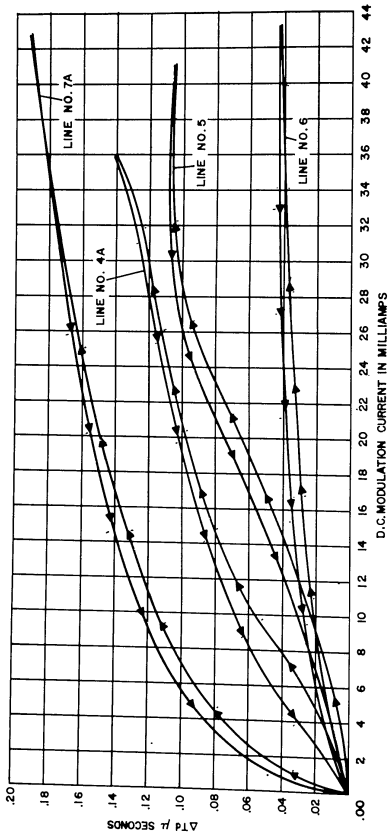

Figure 65. Change in Delay vs. D.C. Modulation Current

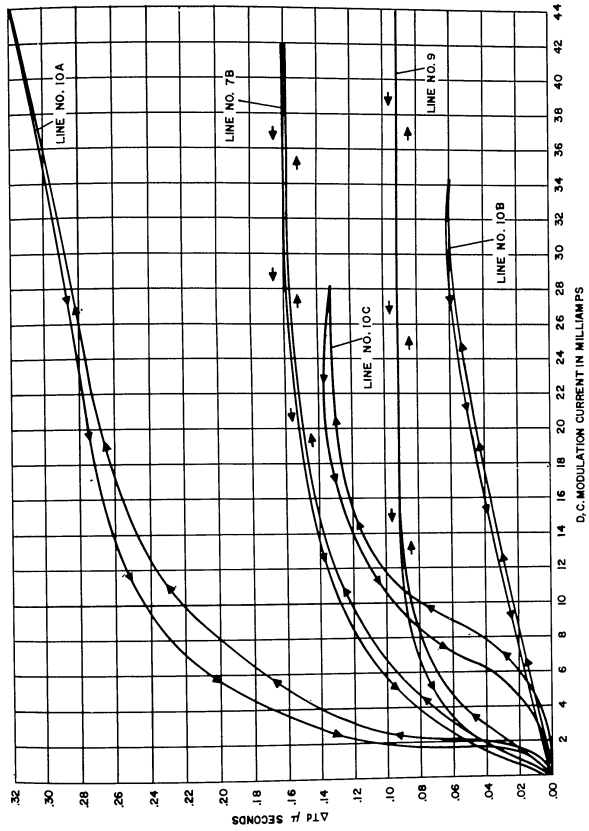

Figure 66. Change in Delay vs. D.C. Modulation Current

STAT

of ± 0.1 μs at 30 mc cannot be achieved. However, where larger attenuations are permissible, it now seems reasonable to obtain ± .05 μs.

All of the delay lines reported in Table XIX were constructed in a similar manner. The rods are closely wound with No. 40 enameled wire. The tubes are coated with an indium-mercury amalgam as the outer conductor. Though amalgam operates rather efficiently, it is somewhat less desirable from the health hazard viewpoint. Other methods should be investigated in order to find simple substitutes.

A further improvement in construction has been incorporated in the latest lines. A glass tube is slipped over the ferrite sleeve. The modulation winding is then wound on the glass rod. It is found that line breakage is reduced and uniformity in winding is increased.

In Figure 67, a photograph is shown of a 6" line. This photograph shows the bread-board model of the device.

Conclusions and Recommendations

As indicated above, it has not been possible to satisfy the ultimate objective of line operation at 30 mc with the indicated change in delay at ±0.1 microsecond. The problem is complicated by an interplay between materials requirements and geometric configuration.

It should be pointed out that the successful construction of the line for operation at 10 mc is a major achievement. Such a component is easily handled and when incorporated in a frequency modulator, will reduce the number of multiplication steps considerably. There is a practical upper limit to the highest starting frequency due to difficulties in obtaining adequate quartz crystals. This is necessary to insure stability. In view of this fact, initial carrier signals at 30 mc probably would not be utilized. However, a 10 mc initial carrier could be used in many common applications. In the present component, all critical specifications have been met. A more than adequate change in time delay is easily achieved. Modulation power requirements have been shown to be insignificantly small. For phase modulation systems which require a constant phase shift in radians, independent of carrier frequency, the present line possibly could be extended to give ±.05 microsecond change in delay at 30 mc.

The results of this effort lead to the following recommendation: Until the utility of the 10 mc carrier line has been shown to be inadequate, no further effort should be expended in developing a 30 mc carrier line giving ±0.1 microsecond change in delay. It has been shown, however, that the present materials and configuration can be used for operation as high as 15 mc and probably with a small amount of additional work, be extended to 20 mc.

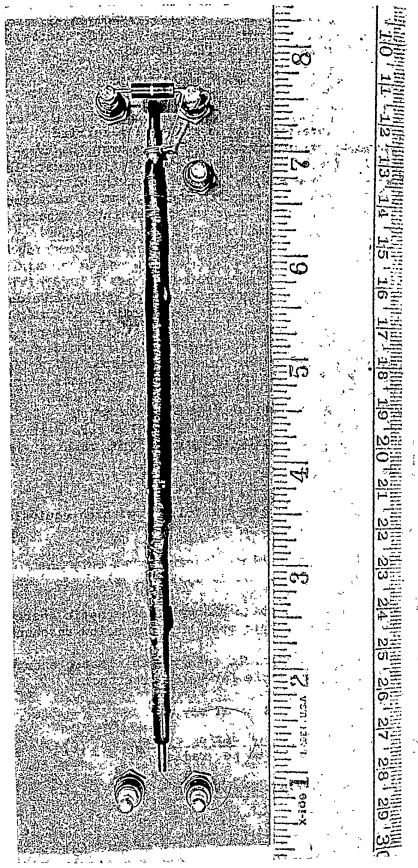

Figure 67. Photograph of Modulated Delay Line

STAT

STAT

SECTION V

MAGNETOSTRICTIVE MATERIALS AND APPLICATIONS

Objective

The objective of this investigation is to develop ferrite materials for dynamic magnetostrictive devices to operate over the temperature range -65°C to 250°C. The desire is to obtain materials suitable for use in such components as filters and oscillators over the frequency range 455 kc to 1000 kc. The maximum temperature coefficient of resonant frequency to be tolerated is 10 ppm per C° over the temperature range of interest.

Material Parameters

The basic parameters with which we are concerned in the development of materials for dynamic magnetostrictive applications are as follows:

k = electromechanical coupling coefficient

Q_m = quality factor for mechanical vibration

f_o = resonant frequency of mechanical vibration in cps

E = effective modulus of elasticity in dynes/cm^2

ρ = density of sample in gm/cm^3

The quantity k is defined by any of the following three equivalent statements:

1. k^2 = ratio of electromagnetic to elastic energy when only an alternating low frequency stress is applied.
2. k^2 = fractional conversion of elastic energy into magnetic energy by an elastically driven sample operating far below resonance.
3. k^2 = fractional conversion of magnetic energy into elastic energy by a magnetically driven sample far below resonance.

The quantity Q_m is defined in the usual way,

$$Q_m = \frac{\text{maximum elastic energy stored during cycle}}{\text{mechanical energy dissipated per radian}} \qquad (2)$$

The quantities f_o, E and ρ are related by

$$f_o = G\sqrt{E/\rho} \qquad (3)$$

where G is a geometrical factor depending on the sample shape and mode of excitation. For a toroid vibrating in simple radial extension

$$G = \frac{1}{2\pi R} \qquad (3')$$

where R is the mean radius of the toroid.

The Equivalent Circuit of a Freely Vibrating Sample

The circuit which we shall use to describe a freely vibrating magnetically driven sample is given in Figure 68.

In Figure 68, L is the inductance of the coil with ferrite core and determines the reactance of the sample far off resonance. R_w is the resistance of the windings; k^2 the square of the electromechanical coupling coefficient; C the equivalent capacitance such that equation (3) is satisfied; and R_m the equivalent resistance which represents the mechanical energy dissipation for the freely vibrating system. (R_m also includes air damping and support damping in the practical case.) The term L/k^2 measures the efficienty of the conversion of magnetic to mechanical energy. For small k the mechanical branch has relatively little effect upon the effective impedance of the sample.

Using the circuit shown in Figure 68, we can now arrive at several useful relationships. In the practical case, the two branches are anti-resonant for the circular frequency given by

$$\omega_a^2 = (2\pi f_a)^2 = \frac{k^2}{(1+k^2)LC} \qquad (4)$$

and the mechanical branch is resonant for the frequency given by

$$\omega_r^2 = (2\pi f_r)^2 = \frac{k^2}{LC} \qquad (5)$$

Using Equations (4) and (5) we have

$$k^2 = \frac{\omega_r^2 - \omega_a^2}{\omega_a^2} \qquad (6)$$

or

$$k^2 = \frac{2(f_r - f_a)}{f_a}$$

for $f_r = f_a$ in the approximation of small k^2.

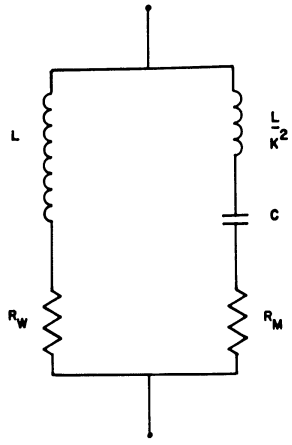

Figure 68. Equivalent Circuit of Freely Vibrating Sample

We see that the electromechanical coupling coefficient can be obtained simply by measuring the resonant and anti-resonant frequencies.

A word about the resonant frequencies f_o, f_a and f_r is now in order. We consider the lossless case, $R_w = R_m = 0$, in the following discussion. The acoustical resonant frequency of a ferromagnet depends upon the experimental method used in exciting the sample. The value of Young's modulus at constant magnetization differs from that obtained at constant field. In the approximation used here, $f_o = f_a$ for constant field and $f_o = f_r$ for constant magnetization. The distinction is of academic interest only in our work except in the determination and interpretation of the temperature coefficients of the frequencies f_a and f_r.

From Equation (2) and Figure 68 we write

$$Q_m = \frac{\omega_a L}{k^2 R_m} \tag{7}$$

or

$$k^2 Q_m = \frac{\omega_a L}{R_m} \tag{8}$$

Now, for $R_w \ll R_m$ and $k^2 Q_m \geq 10$;

$$Z_a = \frac{\omega_a^2 L^2}{R_m} \tag{9}$$

and

$$Z_r = R_m \tag{10}$$

where Z_a and Z_r are the impedances of the sample at the frequencies f_a and f_r, respectively. From Equations (8), (9) and (10) we have

$$k^2 Q_m = \sqrt{Z_a / Z_r} \tag{11}$$

We see that k, Q_m and E can be obtained by measuring the resonant and anti-resonant frequencies, and the ratio of the anti-resonant to the resonant impedance.

Method of Measurement

The basic circuit used for measuring the quantities of interest, f_a, f_r, Z_a and Z_r, is shown in Figure 69.

STAT

STAT

In Figure 69, S is the excitation source V_o and V_S vacuum tube voltmeters and R_o a dropping resistor chosen large in order to maintain constant current to the sample. V_o monitors the drop across R_o so that constant current conditions can be maintained.

Toroidal specimens are prepared for measurement in the following way. The sample is placed in a textolite annular holder which is so designed that the sample makes contact with the holder at only three points. The holder is then wound with an appropriate number of turns. The number of turns chosen depends upon the permeability of the ferrite and the size of the sample. For toroids of one inch diameter and permeability about 30, approximately 200 turns yield a reasonable inductance for mechanical resonance at about 100 kc.

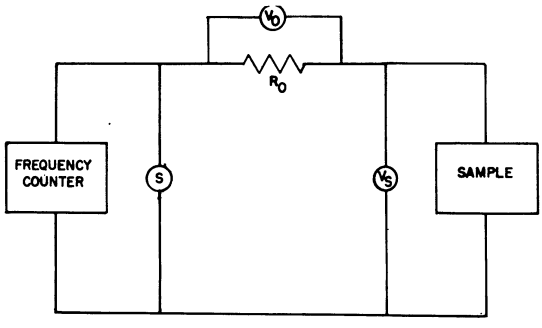

Figure 69. Circuit for Measuring f_a, f_r, Z_a and Z_r for Sample at a Given Magnetic Operating Unit

The magnetostrictive parameters depend upon the magnetic state of the ferrite. In order to insure reproducible results and reproducible magnetic operating points, the following procedure is used. Magnetizing and demagnetizing sources are connected to the sample as shown in Figure 70.

At the start of a series of measurements on a given specimen, the sample is first demagnetized using a 60 cycle AC source with variable amplitude. The present AC source consists of a Variac and an 11 volt, 20 ampere transformer.

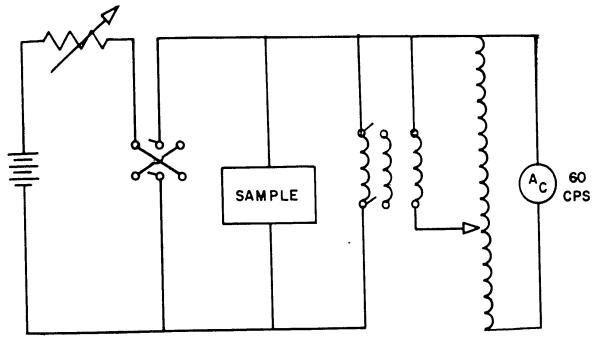

Figure 70. Magnetizing and Demagnetizing Sources

STAT
STAT

The magnetizing current is then applied and its direction reversed several times. The magnetic state attained is then an unambiguous point on the normal magnetization curve. The DC current is then reduced to zero so that the resulting magnetization corresponds to a definite, reproducible remanent point. The values of the magnetization along the normal magnetization curve and at the remanent points are obtained using a flux meter.

The characteristic curve for a vibrating toroidal sample is obtained by measuring the voltage across the sample as a function of driving frequency at constant current. An example of such a characteristic curve is shown in Figure 71.

From Figure 71 f_a, f_r, V_a and V_r can be obtained. V_a and V_r are the voltages across the sample at the anti-resonant point and resonant point, respectively. If the current in the line is maintained constant, then

$$z_a/z_r = V_a/V_r$$

and Equation (11) becomes

$$k^2 Q_m = \sqrt{V_a/V_r} \qquad (12)$$

We see then that for the sample whose characteristic is shown in Figure 71, $V_a/V_r = 400$; from Equation (6), $k^2 = 1.8 \times 10^{-2}$. Therefore, $k = 0.135$ and, using Equation (12), $Q_m = 1100$. From Equations (3) and (3'), we obtain for the elastic modulus (Young's modulus for this case) $E = 1.8 \times 10^{12}$ dynes/cm^2. The sample for which Figure 71 was obtained is a Ni-Zn ferrite (Composition 285, Table IV) operating at a remanent induction of about 1500 gauss. The saturation induction for this sample is 4000 gauss.

Materials

The choice of materials for investigation under this program were governed to a large extent by the proposed temperature range of operation and the requirements on the temperature coefficient of resonant frequency. Composition 285 (see Table IV) exhibits a Curie Temperature greater than 500°C. These materials are expected to have a favorable temperature response to 250°C.

Results of Measurements

In Figure 72 is given a set of characteristics which illustrates the dynamic magnetostrictive response of a specimen as a function of the remanent induction, B_r, of the sample. This family of curves illustrates the dependence of the magnetostrictive and elastic parameters on the magnetic state of the sample.

In Table XX are given the resonant frequency, elastic modulus, the electromechanical coupling coefficient and observed mechanical Q of

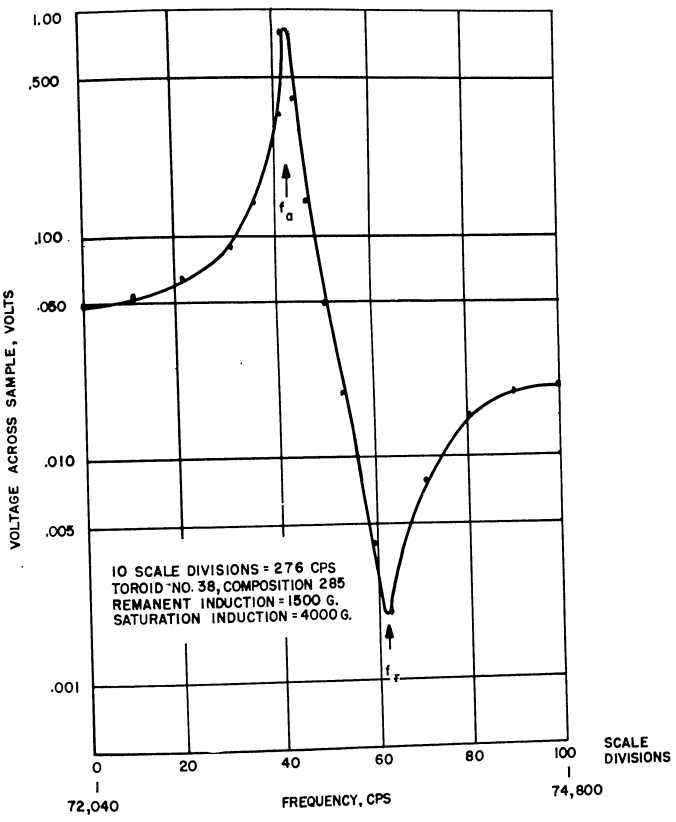

Figure 71. Voltage vs. Frequency for a Magnetically Driven Vibrating Toroidal Sample

STAT

STAT

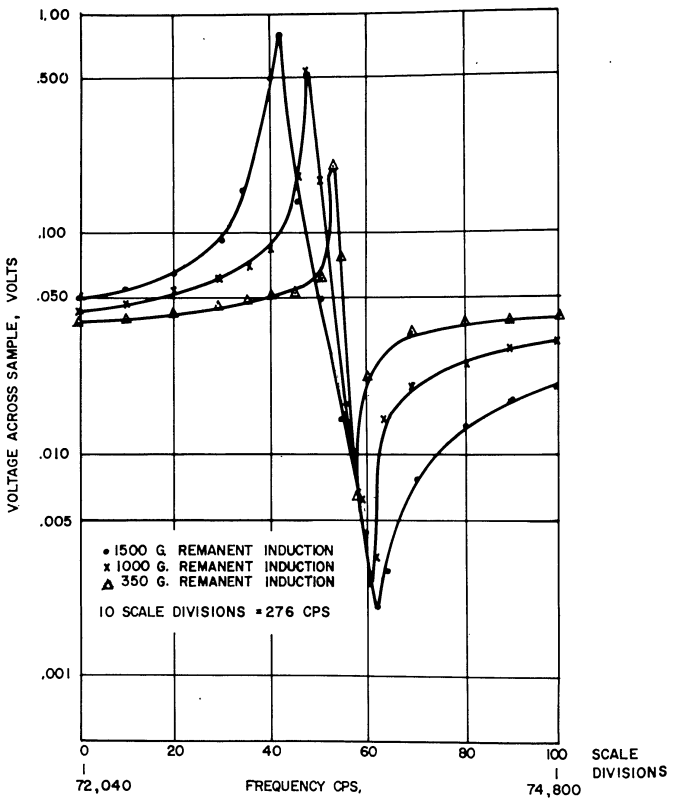

Figure 72. Voltage vs. Frequency for Sample 285.38 Vibrating Radially with Remanent Flux as Parameter

TABLE XX

RESONANT FREQUENCY, f_o, ELASTIC MODULUS, E; ELECTROMECHANICAL COUPLING COEFFICIENT, k; AND OBSERVED MECHANICAL Q, Q_m, FOR COMPOSITION 285 AND PROCESSING TREATMENT AS INDICATED.

Toroid No.	Firing temp. °C	Pressing press, psi.	Pellet size	f_o l:cps.	E dynes per cm^2	k	Q_m
38	1400	13,750	+ 80	73.8	1.8×10^{12}	.135	1100
36	1400	2,400	+ 80	75.8	1.7	.086	2200
53	1100	13,750	- 20	34.4	0.3	.033	1000
22	1400	4,800	+ 20	62.1	1.2	.066	2100
56	1100	2,400	+ 80	55.9	1.2	.027	1300
58	1100	13,750	+ 80	56.6	1.5	.039	2800
69	1400	13,750	- 20	68.4	1.4	.072	600
46	1100	2,400	+ 20	52.0	0.8	.009	500
71	1400	2,400	- 20	53.1	0.7	.066	2100
52	1100	13,750	20 - 40	59.2	1.1	.034	3600
55	1100	2,400	- 20	18.6	0.07	.054	300
28	1400	2,400	20 - 40	73.6	1.5	.080	700

STAT

STAT

various toroids. The data were obtained at room temperature. In performing the experiment, the cores were subjected to a field of approximately 40 oersteds and then allowed to fall to remanence.

The results in Table XX indicate that for Composition 285 larger electromechanical coupling coefficients are obtained for dense bodies fired at relatively high temperatures, 1400°C. However, the temperature coefficient of resonant frequency depends upon the state of internal strain in the sample. Thus, the requirements of temperature stability over the temperature range contemplated, -65°C to 250°C, require a compromise between temperature coefficient and coupling constant.

Figures 73 and 74 give the temperature dependence of f_a and f_r, from room temperature to 250°C, for toroids 285.38 and 285.52, respectively. Composition 285 is prepared using 50 mol% Fe_2O_3, 42 mol% NiO, 7.5 mol% ZnO and 0.5 mol% V_2O_5. Toroid 285.38 was fired at 1400°C and toroid 285.52 at 1100°C.

From Figure 73, it is seen that the temperature variation of f_r and f_a for toroid 285.38 is approximately 100 ppm per °C over the interval 25°C to 250°C. The temperature coefficient of f_r is somewhat greater than that of f_a, the difference being a measure of the decrease of k with temperature over the interval considered.

Figure 74 indicates that the temperature coefficients of f_a and f_r are considerably less for toroid 285.52. In this case, the coefficients are approximately 50 ppm per °C. While this value is still high for the purposes of this development, a clear indication is given as to the strong dependence of the temperature coefficient of resonant frequency upon the processing of the material.

Figure 75 presents the variation of f_a, f_r and k with the current used to bias the sample to remanence. The data are given for toroid 285.52. The decrease in f_r above 0.7 amps may be due to heating of the sample rather than an intrinsic dependence at room temperature. The curves presented in Figure 75 were obtained by biasing the sample with the indicated current, reversing the direction of the current several times, and then decreasing the current to zero. The magnetic state attained, corresponding to each current value, was then an unambiguous point on the normal magnetization curve.

The ΔE effect in a ferromagnetic material is a measure of the variation with state of magnetization of Young's modulus at a given temperature. Figure 75 indicates that the ΔE effect is not large in toroid 285.52 since the change in f_r is small. The electromagnetic coupling coefficient, k, is expected to increase with biasing current so that f_a must decrease as predicted from Equation (6).

Figure 76 shows the dependence of sample voltage, at constant current, on frequency at -174°C and 25°C for toroid 285.56. Between these temperatures, the temperature variation of f_r and f_a is 56 ppm per °C and 65 ppm per °C, respectively. The coupling coefficient, k, is found to be 9.0% at 25°C and 7.5% at -174°C.

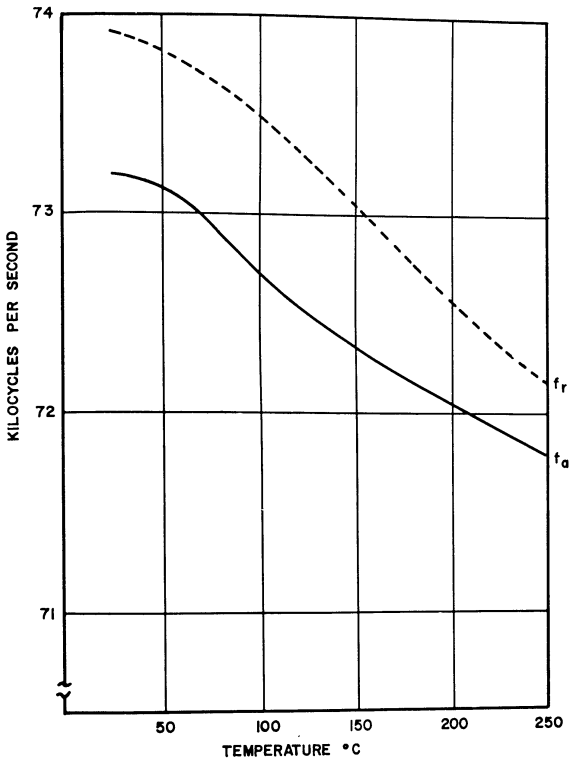

Figure 73. Temperature Variation of f_r and f_a for Toroid 285.38

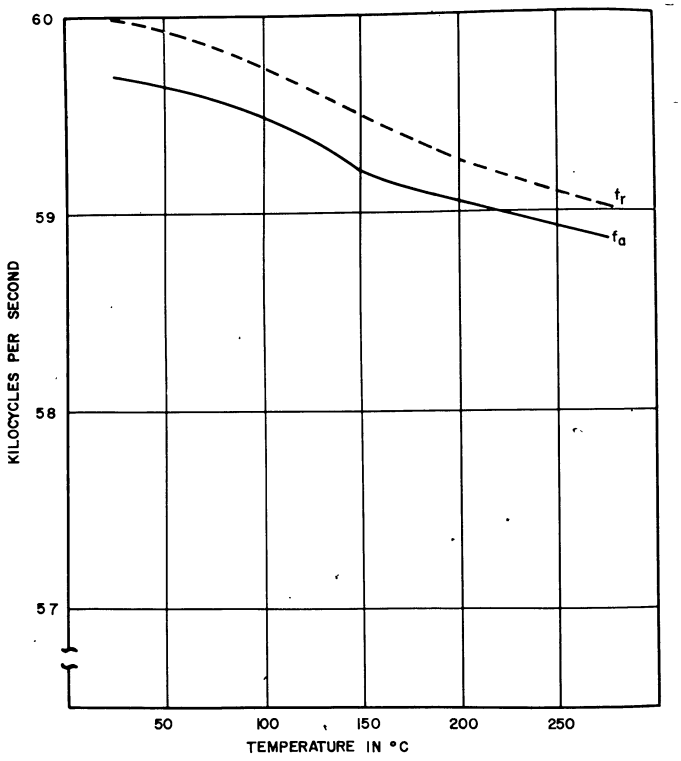

Figure 74. Temperature Variation of f_r and f_a for Toroid 285.52

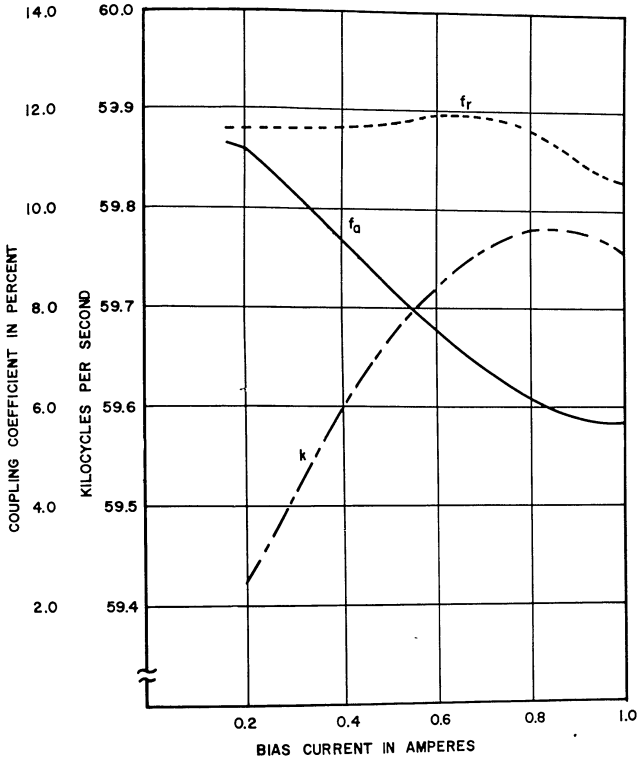

Figure 75. Variation of f_r, f_a and k with Bias Current for Toroid 285.52

STAT
STAT

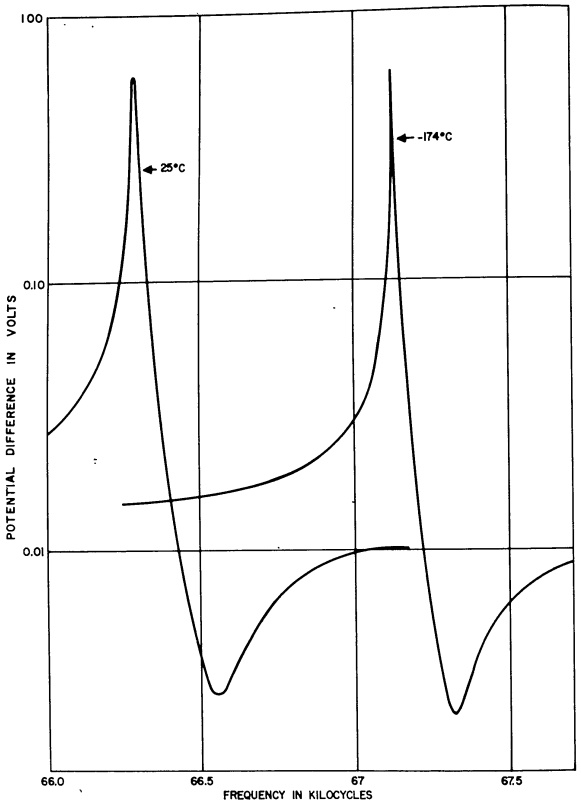

Figure 76. Voltage-Frequency Characteristic for Toroid 285.56

The values of temperature coefficient of resonant frequency and coupling coefficient obtained for toroid 285.56 at low temperatures are very nearly equal to those reported for toroid 285.52. The values obtained for toroid 285.52 were determined from measurements taken between 25°C and 250°C. These two samples were prepared under similar conditions.

Conclusions and Recommendations

Of the various areas of effort investigated during the contract period covered by this report, the development of magnetostrictive materials was the least extensive. As a result, it is difficult to arrive at significant and detailed conclusions. However, the present work has indicated that the temperature interval -65°C to +250°C is too broad to expect a uniformly small temperature coefficient of resonant frequency over the entire interval. The goal of 10 parts per million per degree centigrade was not attained. As a result, no attempt was made to fabricate geometries to give rise to oscillations in the frequency region 455 kc to 1000 kc.

Further effort in this field should be more properly directed toward obtaining specific materials for specified filter application. The temperature coefficient requirement should be stipulated over the smallest temperature interval reasonable.

SECTION VI

CONCLUSIONS

In the body of the text, conclusions and recommendations have been given covering a given phase of effort. In this Section, the pertinent results are summarized and in some respects extended.

Perhaps the most significant accomplishment of the effort covered by this report is the development of a usable modulated ferrite delay line for application at 10 mc. Even though the ultimate goal of a 30 mc carrier line was not achieved, the utility of the device in hand is unquestionable. Operation in a commercial frequency modulating equipment indicated that the present line gives rise to low distortion and that the audio power required for operation is nominal. The necessary total delay and change in delay with field has been obtained using Composition 84 ferrite which was developed under the low signal materials program. Extrusion of this material in rods and tubes of the requisite strength and straightness has been accomplished without the sacrifice of the desirable magnetic properties.

Until the utility of the 10 mc carrier line has been shown to be inadequate, it is recommended that no further effort be expended in developing a 30 mc carrier line giving ± 0.1 microsecond change in delay. It has been shown, however, that the present materials and configuration can be used for operation as high as 15 mc and with a small amount of additional work, be extended to 20 mc. For phase modulation systems which require a constant phase shift in radians, independent of carrier frequency, the present line possibly could be extended to give ± 0.05 microsecond change in delay at 30 mc.

In the development of high power ferrite materials, two Compositions, 704 and 731, are recommended for application to cover the frequency range 20 kc to 1000 kc. These materials exhibit usable permeabilities over the temperature interval -65°C to +250°C. (Characteristic curves are given in the body of the text.)

It is recommended that work in the area of high power ferrite materials development be terminated until the present materials are evaluated in a specific application. After this evaluation, further effort may be fruitful in tailoring specific properties to the needs of a given device. During the course of the present development, high power materials were supplied to the American Research and Manufacturing Corporation for possible application in a rapid response magnetic amplifier being developed under Contract No. AF 33(615)-3377. However, no results have been received to date in connection with the evaluation of these materials.

The broad objectives of the program dealing with the development of low loss, low signal materials were achieved. A series of high Q materials have been made available with permeabilities in the range 12 to 120. The Curie temperatures of these materials lie between 385°C and 500°C and high Q behavior persists over the temperature interval -65°C to +250°C.

In addition, the low signal properties of these materials have been shown to be relatively unaffected by prolonged exposure to high humidity. Of particular importance is the low temperature coefficient of permeability exhibited in the range -55°C to +25°C. In future work, the broad objectives, which applied in the phase of effort currently completed, should be narrowed to stipulate specific low signal parameter values.

Materials developed under the low signal ferrites program have been supplied to the Federal Telecommunications Laboratories for possible application in developments being carried out under Contract AF 33(600)-32060, and to the Emerson Radio and Phonograph Company for possible application in developments being pursued under Contract No. AF 33(600)-31464.

In the development of ferrite materials for magnetostrictive applications, the goal of a temperature coefficient of resonant frequency less than 10 ppm per °C was not achieved. It is recommended that further effort in this field be directed toward obtaining specific materials for specified filter application. The temperature coefficient of resonant frequency requirement should be stipulated over the smallest temperature interval possible.

STAT

STAT

Next 1 Page(s) In Document Denied

STAT

STAT